THE EUROPEAN
PHYSICAL JOURNAL C

Search for a heavy Higgs boson decaying into a Z boson and another heavy Higgs boson in the $\ell\ell bb$ and $\ell\ell WW$ final states in pp collisions at $\sqrt{s} = 13$ TeV with the ATLAS detector

ATLAS Collaboration[⋆]

CERN, 1211 Geneva 23, Switzerland

Abstract A search for a heavy neutral Higgs boson, A, decaying into a Z boson and another heavy Higgs boson, H, is performed using a data sample corresponding to an integrated luminosity of 139 fb^{-1} from proton–proton collisions at $\sqrt{s} = 13$ TeV recorded by the ATLAS detector at the LHC. The search considers the Z boson decaying into electrons or muons and the H boson into a pair of b-quarks or W bosons. The mass range considered is 230–800 GeV for the A boson and 130–700 GeV for the H boson. The data are in good agreement with the background predicted by the Standard Model, and therefore 95% confidence-level upper limits for $\sigma \times B(A \to ZH) \times B(H \to bb$ or $H \to WW)$ are set. The upper limits are in the range 0.0062–0.380 pb for the $H \to bb$ channel and in the range 0.023–8.9 pb for the $H \to WW$ channel. An interpretation of the results in the context of two-Higgs-doublet models is also given.

1 Introduction

After the discovery of a Higgs boson at the Large Hadron Collider (LHC) [1,2], detailed measurements of its properties [3–10] have shown excellent compatibility with the Standard Model (SM) Higgs boson [11–16]. These results indicate that the scalar sector of the theory of the electroweak interaction contains at least a doublet of complex scalar fields. In addition, they constrain the possibilities for additional spin-0 field content in the theory and disfavour parts of the parameter space in models with extended Higgs sectors. These results, however, still allow several extensions of the Higgs sector, such as the two-Higgs-doublet model (2HDM) [17,18], in which large parts of the parameter space are compatible with the existence of a Higgs boson like the one in the SM. In the 2HDM, a second complex doublet of the Higgs fields is added to the single SM Higgs doublet. The model has a weak decoupling limit [19] in which one of its predicted Higgs

bosons has couplings to fermions and vector bosons that are the same as those of the SM Higgs boson at lowest order. In addition, a Higgs sector structure with two complex doublets of fields appears in several new physics scenarios, including supersymmetry [20], dark-matter models [21], axion models [22], electroweak baryogenesis [23] and neutrino mass models [24].

The addition of a second Higgs doublet leads to five Higgs bosons after electroweak symmetry breaking. The phenomenology of such a model is very rich and depends on many parameters, such as the ratio of the vacuum expectation values of the two Higgs doublets ($\tan\beta$) and the Yukawa couplings of the scalar sector [18]. When CP conservation is assumed, the model contains two CP-even Higgs bosons, h and H with $m_H > m_h$, one that is CP-odd, A, and two charged scalars, $H^{\pm}$. There have been many searches for a CP-even Higgs boson at the LHC, in channels that include $H \to WW/ZZ$ [25–30] and $H \to hh$ [31,32], as well as dedicated searches for the heavy CP-odd Higgs boson, as in the $A \to Zh$ channel [33,34]. Some 2HDM searches are agnostic with respect to whether the heavy Higgs bosons are CP-even or CP-odd, for example searches in the $A/H \to \tau\tau/bb$[1] channels [35–37]. In the interpretation of this last category of channels it is usually assumed that both heavy Higgs bosons are degenerate in mass, a hypothesis that is motivated in certain supersymmetric models [20]. Finally, there have been searches for signatures that explicitly assume different masses for the heavy Higgs bosons, for example searches in the $A \to ZH \to \ell\ell bb/\ell\ell\tau\tau$ channels [38–40].

The case in which the heavy Higgs bosons have different masses, in addition to being in an allowed part of the parameter space, is further motivated by electroweak baryogenesis scenarios in the context of the 2HDM [41–44]. For 2HDM electroweak baryogenesis to occur, the requirement $m_A > m_H$ is favoured [41] for a strong first-order phase tran-

---

⋆ e-mail: atlas.publications@cern.ch

[1] To simplify the notation, antiparticles are not explicitly labelled in this paper.
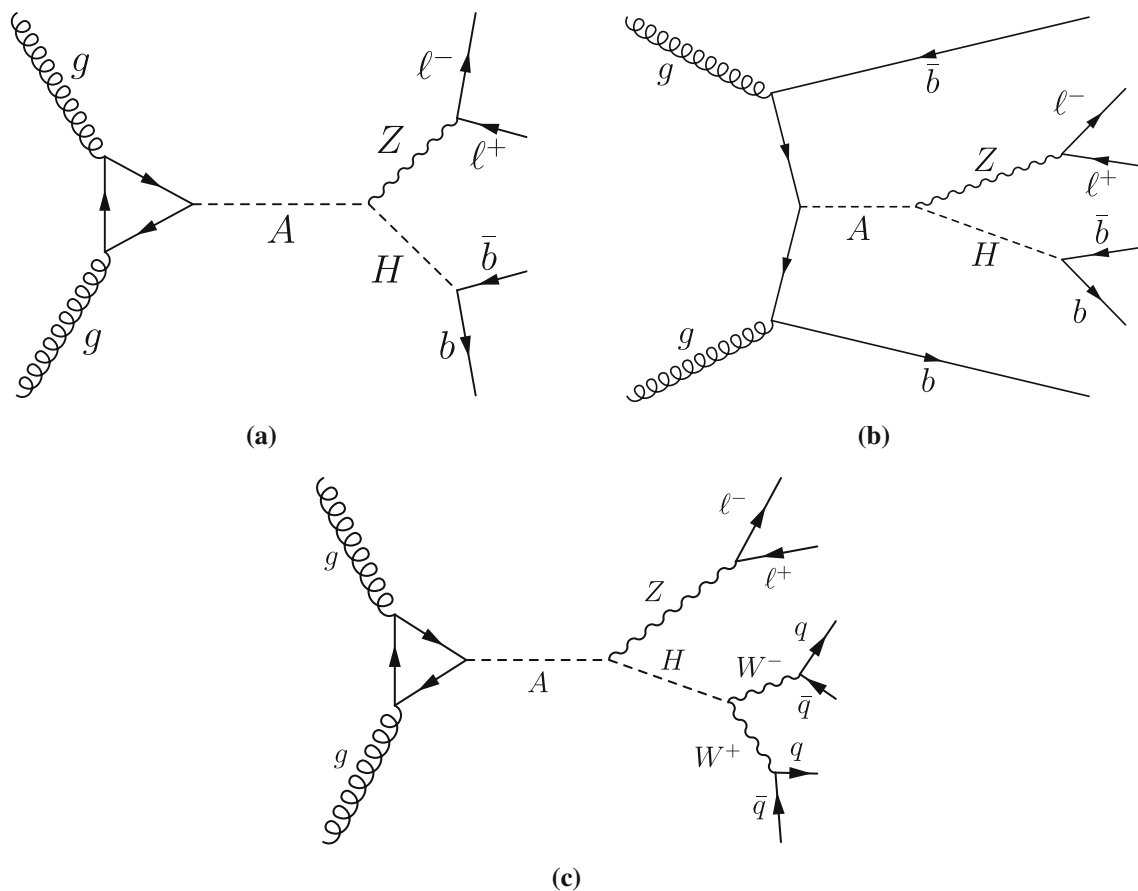
Fig. 1 Example lowest-order Feynman diagrams for **a** gluon–gluon fusion production of A bosons decaying into $ZH \rightarrow \ell\ell bb$, **b** b-associated production of A bosons decaying into $ZH \rightarrow \ell\ell bb$, and **c** gluon–gluon fusion production of A boson decaying into $ZH \rightarrow \ell\ell WW$

sition to take place in the early universe. The A boson mass is also constrained to be less than approximately 800 GeV, whereas the lighter CP-even Higgs boson, h, is required to have properties similar to those of a SM Higgs boson and is assumed to be the Higgs boson with a mass of 125 GeV that was discovered at the LHC [41]. Under such conditions and for large parts of the 2HDM parameter space, the CP-odd Higgs boson, A, decays into ZH [41,45]. At the LHC, the production of the A boson in the relevant 2HDM parameter space proceeds mainly through gluon–gluon fusion and in association with b-quarks (b-associated production).

This search for $A \rightarrow ZH$ decays uses proton–proton collision data at $\sqrt{s} = 13$ TeV corresponding to an integrated luminosity of 139 fb^{-1} recorded by the ATLAS detector at the LHC. The search considers $Z \rightarrow \ell\ell$, where $\ell = e$, μ, to take advantage of the clean leptonic final state. The H boson is studied in the $H \rightarrow bb$ and $H \rightarrow WW$ decay channels. The $H \rightarrow bb$ channel takes advantage of the high branching ratio in large parts of the 2HDM parameter space, especially in the weak decoupling limit, where the H boson decays into weak vector bosons are suppressed. The $H \rightarrow WW$ decay channel is considered in the case where both W bosons

decay hadronically. This heavy Higgs boson decay is dominant in parts of the 2HDM parameter space close to, but not exactly at, the weak decoupling limit [41] and it provides a new way to look for $\ell\ell WW$ resonances in a final state that has been less explored by other LHC searches. Both final states considered allow full reconstruction of the A boson's decay kinematics. This search considers both the gluon–gluon fusion (see Fig. 1a) and b-associated production mechanisms (see Fig. 1b) for the $A \rightarrow ZH \rightarrow \ell\ell bb$ channel. The b-associated production mode of the $A \rightarrow ZH \rightarrow \ell\ell WW$ channel is theoretically allowed, but leads to more complicated jet combinatorics and would necessitate changing the event reconstruction strategy. For this reason, only the gluon–gluon fusion production mode (see Fig. 1c) is considered here.

This article is organised as follows. Section 2 introduces the ATLAS detector. A description of the collision and simulated data samples used in this article is given in Sect. 3. The algorithms used to reconstruct the objects used in this search are described in Sect. 4. The event selection and background estimates for the two channels considered and the modelling of the signal are discussed in Sects. 5 and 6, respectively.

Section 7 is devoted to the description of the systematic uncertainties. The results are discussed in Sect. 8 and the conclusions are given in Sect. 9.

2 ATLAS detector

The ATLAS experiment [46] at the LHC is a general-purpose particle detector with cylindrical geometry and forward–backward symmetry. It includes an inner-detector tracker surrounded by a 2 T superconducting solenoid, electromagnetic and hadronic calorimeters, and a muon spectrometer with a toroidal magnetic field. The inner detector consists of a high-granularity silicon pixel detector, including the insertable B-layer [47,48], a silicon microstrip tracker, and a straw-tube tracker. It provides precision tracking of charged particles with pseudorapidity $|\eta| < 2.5$.[2] The calorimeter system covers the pseudorapidity range $|\eta| < 4.9$. It is composed of sampling calorimeters with either lead/liquid-argon, steel/scintillator-tiles, copper/liquid-argon or tungsten/liquid-argon as the absorber/sensitive material. The muon spectrometer provides muon identification and momentum measurement for $|\eta| < 2.7$. A two-level trigger system [49] is employed to select events to be recorded at an average rate of about 1 kHz for offline analysis.

3 Data and simulated event samples

The data used in this search were collected between 2015 and 2018 from $\sqrt{s} = 13$ TeV proton–proton collisions and correspond to an integrated luminosity of 139 fb^{-1} [50–53], which includes only data-taking periods where all relevant detector subsystems were operational [54]. The data sample was collected using a set of single-muon [55] and single-electron triggers [56]. The single-muon triggers had p_T thresholds in the range of 20–26 GeV for isolated muons and 50 GeV for muons without any isolation requirement. The single-electron triggers employed a range of p_T thresholds in the range 24–300 GeV and a combination of quality and isolation requirements depending on the data-taking period and the p_T threshold.

Simulated signal events with A bosons produced by gluon–gluon fusion were generated at leading order (LO)

with MADGRAPH5_aMC@NLO 2.3.3 [57,58], using PYTHIA 8.210 [59] with a set of tuned parameters called the A14 tune [60] for parton showering. The decays of $H \rightarrow bb$ and WW were considered. Additionally, in the $A \rightarrow ZH \rightarrow \ell\ell bb$ channel, A bosons produced in association with b-quarks were generated at next-to-leading-order (NLO) with MADGRAPH5_aMC@NLO 2.1.2 [58,61,62] following Ref. [63] together with PYTHIA 8.212 and the A14 tune for parton showering. The gluon–gluon fusion production used NNPDF2.3lo [64] as the parton distribution functions (PDFs), while the b-associated production used CT10nlo_nf4 [65]. The signal samples were generated for A bosons with masses in the range of 230–800 GeV (300–800 GeV) and widths up to 20% of the A mass, and for narrow-width H bosons with masses in the range of 130–700 GeV (200–700 GeV) for the $\ell\ell bb$ ($\ell\ell WW$) channel.

Background events from the production of W and Z bosons in association with jets were simulated with SHERPA v2.2.1 [66] using NLO matrix elements (ME) for up to two partons, and LO matrix elements for up to four partons calculated with the Comix [67] and OpenLoops [68,69] libraries. They were matched with the SHERPA parton shower [70] using the MEPS@NLO prescription [71–74] using the set of tuned parameters developed by the SHERPA authors. The NNPDF3.0nnlo set of PDFs [75] was used and the samples were normalised to a next-to-next-to-leading-order (NNLO) prediction [76]. Production of WW, ZZ and WZ pairs was simulated using the same generator and parameters as for the W and Z boson samples.

The production of $t\bar{t}$ events was modelled using the POWHEG -BOXv2 [77–80] generator at NLO with the NNPDF3.0nlo [75] PDF set and the h_{damp} parameter[3] set to 1.5 m_{top} [81]. The events were interfaced to PYTHIA 8.230 to model the parton shower, hadronisation and underlying event, with parameters set according to the A14 tune and using the NNPDF2.3lo set of PDFs. The decays of bottom and charm hadrons were performed by EVT-GEN v1.6.0 [82]. The associated production of a single-top quark and W boson (tW) and single-top production in the s-channel were modelled using the POWHEG-BOXv2 [78–80,83,84] generator at NLO in QCD using the five-flavour scheme and the NNPDF3.0nlo set of PDFs. The diagram removal scheme [85] was used to remove interference and overlap with $t\bar{t}$ production in the case of tW production. The production of $t\bar{t}V$ events was modelled using the MADGRAPH5_AMC@NLO v2.3.3 generator at NLO with the NNPDF3.0nlo PDF set. The events were interfaced to PYTHIA 8.210 using the A14 tune and the

---

[2] ATLAS uses a right-handed coordinate system with its origin at the nominal interaction point (IP) in the centre of the detector and the z-axis along the beam pipe. The x-axis points from the IP to the centre of the LHC ring, and the y-axis points upward. Cylindrical coordinates (r,ϕ) are used in the transverse plane, ϕ being the azimuthal angle around the beam pipe. The pseudorapidity is defined in terms of the polar angle, θ, as $\eta = -\ln\tan(\theta/2)$. Transverse momenta are computed from the three-momenta, $\vec{p}$, as $p_T = |\vec{p}|\sin\theta$.

[3] The h_{damp} parameter is a resummation damping factor and one of the parameters that controls the matching of POWHEG matrix elements to the parton shower and thus effectively regulates the high-p_T radiation against which the $t\bar{t}$ system recoils.

NNPDF2.3lo PDF set. The decays of bottom and charm hadrons were simulated using the EVTGEN v1.2.0 program.

Finally, SM Higgs boson production in association with a vector boson was simulated using POWHEG [78–80,86] and interfaced with PYTHIA 8.186 [87] for parton shower and non-perturbative effects. The POWHEG prediction is accurate to NLO for the Vh boson plus one jet production. The loop-induced $gg \rightarrow Zh$ process was generated separately at LO. The PDF4LHC15 PDF set [88] and the AZNLO tune [89] of PYTHIA 8.186 were used. The simulation prediction was normalised to cross sections calculated at NNLO in QCD with NLO electroweak corrections for $q\bar{q}/qg \rightarrow Vh$ and at NLO and next-to-leading-logarithm accuracy in QCD for $gg \rightarrow Zh$ [90–96].

The effect of multiple interactions in the same and neighbouring bunch crossings (pile-up) was modelled by overlaying the original hard-scattering event with simulated inelastic proton–proton events generated with PYTHIA 8.186 using the NNPDF2.3lo set of PDFs and the A3 tune [97]. The simulated events were weighted to reproduce the distribution of the average number of interactions per bunch crossing ($\langle\mu\rangle$) observed in the data. The $\langle\mu\rangle$ value in the simulation was rescaled by a factor of 1.03 ± 0.07 to improve agreement between data and simulation in the visible inelastic proton–proton cross section [98]. All generated background samples were passed through the GEANT4-based [99] detector simulation [100] of the ATLAS detector. The ATLFAST-II simulation [100] was used for the signal samples to allow for the generation of many different A and H boson masses. The simulated events were reconstructed in the same way as the data.

4 Object reconstruction

Selected events are required to contain at least one vertex having at least two associated tracks with $p_T > 500$ MeV, and the primary vertex is chosen to be the vertex reconstructed with the largest Σp_T^2 of its associated tracks.

Electrons are reconstructed from energy clusters in the electromagnetic calorimeter that are matched to tracks in the inner detector [101]. Electrons are required to have $|\eta| < 2.47$ and $p_T > 7$ GeV. The associated track must have $|d_0|/\sigma_{d_0} < 5$ and $|z_0|\sin\theta < 0.5$ mm, where d_0 (z_0) is the transverse (longitudinal) impact parameter relative to the primary vertex and σ_{d_0} is the error in d_0. To distinguish electrons from jets, isolation and quality requirements are applied. The quality requirements refer to both the inner detector track and the calorimeter shower shape. The isolation requirements are defined using tracking and calorimeter measurements. Electrons used in this search satisfy the 'Loose' quality and isolation requirements.

Muons are reconstructed by matching tracks reconstructed in the inner detector to tracks or track segments in the muon spectrometer [102]. Muons used for this search must have $|\eta| < 2.5$, $p_T > 7$ GeV, $|d_0|/\sigma_{d_0} < 3$, and $|z_0|\sin\theta < 0.5$ mm. They are also required to satisfy 'Loose' isolation requirements, similar to those used for electrons, as well as 'Loose' quality criteria for tracks in the inner detector and muon spectrometer [103].

Jets are reconstructed from topological clusters in the calorimeter system [104], using the anti-k_t algorithm [105, 106] with radius parameter $R = 0.4$. Candidate jets are required to have $p_T > 20$ GeV ($p_T > 30$ GeV) for $|\eta| < 2.5$ ($2.5 < |\eta| < 4.5$) [107]. Low-p_T jets from pile-up are rejected by a multivariate algorithm that uses properties of the reconstructed tracks in the event for jets with $p_T < 60$ GeV and $|\eta| < 2.4$ [108].

Jets containing b-hadrons are identified using a multivariate tagging algorithm (b-tagging) [109,110], which makes use of track impact parameters and reconstructed secondary vertices. The b-tagging algorithm output is used to define a criterion to select jets originating from b-quark hadronisation for jets with $|\eta| < 2.5$. The jets that are selected in this way are referred to as b-jets in the following. The criterion in use has an average efficiency of 70% for jets from b-quarks in simulated $t\bar{t}$ events, with rejection factors of 8.9, 36 and 300 for jets initiated by c-quarks, hadronically decaying τ-leptons and light-flavour quarks or gluons, respectively [110].

Electrons, muons and jets are reconstructed and identified independently. When those objects are spatially close, these algorithms can lead to ambiguous identifications. An overlap removal procedure [111] is therefore applied to remove ambiguities.

The missing transverse momentum, whose magnitude is denoted by E_T^{miss}, is computed as the negative vectorial sum of the transverse momenta of calibrated leptons and jets, plus an additional soft term constructed from all tracks that originate from the primary vertex but are not associated with any identified lepton or jet [112,113].

5 Event selection and background estimation

The final states for the $A \rightarrow ZH \rightarrow \ell\ell\, bb/WW$ decays feature a pair of oppositely charged, same-flavour leptons and either two b-jets or four mostly light-flavour jets from the W bosons decays. Three resonances can be formed by combining the selected objects: (i) the Z boson ($\ell\ell$), (ii) the H boson (bb or $WW \rightarrow 4j$), and (iii) the A boson (ZH system).

Events are required to contain exactly two muons or two electrons. The two muons must have opposite electric charges. This requirement is not applied to electrons, since they have a non-negligible charge misidentification rate due
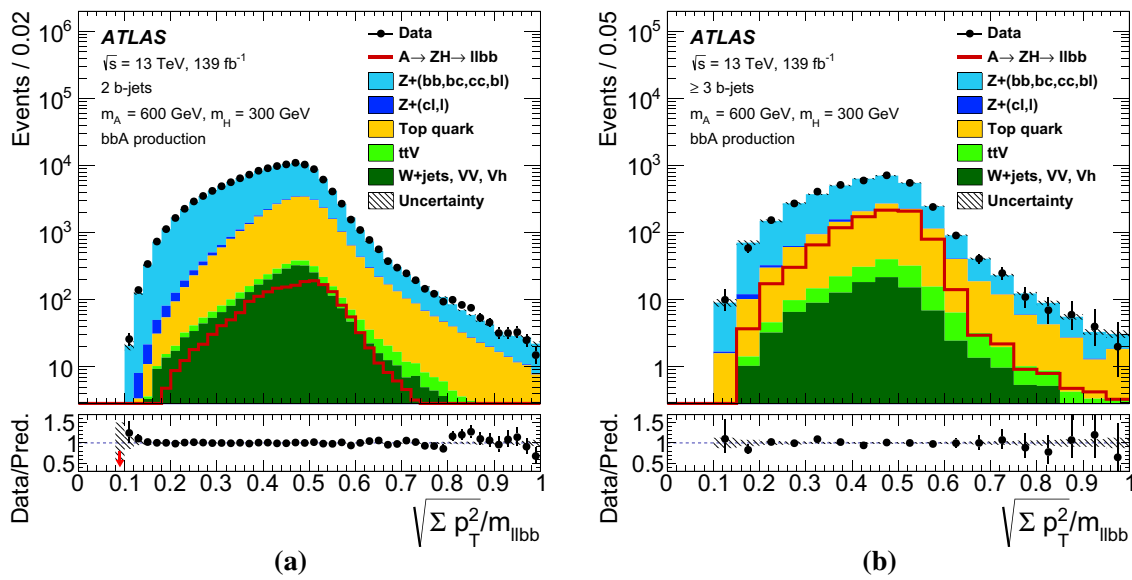
Fig. 2 The $\sqrt{\Sigma p_{\mathrm{T}}^2}/m_{\ell\ell bb}$ distributions shown before the requirement on this variable is applied for events with **a** exactly two b-jets and **b** three or more b-jets. Corrections from a fit to the data are applied to the simulation, as described in Sects. 5.1 and 8. The signal distribution for $(m_A, m_H) = (600, 300)$ GeV is also shown, and is normalised such that the production cross section times the branching ratios $B(A \rightarrow ZH)$ and $B(H \rightarrow bb)$ corresponds to 1 pb. The signal shown includes only A bosons produced in association with b-quarks. The lower panel shows the ratio of the data to the background prediction (black filled circles) and the relative uncertainty, which includes both statistical and systematic components, in the background prediction (hatched area). The notations ttV, VV and Vh refer to top-pair production in association with a vector boson, diboson production and SM Higgs boson production in association with a vector boson, respectively. The production of a Z boson in association with jets is split based on jet flavour. The notation Z+(bb,bc,cc,bl) refers to the case where the jets originate from heavy flavour, which includes at least one jet originating from a b-quark or two jets originating from c-quarks, whereas the notation Z+(cl,l) includes all the remaining cases

to conversions of bremsstrahlung photons. The highest-p_{T} lepton must satisfy $p_{\mathrm{T}} > 27$ GeV in the $\ell\ell bb$ final state, to ensure full efficiency of the single-lepton triggers. This requirement is raised to $p_{\mathrm{T}} > 30$ GeV for the $\ell\ell WW$ final state. The invariant mass of the lepton pair, $m_{\ell\ell}$, must be in the range of 80–100 GeV to be compatible with the mass of the Z boson.

Further event selection criteria are channel-specific, and are described separately in the following sections.

5.1 The $\ell\ell bb$ final state

The events that are used for the $A \rightarrow ZH \rightarrow \ell\ell bb$ search are required to have at least two b-jets, with at least one of them having $p_{\mathrm{T}} > 45$ GeV. The two highest-p_{T} b-jets of the event form the $H \rightarrow bb$ system candidate. The A boson candidate is formed by these two b-jets and, in addition, the two leptons that are matched to the Z boson.

The requirement of a same-flavour lepton pair along with several b-jets implies that the signal region is contaminated by Z boson production in association with jets and backgrounds including top quarks, like $t\bar{t}$ production. The presence of neutrinos in semileptonic top-pair production provides a handle to reduce this background by requiring

$E_{\mathrm{T}}^{\mathrm{miss}}/\sqrt{H_{\mathrm{T}}} < 3.5\,\mathrm{GeV}^{1/2}$, where H_{T} is the scalar sum of the p_{T} of all jets and leptons in the event. The Z+jets background is reduced by requiring $\sqrt{\Sigma p_{\mathrm{T}}^2}/m_{\ell\ell bb} > 0.4$, where $m_{\ell\ell bb}$ is the four-body invariant mass of the two-lepton, two-b-jet system assigned to the A boson candidate and the summation is performed over the p_{T}^2 of these objects. This discriminating variable is chosen because the signal distributions are similar across the two production mechanisms and the m_A and m_H range used in the search. The requirement is optimised separately for each signal hypothesis and, subsequently, an average value is chosen. The distribution of the $\sqrt{\Sigma p_{\mathrm{T}}^2}/m_{\ell\ell bb}$ variable is shown in Fig. 2 separately for the cases where exactly two b-jets and three or more b-jets are present in the event. The distribution is shown before the $\sqrt{\Sigma p_{\mathrm{T}}^2}/m_{\ell\ell bb} > 0.4$ requirement is applied.

The two signal production mechanisms, gluon–gluon fusion and b-associated production, differ mainly in the number of heavy-flavour jets that are produced in association with the A boson. This motivates a categorisation based on the number of b-jets present in the event. In particular, two categories are defined: the $n_b = 2$ category, which contains events with exactly two b-jets, and the $n_b \geq 3$ category, which contains events with three or more b-jets. For gluon–

Table 1 Summary of the event selection for signal and control regions in the $A \to ZH \to \ell\ell bb$ channel

	$n_b = 2$ category Exactly 2 b-tagged jets	$n_b \geq 3$ category At least 3 b-tagged jets
Single-electron or single-muon trigger Exactly 2 leptons (e or μ) ($p_T > 7$ GeV) with the leading one having $p_T > 27$ GeV Opposite electric charge for $\mu\mu$ pairs; $\,$ 80 GeV $< m_{\ell\ell, \, e\mu} < 100$ GeV, $\ell = e, \, \mu$ At least 2 b-jets ($p_T > 20$ GeV) with one of them having $p_T > 45$ GeV $E_T^{\mathrm{miss}}/\sqrt{H_T} < 3.5$ GeV$^{1/2}$, $\sqrt{\Sigma p_T^2}/m_{\ell\ell bb} > 0.4$		
Signal region	ee or $\mu\mu$ pair $0.85 \cdot m_H - 20$ GeV $< m_{bb} < m_H + 20$ GeV	ee or $\mu\mu$ pair $0.85 \cdot m_H - 25$ GeV $< m_{bb} < m_H + 50$ GeV
Z+jets control region	ee or $\mu\mu$ pair $m_{bb} < 0.85 \cdot m_H - 20$ GeV or $m_{bb} > m_H + 20$ GeV	ee or $\mu\mu$ pair $m_{bb} < 0.85 \cdot m_H - 25$ GeV or $m_{bb} > m_H + 50$ GeV
Top control region	$e\mu$ pair $0.85 \cdot m_H - 20$ GeV $< m_{bb} < m_H + 20$ GeV	$e\mu$ pair $0.85 \cdot m_H - 25$ GeV $< m_{bb} < m_H + 50$ GeV

gluon fusion production, more than 95% of the events passing the above selection fall into the $n_b = 2$ category. For b-associated production, only 25–35% of the selected events fall into the $n_b \geq 3$ category, and the others enter the $n_b = 2$ category. This is because of the relatively soft p_T spectrum of the associated b-jets and the geometric acceptance of the tracker.

Finally, the invariant mass m_{bb} of the b-jets that are assigned to the H boson must be compatible with the assumed H boson mass. This is ensured by requiring m_{bb} to be within optimised boundaries that depend on the assumed m_H: $0.85 \cdot m_H - 20$ GeV $< m_{bb} < m_H + 20$ GeV for the $n_b = 2$ category, and $0.85 \cdot m_H - 25$ GeV $< m_{bb} < m_H + 50$ GeV for the $n_b \geq 3$ category. The wider window for $n_b \geq 3$ is motivated by a slightly poorer resolution due to potential b-jet misassignments. The b-jets that are matched to the H boson are the highest-p_T b-jets in the event and, hence, in the case of b-associated production, where more b-jets are present, may not be the ones that actually come from the $H \to bb$ decay. In b-associated production, the fraction of A bosons for which the correct b-jets are chosen is in the range 50–90% for the $n_b \geq 3$ category and is at least 65% for the $n_b = 2$ category.

The signal efficiency in the $n_b = 2$ category after the m_{bb} window requirement is 5.1–11% (2.5–6.6%) for gluon–gluon fusion (b-associated) production, depending on the m_A and m_H values. Similarly, the efficiency in the $n_b \geq 3$ category after the m_{bb} window requirement is 1.3–3.2% for b-associated production. The quoted numbers refer to the efficiencies for A bosons decaying into ZH, with $Z \to ee/\mu\mu/\tau\tau$ and $H \to bb$, to pass the event selection for each of the categories. The inclusion of $Z \to \tau\tau$ in this definition lowers the quoted signal efficiency because these decays have a very small efficiency to pass in this selection

(which aims at $Z \to ee/\mu\mu$). The signal region selection is summarised in Table 1.

The $m_{\ell\ell bb}$ distribution after the m_{bb} requirement is the final discriminating variable, which is fitted to obtain the result of the search in this channel. To improve the $m_{\ell\ell bb}$ resolution, the bb system's four-momentum components are scaled to match the assumed H boson mass and the $\ell\ell$ system's four-momentum components are scaled to match the Z boson mass. This procedure, performed after the event selection, improves the $m_{\ell\ell bb}$ resolution by a factor of two without significantly distorting the background distributions, resulting in an A boson mass resolution that is at best about 1% and up to 4% for gluon–gluon fusion, up to 10% for b-associated production in the $n_b = 2$ category and up to 16% for b-associated production in the $n_b \geq 3$ category, depending on the m_A and m_H values.

Despite the dedicated selection criteria against Z+jets and top-quark production, these background processes dominate the signal region: the Z+jets contribution is ∼60–70% depending on the n_b category, while the top-quark contribution is ∼30–35%. In the $n_b \geq 3$ category, other processes ($t\bar{t}V$, dibosons, Vh) contribute up to ∼5% of the total background, while their contribution to the $n_b = 2$ category is less than 1%. The accurate determination of Z+jets and top-quark contributions is paramount for the sensitivity of this search. Their estimation employs a combination of data-driven corrections to simulated events.

The most abundant background in this channel is from Z+jets production. The normalisation of this process is constrained by a control region defined by inverting the m_{bb} window criterion for each H boson mass hypothesis (see also Table 1). The control regions are distinct for the $n_b = 2$ and $n_b \geq 3$ categories, since the accuracy of the background simulation depends on the number of b-jets present in the event. The modelling of the Z+jets simulated events is exam-
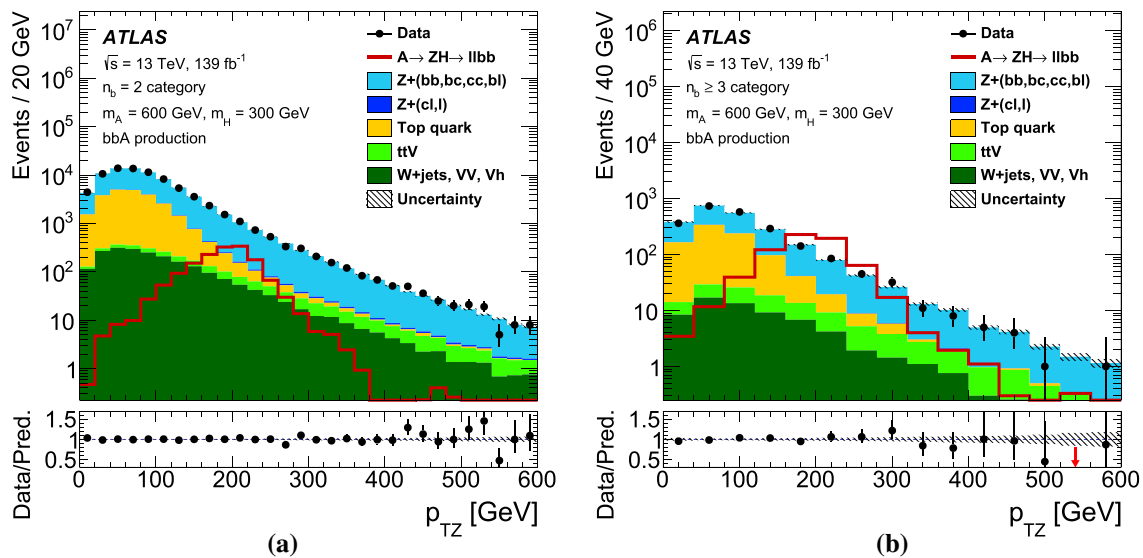
Fig. 3 The p_{TZ} distributions for **a** the $n_b = 2$ and **b** the $n_b \geq 3$ category. The events are required to satisfy all the signal region criteria with the exception of the m_{bb} window requirement. The same conventions as in Fig. 2 are used

ined extensively in a number of kinematic variables, including the p_T of the Z boson (p_{TZ}), the m_{bb} distribution and the $\sqrt{\Sigma p_T^2}/m_{\ell\ell bb}$ distribution. The simulated distributions of these variables are compared against data in a control region that requires two jets with exactly one of them being a b-jet, as well as an early selection stage, before the m_{bb} window and $\sqrt{\Sigma p_T^2}/m_{\ell\ell bb}$ requirements. For this early selection stage, it was verified that even those signals that were already excluded in Ref. [39] would be washed out by the background and would not bias the results. These regions are not used in the likelihood fit described in Sect. 8 and thus they are not included in Table 1. As a result of these studies, corrections to the distributions of p_{TZ}, m_{bb} and $\sqrt{\Sigma p_T^2}/m_{\ell\ell bb}$ in the simulated Z+jets events are applied. The corrections are found to be uncorrelated and they are applied sequentially. The most significant effect on the sensitivity of this search (see also Sect. 7) is due to the corrections to the modelling of the p_{TZ} distribution, which range from +5 to −10% for most of the Z+jets events. As an example, Fig. 3 compares the p_{TZ} distributions in data with the background model after all corrections used in this search for events that satisfy all the requirements of the signal region with the exception of the m_{bb} window requirement, separately for $n_b = 2$ and $n_b \geq 3$ categories.

Top-quark production is heavily dominated by $t\bar{t}$ production in which both top quarks decay semileptonically. Therefore, it is possible to define a pure top-quark control region by keeping the same selection as discussed previously, apart from an opposite-flavour lepton criterion, i.e. an $e\mu$ pair is required instead of an ee or $\mu\mu$ pair (see also Table 1). This region is used for top-pair production normalisation, and also

to check that kinematic distributions such as the top-quark p_T spectrum are adequately modelled in simulation. Different control regions are used in the $n_b = 2$ and $n_b \geq 3$ categories. This is because in the $n_b \geq 3$ category the top-quark background is dominated by top-quark pair production in association with jets, which is more difficult to model than the inclusive top-quark pair production that dominates the top-quark background in the $n_b = 2$ category. Finally, the m_{bb} window requirement is also applied to the top-quark control region, resulting in a separate control region for each m_H hypothesis tested in the search. Good agreement within uncertainties is observed between data and simulation in the shape of all variables considered.

Backgrounds from diboson, 'single-top-quark', and SM Higgs boson production, as well as $t\bar{t}$ production in association with a vector boson are minor contributions to the total background composition. The shapes of their distributions are taken from simulation, whereas they are normalised using precise inclusive cross sections calculated from theory. The diboson samples are normalised using NNLO cross sections [114–117]. Single-top-quark production and top-quark-pair production in association with vector bosons are normalised to NLO cross sections from Refs. [118–120] and Ref. [58], respectively. The normalisation of SM Higgs boson production in association with a vector boson follows the recommendations of Ref. [63] using NNLO QCD and NLO electroweak corrections.

5.2 The $\ell\ell WW$ final state

The decay $A \to ZH \to \ell\ell WW$ features a pair of electrons or muons and four jets from the hadronic W boson decays.
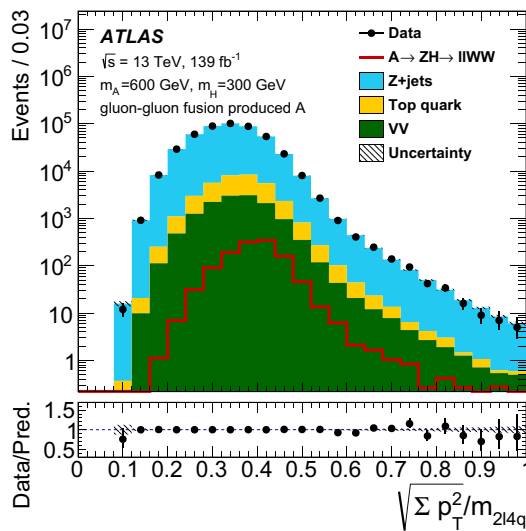
Fig. 4 The $\sqrt{\Sigma p_\mathrm{T}^2}/m_{2\ell 4q}$ distribution shown before the requirement on this variable is applied. Corrections from a fit to the data are applied to the simulation, as described in Sects. 5.2 and 8. The notation VV in the legend corresponds to the production of diboson events. The signal distribution for $(m_A, m_H) = (600, 300)$ GeV is also shown, and is normalised such that the production cross section times the branching ratios $B(A \to ZH)$ and $B(H \to WW)$ corresponds to 1 pb. The lower panel shows the ratio of the data to the background prediction (black filled circles) and the relative uncertainty, which includes both statistical and systematic components, in the background prediction (dashed area)

The selected events are required to have at least four jets with the highest- and second-highest-p_T jets satisfying $p_\mathrm{T} > 40$ GeV and $p_\mathrm{T} > 30$ GeV, respectively. In addition, the lowest-p_T electrons or muons are required to have $p_\mathrm{T} > 15$ GeV.

The selection of the correct jet pairs in the reconstruction of the two W boson candidates is important for improving the signal resolution and suppressing backgrounds. For this task, all possible jet pairs that can be formed by considering up to the five highest-p_T jets in the event are taken into account. A set of requirements on kinematic variables, such as the angular distances between the jets within a pair, the jet transverse momenta and the reconstructed masses of the W, H and A boson candidates, is optimised to test the various combinations for compatibility with the signal hypothesis so that the signal efficiency and background rejection are maximised. This procedure results in a signal efficiency that ranges from 50 to 70% depending on m_A and m_H, whereas for background processes the efficiency is about 40%. The fraction of events in which the correct jet pairs are assigned to the W boson candidates after this procedure is in the range from 50 to 70%, depending on the m_A and m_H values.

The main background in this channel is from the production of a Z boson in association with jets. A criterion similar to that in the $\ell\ell bb$ channel is employed to discriminate

against it: $\sqrt{\Sigma p_\mathrm{T}^2}/m_{2\ell 4q} > 0.3$, where $m_{2\ell 4q}$ is the six-body invariant mass of the two-lepton, four-jet system assigned to the A boson and the summation is performed over the p_T^2 of these objects. This discriminating variable is chosen for the same reasons as in the $\ell\ell bb$ channel and it is optimised following the same considerations. The distribution of this variable before the requirement is applied is shown in Fig. 4.

Finally, the invariant mass of the four selected jets, m_{4q}, must be compatible with the assumed H boson mass. This is ensured by requiring m_{4q} to be within optimised boundaries that depend on m_H: $m_H - 53$ GeV $< m_{4q} < 0.97 \cdot m_H + 54$ GeV. After this requirement the signal efficiency for A bosons decaying into ZH with $Z \to ee/\mu\mu/\tau\tau$ and $H \to WW \to qqqq$ is 6.5–11%, depending on the m_A and m_H values. The signal region selection is summarised in Table 2.

The $m_{2\ell 4q}$ distribution after the m_{4q} requirement is the final discriminating variable, which is fitted to obtain the results of the search in this channel. To improve the $m_{2\ell 4q}$ resolution, the four-jet system's four-momentum components are scaled to match the assumed H boson mass and the $\ell\ell$ system's four-momentum components are scaled to match the Z boson mass. The final A boson mass resolution is in the range from 1% to 17% of m_A, depending on the m_A and m_H values.

The dominant backgrounds after the event selection are from Z+jets ($\sim$90% of total background), top-quark ($\sim$5%), and diboson ($\sim$5%) production. Smaller backgrounds (W+jets, $t\bar{t}h$, $t\bar{t}V$ and Vh) contribute less than 1% to the total background and are not included in the background composition.

The shape of the Z+jets background is taken from simulation combined with data-driven corrections, and the normalisation is constrained by the control region outside the m_{4q} mass window of each signal region (see Table 2), using a procedure similar to that in the $\ell\ell bb$ channel. To address shape differences between distributions of kinematic variables in data and simulated backgrounds, two corrections are applied to the p_T of the Z boson candidates and to the leading jet's p_T. Those corrections are derived from a control region orthogonal to the signal region, obtained by selecting $\sqrt{\Sigma p_\mathrm{T}^2}/m_{2\ell 4q} < 0.3$. This region is not used subsequently in the likelihood fit described in Sect. 8 and therefore it is not included in Table 2. The corrections are found to be uncorrelated and they are applied sequentially. The correction to the p_{TZ} distribution in the simulation is as large as 20% at low p_{TZ} values and it becomes smaller as p_{TZ} increases, whereas the correction to the leading jet's p_T does not exceed ± 10%. The distributions of the p_T of the Z boson candidates and of the leading jet's p_T, after the reweighting, are shown in Fig. 5 for events satisfying all requirements for the signal region with the exception of the m_{4q} window cut.

Table 2 Summary of the event selection for signal and control regions in the $A \to ZH \to \ell\ell WW$ channel

	Single-electron or single-muon trigger
	Exactly 2 leptons (e or μ) ($p_T > 15$ GeV) with the leading one having $p_T > 30$ GeV
	Opposite electric charge for $\mu\mu$ pairs; 80 GeV $< m_{\ell\ell, e\mu} <$ 100 GeV, $\ell = e, \mu$
	At least 4 jets ($p_T > 20$ GeV) with leading and second leading jets having $p_T > 40$, 30 GeV
	Jets chosen with a dedicated discriminant
	$\sqrt{\Sigma p_T^2}/m_{2\ell 4q} > 0.3$
Signal region	ee or $\mu\mu$ pair
	$m_H - 53$ GeV $< m_{4q} < 0.97 \cdot m_H + 54$ GeV
Z+jets control region	ee or $\mu\mu$ pair
	$m_{4q} < m_H - 53$ GeV
	or $m_{4q} > 0.97 \cdot m_H + 54$ GeV
Top control region	$e\mu$ pair
	$m_H - 53$ GeV $< m_{4q} < 0.97 \cdot m_H + 54$ GeV
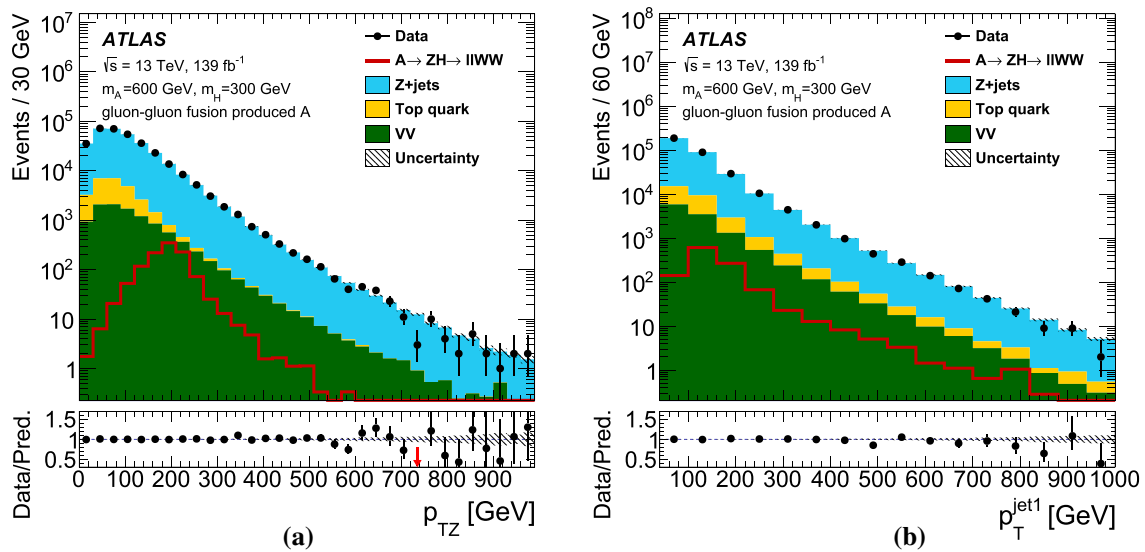
Fig. 5 The distributions of **a** the p_T of the Z boson candidates and **b** the leading jet's p_T in the $\ell\ell WW$ channel. The events are required to satisfy all the signal region criteria with the exception of the m_{4q} window requirement. Data-driven corrections are applied, as described in the text. The same conventions as in Fig. 4 are used

The top-quark background shape is taken from simulated events. The normalisation is constrained using a high-purity control region defined by keeping the same selection as for the signal region, but replacing the electron or muon pairs by opposite-flavour leptons ($e\mu$ pairs), as indicated in Table 2. The single-top-quark, Z+jets and diboson production contributions in this control region are estimated from simulation. The diboson background shape and normalisation are taken from the simulated samples, using the same cross-section calculation as in the $\ell\ell bb$ channel.

6 Signal modelling

This analysis searches for two new particles, with their mass hypotheses considered in the two-dimensional space m_A–m_H, with good mass resolution of the A and H reconstructed

final states. The investigation of the relevant phase space requires a large number of signal mass hypotheses to be tested. In addition, various new physics scenarios which are of interest for this search, like the 2HDM, include A bosons with natural widths comparable to, or larger than, the experimental mass resolution for large parts of the parameter space in which this search has sensitivity. The H bosons are considered to always have negligible natural width, in accordance with the 2HDM scenarios used to interpret this search (see Sect. 8). For these reasons, the $m_{\ell\ell bb}$ and $m_{2\ell 4q}$ distributions can be simulated only for some (m_A, m_H) points and an interpolation using analytic functions is employed for the rest, following a procedure similar to that used in Ref. [39].

In the cases where the natural widths of both the A and H bosons are much smaller than the experimental mass resolution, the modelling of the mass distributions uses two
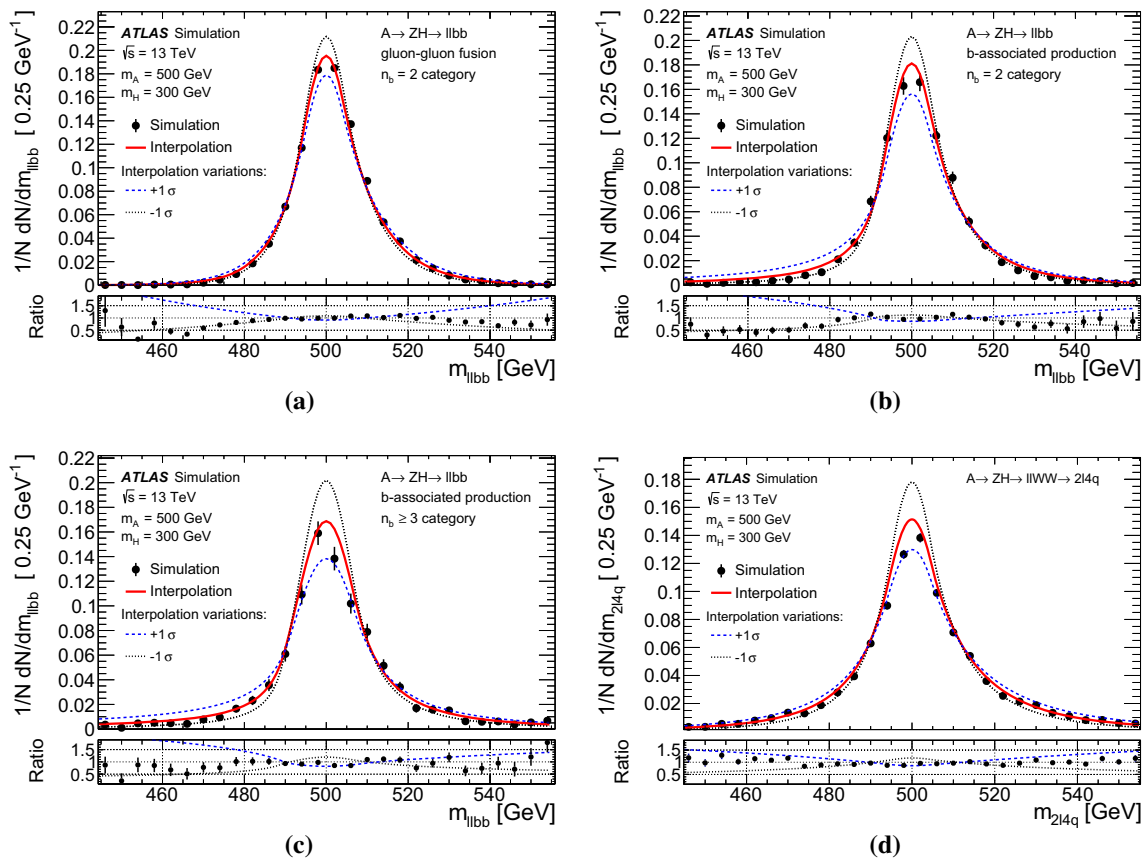
Fig. 6 Signal $m_{\ell\ell bb}$ or $m_{2\ell 4q}$ distributions assuming $m_A = 500$ GeV and $m_H = 300$ GeV for the following cases: $\ell\ell bb$ channel: **a** gluon–gluon fusion in the $n_b = 2$ category, **b** b-associated production in the $n_b = 2$ category, and **c** b-associated production in the $n_b \geq 3$ category; **d** $\ell\ell WW$ channel. In the upper panels, the black filled circles correspond to the simulated distributions, which are compared against the interpolated parameterised signal distributions shown as solid red curves. Also in the same panels, the shape variations of the interpolated parameterised signal distributions are shown in dotted blue $(+1\sigma)$ and black (-1σ) lines. In the lower panels, the black filled circles correspond to the ratio of the simulation to the interpolated parameterised curve. The dotted blue (black) line corresponds to the ratio of the $+1\sigma$ (-1σ) shape variation of the interpolated curve to the interpolated curve

types of parametric functions. First, an *ExpGaussExp* (EGE) function [39,121] provides a good description of gluon–gluon fusion production of A bosons in the $n_b = 2$ category of the $\ell\ell bb$ channel. Second, a double-Gaussian Crystal Ball (DSCB) function [39,122] gives a good description of gluon–gluon fusion production in the $\ell\ell WW$ channel and b-associated production in both the $n_b = 2$ and $n_b \geq 3$ categories of the $\ell\ell bb$ channel.

Both the EGE and DSCB functions have a Gaussian core but they differ in the way the tails are treated. The tails of the EGE function are exponential, described by two parameters, whereas DSCB has power-law tails described by four extra parameters. The values of the function parameters are extracted from unbinned maximum-likelihood fits to the simulated $m_{\ell\ell bb}$ and $m_{2\ell 4q}$ distributions. Polynomial functions are used to interpolate the parameters to mass points that were not simulated. These interpolated parametric functions are used to model the signal mass shapes for all the signal assumptions considered in this search. The fit uncertainties

of the DSCB and EGE function parameters, as well as the parameters of the polynomial functions used for the interpolation, are used to derive a shape uncertainty for each of the interpolated distributions.

A typical example of the result of the signal parameterisation is shown in Fig. 6 for the $(m_A, m_H) = (500, 300)$ GeV mass point. The figure shows a comparison of the simulated mass distribution and the interpolated parametric function, as well as the shape variation that is taken as an estimate of the systematic uncertainty from the procedure. In general, the cores of the $m_{\ell\ell bb}$ and $m_{2\ell 4q}$ distributions are well-parameterised by the chosen functional forms. There are some small differences between the function description and the simulated distribution in the tails of the distributions, but those have negligible effects on the final results and they are covered by interpolation uncertainties.

The parameterisation procedure described in the previous paragraph is modified to allow for cases where the width of the A boson is comparable to, or larger than, the experimen-

tal mass resolution. This can be modelled by convolving a modified Breit–Wigner distribution[4] with the EGE or DSCB function. This procedure is valid as long as the width of the H boson remains narrow relative to the experimental resolution, which is the case for the 2HDM scenarios considered in Sect. 8. Widths of up to approximately 20% of the A boson mass are considered, which is the range relevant to the sensitive parameter space of the 2HDM scenarios that are of interest for this search.

Finally, the signal efficiencies for the interpolated mass points are obtained through separate two-dimensional interpolations on the (m_A, m_H) plane using thin-plate splines [123].

7 Systematic uncertainties

Several sources of systematic uncertainty in the signal and background estimates are considered, including experimental and theoretical sources. Experimental uncertainties comprise those in the luminosity measurement [124] (obtained using the LUCID-2 detector [53]), trigger, object identification, energy/momentum scale and resolution as well as underlying-event and pile-up modelling [98,102,103,107]. These uncertainties impact the simulations of signal and background processes.

The signal and background modelling have associated theoretical uncertainties. For the signal modelling, the uncertainties due to the factorisation and renormalisation scale choice, the initial- and final-state radiation treatment and the PDF choice are considered. No additional signal modelling uncertainties related to model-specific cross-section predictions, such as the 2HDM predictions used in Sect. 8, are considered. The renormalisation and factorisation scales are varied up and down separately by a factor of two, and the largest deviation from the nominal signal is taken as the estimated uncertainty. The uncertainties due to initial- and final-state radiation as well as the multiple parton interaction modelling are estimated using a subset of A14 tuning variations [60]. PDF uncertainties are computed using the prescription from PDF4LHC15 [88], which include the envelope of three PDF sets, namely CT14, MMHT2014 and NNPDF3.0.

Additional systematic uncertainties are assigned to cover the differences in signal efficiencies and $m_{\ell\ell bb}$ and $m_{\ell\ell WW}$ resolution differences between the interpolations and the simulations, as shown by the dotted blue and black lines in the lower panels of Fig. 6.

For the background modelling, the most important sources of systematic uncertainty are the modelling of shapes of several kinematic distributions of Z+jets events. In the $\ell\ell bb$ channel, they arise from the shape corrections for the p_{TZ},

$\sqrt{\Sigma p_T^2}/m_{\ell\ell bb}$ and m_{bb} variables described in Sect. 5.1. An uncertainty is estimated by comparing the corrections and the agreement between the background prediction and the data for various variables and among various control regions. For each of the corrections, the applied uncertainty is half the size of the correction in the $n_b = 2$ category, and the full size of the correction in the $n_b \geq 3$ category. In the $\ell\ell WW$ channel, the uncertainties are due to the shapes of the p_{TZ} and leading-jet p_T distributions (Sect. 5.2). The uncertainty is estimated similarly to that in the $\ell\ell bb$ channel and is half the size of the correction. For other background processes, modelling uncertainties are obtained by varying the factorisation and renormalisation scales, and the amount of initial- and final-state radiation.

The effect of these systematic uncertainties on the search is studied using a signal-strength parameter μ for hypothesised signal production (see also Sect. 8). The uncertainties found to have the largest impact depend on the choice of (m_A, m_H) signal point. Table 3 shows the relative uncertainties in the μ value from the leading sources of systematic uncertainty for two example mass points of gluon–gluon fusion and b-associated production for the $\ell\ell bb$ channel. The uncertainties are evaluated using an Asimov dataset [125] generated with the signal cross section set to the expected limits for the particular (m_A, m_H) signal point, considering a narrow-width A boson. Table 4 shows the same information for the $\ell\ell WW$ channel. The leading sources of systematic uncertainty are similar for other mass points studied and for larger A boson widths.

For the $\ell\ell bb$ channel, the most relevant sources of systematic uncertainty are the background modelling, the signal interpolation, and the jet energy scale and resolution. The limited size of the simulated samples has a higher impact at low masses, since at higher masses other sources are more dominant. Other systematic uncertainties with non-negligible impact include those associated with b-tagging and theoretical errors. In the $\ell\ell WW$ channel, the most relevant systematic uncertainties are those related to the jet energy scale and resolution, as expected in a channel with four jets in the final state. The limited size of the simulated samples, the background modelling and the signal interpolation also have a non-negligible impact on the signal-strength parameter. In both channels, the data statistical uncertainties have lower impact at low masses compared to the systematic uncertainties. In addition, the search sensitivity is affected at high masses by the limited size of the data sample, an effect which is more pronounced in the $\ell\ell bb$ channel.

8 Results

The $m_{\ell\ell bb}$ and $m_{2\ell 4q}$ distributions are expected to exhibit a resonant structure if signal events are present, while

---

[4] The modification is the multiplication of the Breit–Wigner distribution with a log-normal distribution to account for the distortion due to the event selection.

Table 3 The effect of the most important sources of uncertainty on the signal-strength parameter at two example mass points of $(m_A, m_H) = (230, 130)$ GeV and $(m_A, m_H) = (700, 200)$ GeV in the $\ell\ell bb$ channel, for both gluon–gluon fusion and b-associated production of a narrow-width A boson. The signal cross sections are taken to be the expected median upper limits (see Sect. 8) and they correspond to values that are shown next to the indicated mass points. JES and JER stand for jet energy scale and jet energy resolution, 'Sim. stat.' for simulation statistics, 'Sig. interp.' for signal interpolation, and 'Bkg. model.' for the background modelling. 'Theory' refers to theoretical uncertainties in the signal samples due to the PDF choice, factorisation and renormalisation scales, and initial- and final-state radiation

$A \rightarrow ZH \rightarrow \ell\ell bb$

| Gluon–gluon fusion production | | | | b-associated production | | | |
| (230, 130) GeV, 0.31 pb | | (700, 200) GeV, 0.017 pb | | (230, 130) GeV, 0.16 pb | | (700, 200) GeV, 0.018 pb | |
Source	$\Delta\mu/\mu$ [%]	Source	$\Delta\mu/\mu$ [%]	Source	$\Delta\mu/\mu$ [%]	Source	$\Delta\mu/\mu$ [%]
Data stat.	28	Data stat.	45	Data stat.	33	Data stat.	46
Total syst.	36	Total syst.	26	Total syst.	33	Total syst.	25
Sim. stat.	19	Sim. stat.	7.2	Sim. stat.	18	Sim. stat.	7.2
Sig. interp.	9.9	Sig. interp.	8.7	Sig. interp.	13	Sig. interp	13
Bkg. model.	19	Bkg. model.	18	Bkg. model.	15	Bkg. model.	16
JES/JER	20	JES/JER	18	JES/JER	14	JES/JER	16
b-tagging	7.5	b-tagging	12	b-tagging	9.5	b-tagging	12
Theory	7.4	Theory	9.5	Theory	5.0	Theory	7.1

Table 4 The effect of the most important sources of uncertainty on the signal-strength parameter at two example mass points of $(m_A, m_H) = (500, 300)$ GeV and $(m_A, m_H) = (700, 200)$ GeV in the $\ell\ell WW$ channel for gluon–gluon fusion production of a narrow-width A boson. The same notation as in Table 3 is used

$A \rightarrow ZH \rightarrow \ell\ell WW$

| Gluon–gluon fusion production | | | |
| (500, 300) GeV, 0.70 pb | | (700, 200) GeV, 0.38 pb | |
Source	$\Delta\mu/\mu$ [%]	Source	$\Delta\mu/\mu$ [%]
Data stat.	32	Data stat.	33
Total syst.	42	Total stat.	38
Sim. stat.	24	Sim. stat.	19
Sig. interp.	14	Sig. interp.	12
Bkg. model.	14	Bkg. model.	16
JES/JER	30	JES/JER	23
Theory	6.5	Theory	7.6

background events result in a smoothly falling spectrum. Therefore, those are chosen as the final variables to discriminate between signal and background. The shape differences between the signal and background contributions in the $m_{\ell\ell bb}$ and $m_{2\ell 4q}$ distributions are exploited through binned maximum-likelihood fits of the signal-plus-background hypotheses to extract potential signal contributions. The fits are based on the statistical framework described in Refs. [125–127]. For a given mass hypothesis of (m_A, m_H), the likelihood is constructed as the product of Poisson probabilities for event yields in the $m_{\ell\ell bb}$ or $m_{2\ell 4q}$ bins:

$$L(\mu, \vec{\alpha}, \vec{\theta} | m_A, m_H)$$
$$= \prod_{i=\text{bins}} \text{Poisson}\left(N_i \middle| \left(\mu \times S_i(m_A, m_H, \vec{\theta}) + B_i(\vec{\alpha}, \vec{\theta})\right)\right) \cdot G(\vec{\theta}),$$

where N_i is the number of observed events, and $S_i(m_A, m_H, \vec{\theta})$ and $B_i(\vec{\alpha}, \vec{\theta})$ are the expected number of signal events and estimated number of background events in bin i. The vector $\vec{\alpha}$ represents free background normalisation scale factors (described later) and the vector $\vec{\theta}$ denotes all non-explicitly listed parameters of the likelihood function such as nuisance parameters associated with systematic uncertainties. Systematic uncertainties are incorporated in the likelihood as nuisance parameters with either Gaussian or log-normal constraint terms, denoted by $G(\vec{\theta})$ in the formula above. The parameter of interest, μ, is a multiplicative factor applied to the expected signal rate. The $m_{\ell\ell bb}$ and $m_{2\ell 4q}$ bin widths are chosen according to the expected detector resolution and taking into account the statistical uncertainty in the number of simulated background events. The bin centres are adjusted such that at least 65% of the test signal is contained in one bin.

For each bin, S_i is calculated from the total integrated luminosity, the assumed cross section times branching ratio for the signal and its selection efficiency. The sum of all background contributions in the bin, B_i, is estimated from simulation, which includes the modelling corrections discussed in Sects. 5.1 and 5.2. The number of events in the $t\bar{t}$ and Z+jets control regions is included in the likelihood calculation to constrain their normalisation in the signal regions. This is achieved by introducing two free normalisation scale factors per channel, represented by $\vec{\alpha}$ in the likelihood description earlier in this section. In the $\ell\ell bb$ channel these scale factors apply to the $t\bar{t}$ contribution and the heavy-flavour component of the Z+jets contribution, whereas the rest of the contributions in the control region are estimated from simulation. In the $\ell\ell WW$ channel the scale factors apply to the $t\bar{t}$ contri-

(a)

(b)
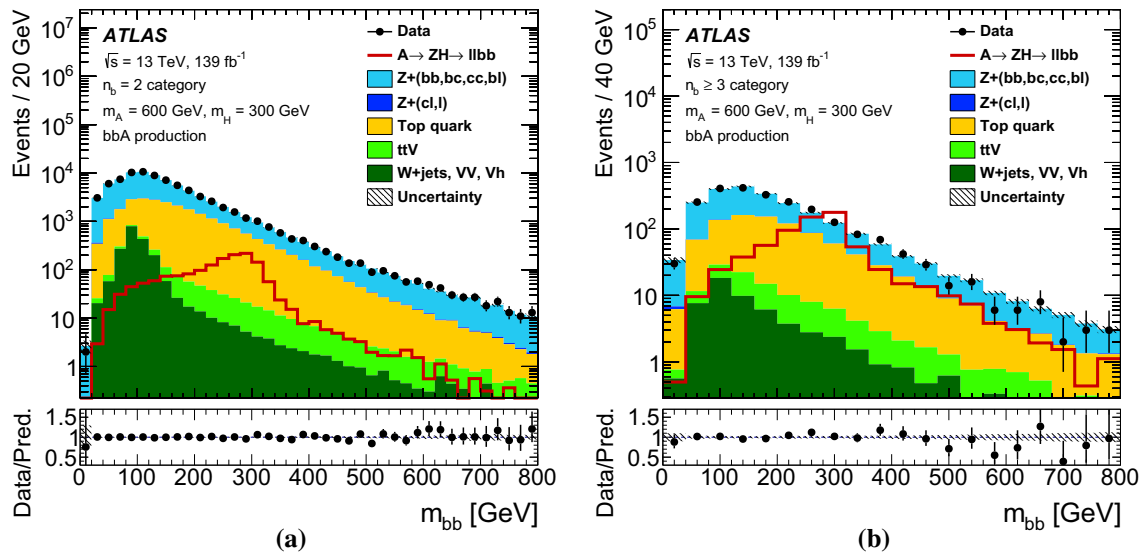
Fig. 7 The m_{bb} distribution before any m_{bb} window cuts for the **a** $n_b = 2$ and **b** $n_b \geq 3$ categories. The signal distribution for $(m_A, m_H) = (600, 300)$ GeV is also shown, and is normalised such that the

production cross section times the branching ratios $B(A \rightarrow ZH)$ and $B(H \rightarrow bb)$ corresponds to 1 pb. The same conventions as in Fig. 2 are used

bution and the flavour-inclusive Z+jets contribution. Typical values of the scale factors are close to unity with the exception of Z+jets in the $\ell\ell bb$ channel, which is scaled by a factor of 1.2, and $t\bar{t}$ in the $\ell\ell bb$ $n_b \geq 3$ category, which is typically scaled by a factor of 1.4.

The signals that are fitted in each category are motivated by signal efficiency considerations and the interpretation of the search in the context of the 2HDM. In the $\ell\ell bb$ channel the following fits are performed. First, A bosons produced by gluon–gluon fusion are considered in the $n_b = 2$ category. Second, a combined fit for the b-associated production mechanism in both the $n_b = 2$ and $n_b \geq 3$ categories is performed. Finally, there is a combination of the b-associated production fit with the gluon–gluon fusion fit, which is interpreted in the context of the 2HDM. In the $\ell\ell WW$ channel, only A bosons produced by gluon–gluon fusion are considered and, hence, it is the only fit that is considered.

8.1 $A \rightarrow ZH \rightarrow \ell\ell bb$ results

The $m_{\ell\ell bb}$ distributions from different m_{bb} mass windows are scanned for potential excesses beyond the background expectations through signal-plus-background fits. The scan is performed in steps of 10 GeV for both the m_A range 230–800 GeV and the m_H range 130–700 GeV, such that $m_A - m_H \geq 100$ GeV. The step sizes are chosen to be compatible with the detector resolution for $m_{\ell\ell bb}$ and m_{bb}. In total, there are 58 m_{bb} windows that are probed for the $n_b = 2$ and $n_b \geq 3$ categories. The overall number of (m_A, m_H) signal hypotheses that are tested is 1711 per category.

Figure 7 shows the distribution of the H boson candidate mass m_{bb} before the m_{bb} window requirement in each

of the two categories. Typical examples of $m_{\ell\ell bb}$ distributions after the application of the m_{bb} window requirement are shown in Fig. 8a–d. In particular, the m_{bb} window defined for $m_H = 300$ GeV is shown in Fig. 8a, b for the $n_b = 2$ and $n_b \geq 3$ categories, respectively. On the same figures, a signal distribution is shown as well, which corresponds to gluon–gluon fusion production in Fig. 8a and b-associated production in Fig. 8b, for the $(m_A, m_H) = (600, 300)$ GeV signal point. Similarly, an m_{bb} window defined for $m_H = 500$ GeV is shown Fig. 8c, d for the $n_b = 2$ and $n_b \geq 3$ categories, respectively. The signal distribution for the $(m_A, m_H) = (670, 500)$ GeV signal point is also shown for gluon–gluon fusion production in Fig. 8c and b-associated production in Fig. 8d.

In all cases, the data are found to be well described by the background model. The most significant excess for the gluon–gluon fusion production signal assumption is at the $(m_A, m_H) = (610, 290)$ GeV signal point, for which the local (global) significance [128] is 3.1 (1.3) standard deviations. For b-associated production, the most significant excess is at the $(m_A, m_H) = (440, 220)$ GeV signal point, for which the local (global) significance is 3.1 (1.3) standard deviations. The significances are calculated for each production process separately, ignoring the contribution from the other.

In the absence of any statistically significant excess, the results of the search in this channel are interpreted as upper limits on the production cross section of an A boson decaying into ZH followed by the $H \rightarrow bb$ decay, $\sigma \times B(A \rightarrow ZH) \times B(H \rightarrow bb)$. The cross-section upper limits consider A bosons that are produced only by a single mechanism, i.e. either gluon–gluon fusion or b-associated produc-
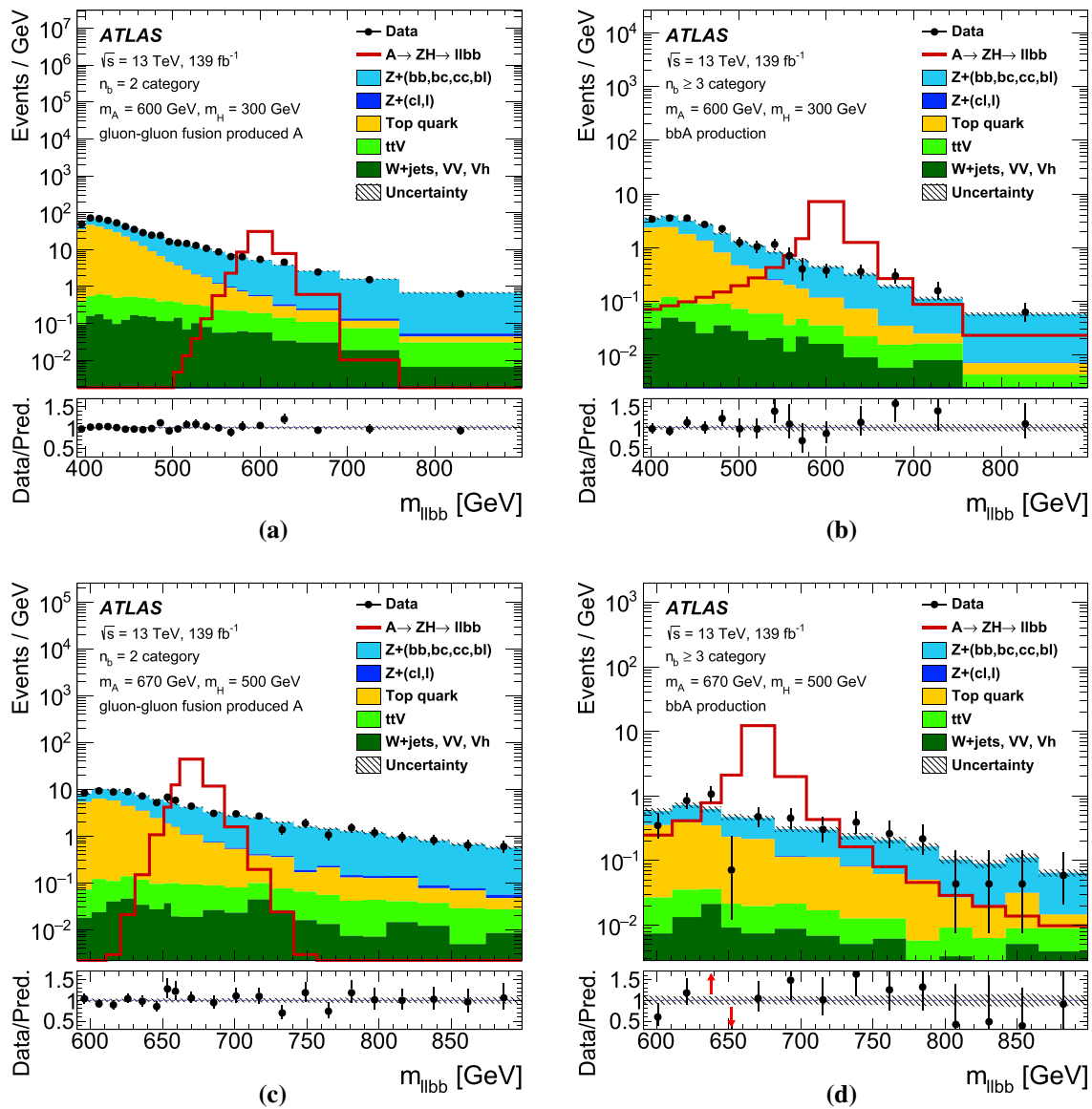
Fig. 8 The $m_{\ell\ell bb}$ mass distribution for the m_{bb} windows defined for $m_H = 300$ GeV and $m_H = 500$ GeV for **a**, **c** the $n_b = 2$ and **b**, **d** the $n_b \geq 3$ category, respectively. Signal distributions with $(m_A, m_H) = (600, 300)$ GeV and $(m_A, m_H) = (670, 500)$ GeV are also shown for gluon–gluon fusion production in (**a**, **c**) and b-associated production in **b**, **d**. The number of entries shown in each bin is the number of events in that bin divided by the width of the bin. The same conventions as in Fig. 2 are used

tion. Modified frequentist [129] 95% confidence level (CL) upper limits on the production cross section of this process are obtained using the asymptotic approximation [125] for the various signal hypotheses that are tested. In particular, expected and observed upper limits for gluon–gluon fusion production of narrow-width A bosons in the $n_b = 2$ category are shown in Fig. 9a, b, respectively. For b-associated production of narrow-width A bosons, the expected and observed limits for the combination of the $n_b = 2$ and $n_b \geq 3$ categories are shown in Fig. 9c, d, respectively. The upper limits for gluon–gluon fusion vary from 6.2 fb for $(m_A, m_H) = (780, 129)$ GeV to 380 fb for $(m_A, m_H) = (250, 150)$ GeV. This is to be compared with the correspond-

ing expected limits of 15 fb and 240 fb for these two signal hypotheses. For b-associated production the upper limit varies from 6.8 fb for $(m_A, m_H) = (760, 220)$ GeV to 210 fb for $(m_A, m_H) = (230, 130)$ GeV, whereas the corresponding expected limits are 15 fb and 160 fb.

Upper limits are also calculated for signal assumptions where the natural width of the A boson is large in comparison with the experimental mass resolution, which is needed for the interpretation of the search in the context of the 2HDM. The cross-section upper limit decreases as the natural width of the A boson increases. In particular, a gluon–gluon produced A boson with a natural width of 10% of its mass has a cross-section upper limit that is reduced on average
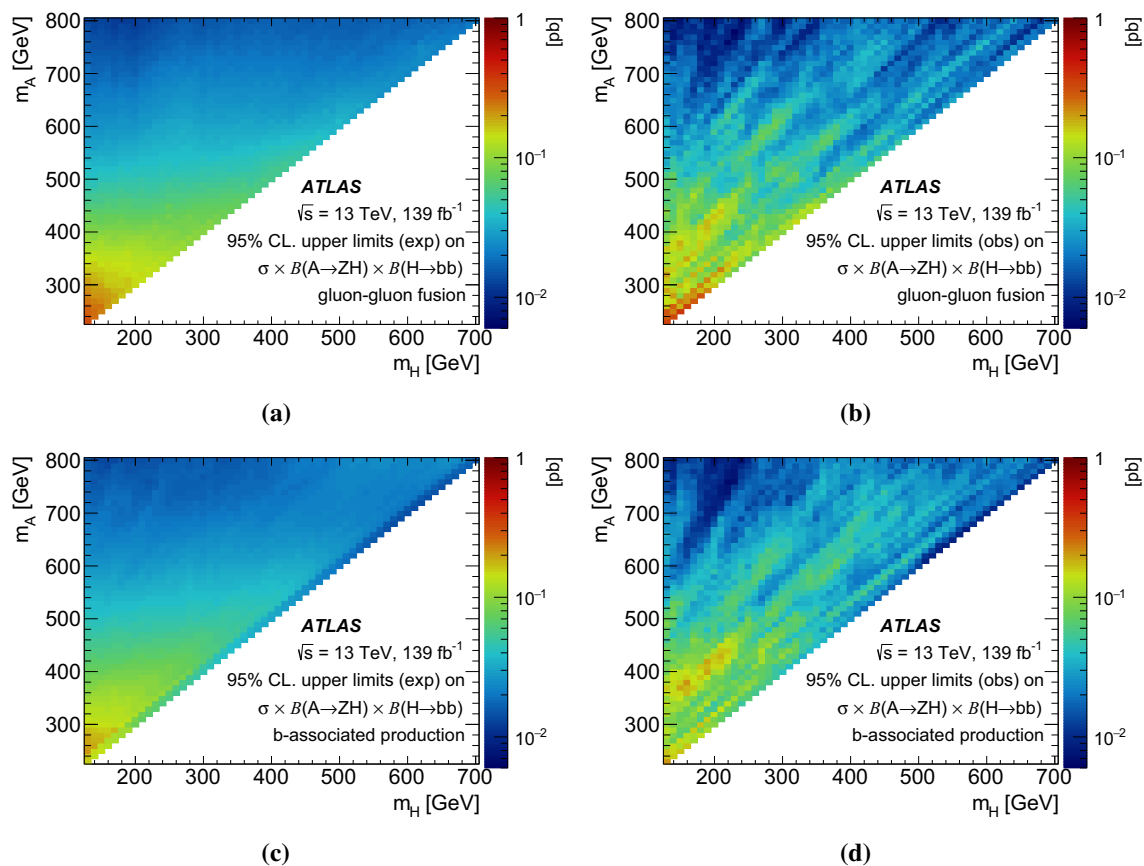
Fig. 9 Upper bounds at 95% CL on the production cross section times the branching ratio $B(A \rightarrow ZH) \times B(H \rightarrow bb)$ in pb for **a**, **b** gluon–gluon fusion and **c**, **d** b-associated production. The expected upper limits are shown in (**a**) and (**c**) and the observed upper limits are shown in **b** and **d**

by a factor of approximately 3 from the narrow-width case. This factor becomes approximately 4 when the natural width increases to 20%. The A bosons from b-associated production have worse experimental mass resolution and the deterioration of the limit is on average smaller: the upper limits are reduced by a factor of about 1.9 (2.3) for a natural width of 10% (20%).

The results for A boson natural widths that are comparable to, or larger than, the experimental mass resolution are used for the interpretation of the search in the context of the CP-conserving 2HDM. The 2HDM benchmark against which the search results are compared has three free parameters: m_A, m_H and $\tan \beta$. In addition, there are four ways to assign the Yukawa couplings to fermions, defining type-I, type-II, lepton-specific and flipped 2HDMs. The remaining parameters are fixed. The mass of the lightest Higgs boson in the model is fixed to 125 GeV and its couplings are set to be the same as those of the SM Higgs boson by choosing $\cos(\beta - \alpha) = 0$ [19], which is known as the 2HDM weak decoupling limit. The charged Higgs boson is assumed to have the same mass as the A boson and the potential parameter m_{12}^2 [18] is fixed to $m_A^2 \tan \beta / (1 + \tan^2 \beta)$.

The cross sections for A boson production in the 2HDM are calculated using corrections at up to NNLO in QCD for gluon–gluon fusion and b-associated production in the five-flavour scheme as implemented in SusHi [130–133]. For b-associated production a cross section in the four-flavour scheme is also calculated as described in Refs. [134,135] and the results are combined with the five-flavour scheme calculation following Ref. [136]. The Higgs boson widths and branching ratios are calculated using 2HDMC [137]. The procedure for the calculation of the cross sections and branching ratios, as well as for the choice of 2HDM parameters, follows Ref. [63].

The interpretation of the search in the 2HDM is performed in the (m_H, m_A) plane, as shown in Fig. 10. In this plot, colour-shaded areas indicate expected and observed exclusions for various $\tan \beta$ values. There is one plot for each of the four 2HDM types. For the type-I and lepton-specific 2HDMs, only gluon–gluon fusion production is relevant. The exclusion region reaches $m_H \lesssim 350$ GeV for $\tan \beta = 1$ and the sensitivity decreases for larger $\tan \beta$ values. In type-I 2HDM for instance, for $\tan \beta = 10$ the exclusion reaches $m_H \lesssim 320$ GeV and $m_A \lesssim 500$ GeV. The limiting value at $m_H \simeq 350$ GeV is due to the drop of the $H \rightarrow bb$ branching ratio, which competes with $H \rightarrow t\bar{t}$ at larger m_H values. The type-II and flipped 2HDMs are dominated by A bosons from b-associated production as $\tan \beta$ increases, although
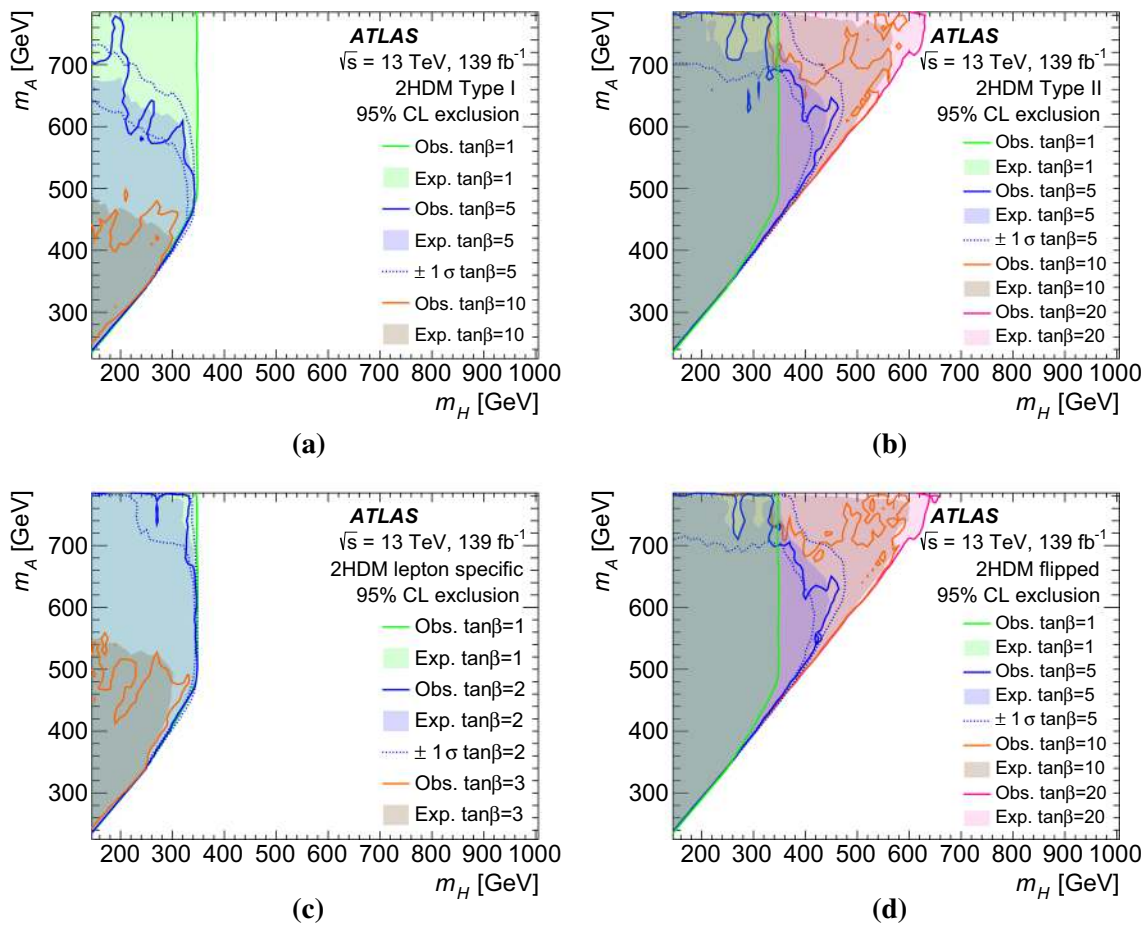
Fig. 10 Observed and expected 95% CL exclusion regions for the $\ell\ell bb$ channel in the (m_H, m_A) plane for various $\tan\beta$ values for the **a** type-I, **b** type-II, **c** lepton-specific and **d** flipped 2HDM, with $\cos(\beta - \alpha) = 0$

gluon–gluon fusion is still important for $\tan\beta \approx 1$. Like the type-I and lepton-specific 2HDMs, the type-II and flipped 2HDMs provide similar constraints because they only differ in the lepton Yukawa couplings. The contribution from b-associated signal production increases the sensitivity at large $\tan\beta$ values, excluding $m_H \lesssim 650$ GeV for $\tan\beta = 20$. The search sensitivity deteriorates at lower $\tan\beta$ values, excluding $m_H \lesssim 350$ GeV for $\tan\beta = 1$.

8.2 $A \rightarrow ZH \rightarrow \ell\ell WW$ results

The $m_{2\ell 4q}$ distributions from different m_{4q} mass windows are scanned for possible excesses using a procedure similar to the one in the $\ell\ell bb$ channel. The scan is performed in steps of 10 GeV for both the m_A range 300–800 GeV and the m_H range 200–700 GeV, such that $m_A - m_H \geq 100$ GeV. This gives in total 51 m_{4q} mass windows and the overall number of (m_A, m_H) signal hypotheses that are tested is 1326.

Figure 11 shows the distribution of the H boson candidate mass m_{4q} before the m_{4q} window requirement. Typical examples of $m_{2\ell 4q}$ distributions after the application
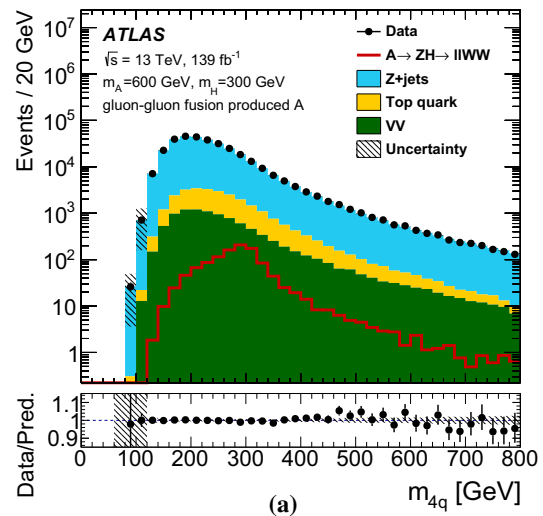
Fig. 11 The m_{4q} distribution before any m_{4q} window cuts. The same conventions as in Fig. 4 are used

of the m_{4q} window requirement are shown in Fig. 12a, b, referring to m_{4q} windows defined for $m_H = 300$ GeV and $m_H = 500$ GeV, respectively. Signal distributions corre-

(a)

(b)
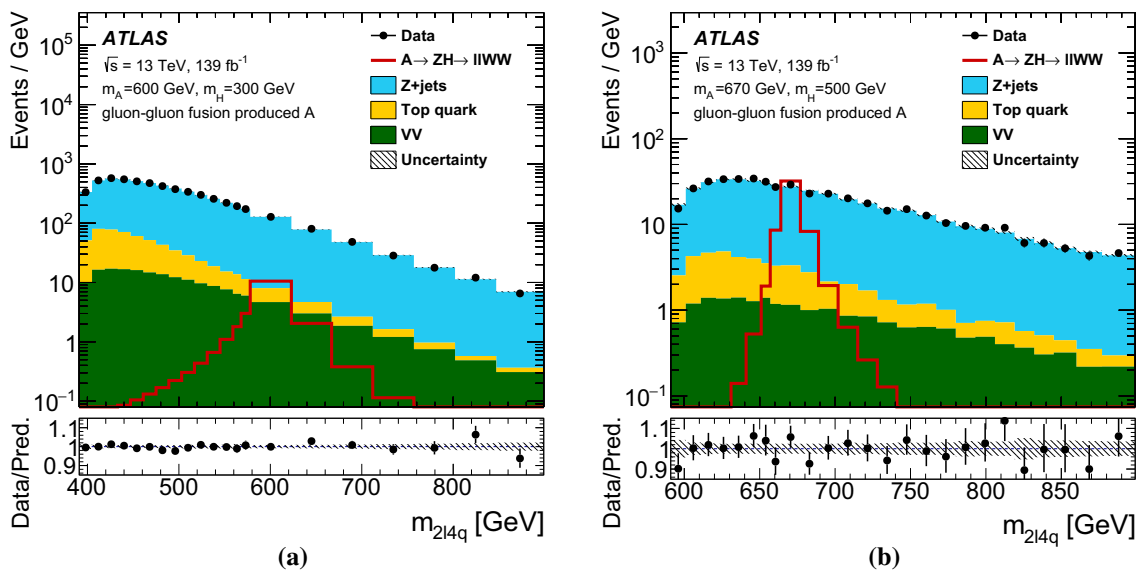
Fig. 12 The $m_{2\ell 4q}$ mass distribution for the m_{4q} windows defined for **a** $m_H = 300$ GeV and **b** $m_H = 500$ GeV. Signal distributions are also shown with $(m_A, m_H) = (600, 300)$ GeV and $(m_A, m_H) =$ (670, 500) GeV. The number of entries shown in each bin is the number of events in that bin divided by the width of the bin. The same conventions as in Fig. 4 are used

(a)

(b)
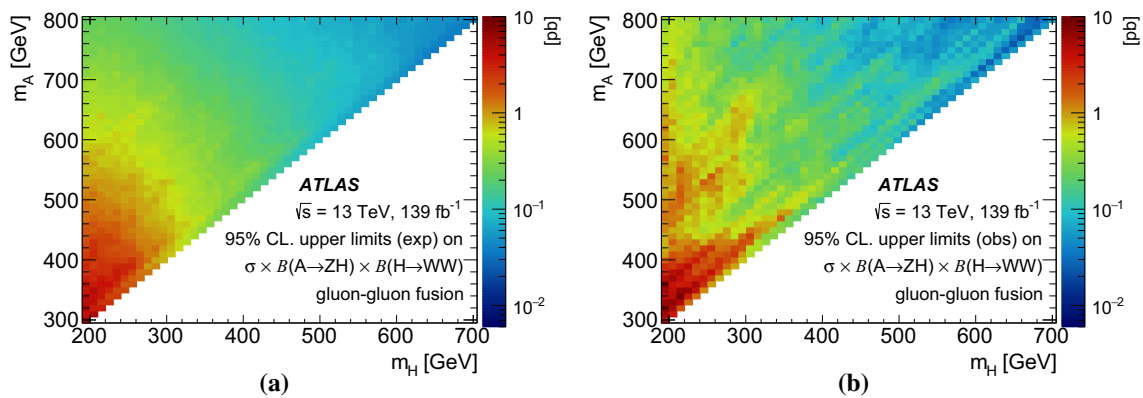
Fig. 13 Expected (**a**) and observed (**b**) upper bounds at 95% CL on the production cross section times the branching ratio $B(A \to ZH) \times B(H \to WW)$ in pb

sponding to the $(m_A, m_H) = (600, 300)$ GeV signal point for Fig. 12a and the $(m_A, m_H) = (670, 500)$ GeV signal point for Fig. 12b are also shown.

In all cases, the data are found to be well described by the background model. The most significant excess is at the $(m_A, m_H) = (440, 310)$ GeV signal point, for which the local (global) significance is 2.9 (0.82) standard deviations.

Using the same method as for the $\ell\ell bb$ channel, constraints on the production of $A \to ZH$ followed by $H \to WW$ decay are derived. The 95% CL upper limits are shown in Fig. 13 for a narrow-width A boson produced via gluon–gluon fusion. The upper limit varies from 0.023 pb for the $(m_A, m_H) = (770, 660)$ GeV signal point to 8.9 pb for the $(m_A, m_H) = (340, 220)$ GeV signal point. This is to be compared with the corresponding expected limits of 0.041 pb and 3.6 pb for these two signal points. The upper limits determine

orate when the natural width of the A boson is comparable to, or larger than, the experimental mass resolution. In particular, for a natural width that is 10% of m_A the upper limits decrease on average by a factor of 3. This factor becomes approximately 5 when the natural width increases to 20%.

The sensitivity of the $\ell\ell WW$ channel in the context of the CP-conserving 2HDM was examined. The same 2HDM calculations as in the $\ell\ell bb$ channel are used and the only differences are related to the parameter space of the model that is probed. In particular, because only A bosons produced by gluon–gluon fusion are studied in this search, only type-I and lepton-specific 2HDMs are considered. In addition, the partial width $\Gamma(H \to WW)$ vanishes when $\cos(\beta - \alpha) = 0$ and is maximal at $|\cos(\beta - \alpha)| = 1$, whereas for the partial width $\Gamma(A \to ZH)$ the opposite is true, i.e. it vanishes when $|\cos(\beta - \alpha)| = 1$ and it is maximal when $\cos(\beta - \alpha) = 0$.
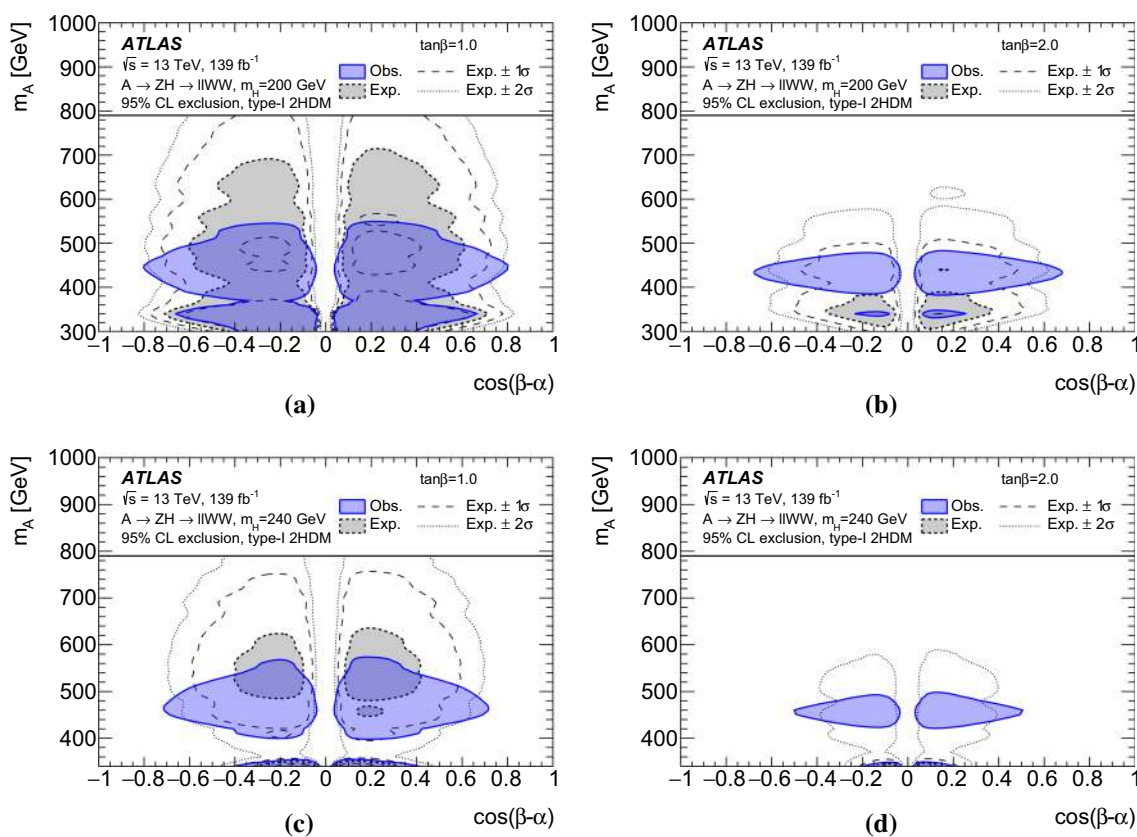
Fig. 14 Observed and expected 95% CL exclusion regions in the $(\cos(\beta - \alpha), m_A)$ plane for various $\tan \beta$ values for **a**, **b** $m_H = 200$ GeV and **c**, **d** $m_H = 240$ GeV in the context of type-I 2HDM for the $\ell\ell WW$ channel

These observations imply that this channel should be most sensitive between these two extreme values of $|\cos(\beta - \alpha)|$.

The interpretation of the observed and expected upper limits on the cross section times branching ratio in the context of the type-I and lepton-specific 2HDM scenarios show that the $\ell\ell WW$ channel has little sensitivity in regions that are not already excluded by the 125 GeV Higgs boson coupling measurements [3], an analysis that also provides similar limits in this parameter space. In particular, for the m_A range considered in this channel, there is sensitivity up to $m_H < 250$ GeV and for $\tan \beta < 4$. Some examples of 95% CL excluded regions in the plane defined by m_A and $\cos(\beta - \alpha)$ for $m_H = 200$ GeV and $m_H = 240$ GeV are shown in Fig. 14 for the type-I 2HDM. The results are very similar for the lepton-specific 2HDM, since the only difference between the two 2HDM types is the lepton Yukawa couplings, which only affect the total width.

9 Conclusion

Data recorded by the ATLAS experiment at the LHC, corresponding to an integrated luminosity of 139 fb^{-1} from proton–proton collisions at a centre-of-mass energy 13 TeV,

are used to search for a heavy Higgs boson, A, decaying into ZH, where H denotes another heavy Higgs boson with mass $m_H > 125$ GeV. Two final states were considered, where the H boson decays into a pair of b-quarks or W bosons, and in both cases the Z boson decays into a pair of electrons or muons. In the $\ell\ell bb$ channel, the A boson is assumed to be produced via either gluon–gluon fusion or b-associated production. In the $\ell\ell WW$ channel, only gluon–gluon fusion production is considered. No significant deviation from the SM background predictions is observed in the $ZH \rightarrow \ell\ell bb$ and $ZH \rightarrow \ell\ell WW \rightarrow \ell\ell qqqq$ final states that are considered in this search. Considering each channel and each production process separately, upper limits are set at the 95% confidence level for $\sigma \times B(A \rightarrow ZH) \times B(H \rightarrow bb$ or $H \rightarrow WW)$. For $\ell\ell bb$, upper limits are set in the range 6.2–380 fb for gluon–gluon fusion and 6.8–210 fb for b-associated production of a narrow A boson in the mass range 230–800 GeV, assuming the H boson is in the mass range 130–700 GeV. For $\ell\ell WW$, the observed upper limits are in the range 0.023–8.9 pb for gluon–gluon fusion production of a narrow A boson in the mass range 300–800 GeV, assuming the H boson is in the mass range 200–700 GeV. Taking into account both production processes, the $\ell\ell bb$ search tightens the constraints on the 2HDM scenario in the case of large mass splittings between

its heavier neutral Higgs bosons. The $\ell\ell WW$ channel has not been explored previously at the LHC, and this search explicitly demonstrates its potential to constrain 2HDM parameters away from the weak decoupling limit.

Data Availability Statement This manuscript has no associated data or the data will not be deposited. [Authors' comment: "All ATLAS scientific output is published in journals, and preliminary results are made available in Conference Notes. All are openly available, without restriction on use by external parties beyond copyright law and the standard conditions agreed by CERN. Data associated with journal publications are also made available: tables and data from plots (e.g. cross section values, likelihood profiles, selection efficiencies, cross section limits, ...) are stored in appropriate repositories such as HEPDATA (http://hepdata.cedar.ac.uk/). ATLAS also strives to make additional material related to the paper available that allows a reinterpretation of the data in the context of new theoretical models. For example, an extended encapsulation of the analysis is often provided for measurements in the framework of RIVET (http://rivet.hepforge.org/). This information is taken from the ATLAS Data Access Policy, which is a public document that can be downloaded from http://opendata.cern.ch/record/413 [opendata.cern.ch].]

References

1. ATLAS Collaboration, Observation of a new particle in the search for the Standard Model Higgs boson with the ATLAS detector at the LHC. Phys. Lett. B **716**, 1 (2012). arXiv:1207.7214 [hep-ex]
2. CMS Collaboration, Observation of a new boson at a mass of 125 GeV with the CMS experiment at the LHC. Phys. Lett. B **716**, 30 (2012). arXiv:1207.7235 [hep-ex])
3. ATLAS Collaboration, Combined measurements of Higgs boson production and decay using up to 80fb^{-1} of proton-proton collision data at $\sqrt{s} = 13\,TeV$ collected with the ATLAS experiment. Phys. Rev. D **101**, 012002 (2020). arXiv:1909.02845 [hep-ex]
4. ATLAS Collaboration, CP Properties of Higgs boson interactions with top quarks in the $t\bar{t}H$ and tH processes using $H \rightarrow \gamma\gamma$ with the ATLAS detector. Phys. Rev. Lett. **125**, 061802 (2020). arXiv:2004.04545 [hep-ex]
5. ATLAS Collaboration, Test of CP invariance in vector-boson fusion production of the Higgs boson in the $H \rightarrow \tau\tau$ channel in proton-proton collisions at $\sqrt{s} = 13\,TeV$ with the ATLAS detector. Phys. Lett. B **805**, 135426 (2020). arXiv:2002.05315 [hep-ex]
6. ATLAS Collaboration, Study of the spin and parity of the Higgs boson in diboson decays with the ATLAS detector. Eur. Phys. J. C **75**, 476 (2015). arXiv:1506.05669 [hep-ex]. [Erratum: Eur. Phys. J. C **76**, 152 (2016)]
7. CMS Collaboration, Measurement and interpretation of differential cross sections for Higgs boson production at $\sqrt{s} = 13\,TeV$. Phys. Lett. B **792**, 369 (2019). arXiv:1812.06504 [hep-ex]
8. CMS Collaboration, Combined measurements of Higgs boson couplings in proton-proton collisions at $\sqrt{s} = 13\,TeV$. Eur. Phys. J. C **79**, 421 (2019). arXiv:1809.10733 [hep-ex])
9. CMS Collaboration, Measurements of $t\bar{t}$H production and the CP structure of the Yukawa interaction between the Higgs boson and top quark in the diphoton decay channel. Phys. Rev. Lett. **125**, 061801 (2020). arXiv:2003.10866 [hep-ex]
10. ATLAS and CMS Collaborations, Measurements of the Higgs boson production and decay rates and constraints on its couplings from a combined ATLAS and CMS analysis of the LHC pp collision data at $\sqrt{s} = 7\,and\,8\,TeV$. JHEP **08**, 045 (2016). arXiv:1606.02266 [hep-ex]
11. F. Englert, R. Brout, Broken symmetry and the mass of gauge vector mesons. Phys. Rev. Lett. **13**, 321 (1964)
12. P.W. Higgs, Broken symmetries, massless particles and gauge fields. Phys. Lett. **12**, 132 (1964)
13. P.W. Higgs, Broken symmetries and the masses of gauge bosons. Phys. Rev. Lett. **13**, 508 (1964)
14. G.S. Guralnik, C.R. Hagen, T.W.B. Kibble, Global conservation laws and massless particles. Phys. Rev. Lett. **13**, 585 (1964)
15. P.W. Higgs, Spontaneous symmetry breakdown without massless bosons. Phys. Rev. **145**, 1156 (1966)
16. T.W.B. Kibble, Symmetry breaking in non-Abelian gauge theories. Phys. Rev. **155**, 1554 (1967)

17. T.D. Lee, A theory of spontaneous T violation. Phys. Rev. D **8**, 1226 (1973)

18. G. Branco et al., Theory and phenomenology of two-Higgs-doublet models. Phys. Rep. **516**, 1 (2012). arXiv:1106.0034 [hep-ph]

19. J.F. Gunion, H.E. Haber, CP-conserving two-Higgs-doublet model: the approach to the decoupling limit. Phys. Rev. D **67**, 075019 (2003)

20. A. Djouadi, The anatomy of electroweak symmetry breaking Tome II: the Higgs bosons in the minimal supersymmetric model. Phys. Rep. **459**, 1 (2008). arXiv:hep-ph/0503173

21. J. Abdallah et al., Simplified models for dark matter searches at the LHC. Phys. Dark Univ. **9–10**, 8 (2015). arXiv:1506.03116 [hep-ph]

22. J.E. Kim, G. Carosi, Axions and the strong CP problem. Rev. Mod. Phys. **82**, 557 (2010). arXiv:0807.3125 [hep-ph]

23. A.G. Cohen, D.B. Kaplan, A.E. Nelson, Progress in electroweak baryogenesis. Ann. Rev. Nucl. Part. Sci. **43**, 27 (1993). arXiv:hep-ph/9302210

24. S.F. King, Neutrino mass models. Rep. Prog. Phys. **67**, 107 (2004). arXiv:hep-ph/0310204

25. ATLAS Collaboration, Searches for heavy ZZ and ZW resonances in the $\ell\ell qq$ and $vvqq$ final states in pp collisions at $\sqrt{s} = 13\,TeV$ with the ATLAS detector. JHEP **03**, 009 (2018). arXiv:1708.09638 [hep-ex]

26. ATLAS Collaboration, Search for WW/WZ resonance production in ℓvqq final states in pp collisions at $\sqrt{s} = 13\,TeV$ with the ATLAS detector. JHEP **03**, 042 (2018). arXiv:1710.07235 [hep-ex]

27. ATLAS Collaboration, Search for heavy diboson resonances in semileptonic final states in pp collisions at $\sqrt{s} = 13\,TeV$ with the ATLAS detector (2020). arXiv:2004.14636 [hep-ex]. https://doi.org/10.1007/JHEP10(2020)061

28. ATLAS Collaboration, Search for diboson resonances in hadronic final states in 139 fb^{-1} of pp collisions at $\sqrt{s} = 13\,TeV$ with the ATLAS detector. JHEP **09**, 091 (2019). arXiv:1906.08589 [hep-ex]

29. CMS Collaboration, Search for a heavy Higgs boson decaying to a pair of W bosons inproton-proton collisions at $\sqrt{s} = 13\,TeV$. JHEP **03**, 034 (2020). arXiv:1912.01594 [hep-ex]

30. CMS Collaboration, Search for a new scalar resonance decaying to a pair of Z bosons in proton-proton collisions at $\sqrt{s} = 13\,TeV$. JHEP **06**, 127 (2018). arXiv:1804.01939 [hep-ex]

31. ATLAS Collaboration, Combination of searches for Higgs boson pairs in pp collisions at $\sqrt{s} = 13\,TeV$ with the ATLAS detector. Phys. Lett. B **800**, 135103 (2020). arXiv:1906.02025 [hep-ex]

32. CMS Collaboration, Combination of searches for Higgs boson pair production in proton-proton collisions at $\sqrt{s} = 13\,TeV$. Phys. Rev. Lett. **122**, 121803 (2019). arXiv:1811.09689 [hep-ex]

33. ATLAS Collaboration, Search for heavy resonances decaying into a W or Z boson and a Higgs boson in final states with leptons and b-jets in 36 fb^{-1} of $\sqrt{s} = 13\,TeV$ pp collisions with the ATLAS detector. JHEP **03**, 174 (2018). arXiv:1712.06518 [hep-ex]. [Erratum: JHEP **11**, 051 (2018)]

34. CMS Collaboration, Search for a heavy pseudoscalar Higgs boson decaying into a 125 GeV Higgs boson and a Z boson in final states with two tau and two light leptons at $\sqrt{s} = 13\,TeV$. JHEP **03**, 065 (2020). arXiv:1910.11634 [hep-ex])

35. ATLAS Collaboration, Search for heavy Higgs bosons decaying into two tau leptons with the ATLAS detector using pp collisions at $\sqrt{s} = 13\,TeV$. Phys. Rev. Lett. **125**, 051801 (2020). arXiv:2002.12223 [hep-ex]

36. CMS Collaboration, Search for beyond the standard model Higgs bosons decaying into a b$\bar{b}$ pair in pp collisions at $\sqrt{s} = 13\,TeV$. JHEP **08**, 113 (2018). arXiv:1805.12191 [hep-ex]

37. CMS Collaboration, Search for additional neutral MSSM Higgs bosons in the $\tau\tau$ final state in proton-proton collisions at $\sqrt{s} = 13\,TeV$. JHEP **09**, 007 (2018). arXiv:1803.06553 [hep-ex]

38. CMS Collaboration, Search for neutral resonances decaying into a Z boson and a pair of b jets or τ leptons. Phys. Lett. B **759**, 369 (2016). arXiv:1603.02991 [hep-ex]

39. ATLAS Collaboration, Search for a heavy Higgs boson decaying into a Z boson and another heavy Higgs boson in the $\ell\ell bb$ final state in pp collisions at $\sqrt{s} = 13\,TeV$ with the ATLAS detector. Phys. Lett. B **783**, 392 (2018). arXiv:1804.01126 [hep-ex]

40. CMS Collaboration, Search for new neutral Higgs bosons through the $H \rightarrow ZA \rightarrow \ell^+\ell^- b\bar{b}$ process in pp collisions at $\sqrt{s} = 13\,TeV$. JHEP **03**, 055 (2020). arXiv:1911.03781 [hep-ex]

41. G.C. Dorsch, S.J. Huber, K. Mimasu, J.M. No, Echoes of the electroweak phase transition: discovering a second Higgs doublet through $A_0 \rightarrow ZH_0$. Phys. Rev. Lett. **113**, 211802 (2014). arXiv:1405.5537 [hep-ph]

42. N. Turok, J. Zadrozny, Electroweak baryogenesis in the two-doublet model. Nucl. Phys. B **358**, 471 (1991)

43. L. Fromme, S.J. Huber, M. Seniuch, Baryogenesis in the two-Higgs doublet model. JHEP **11**, 038 (2006). arXiv:hep-ph/0605242

44. P. Basler, M. Krause, M. Mühlleitner, J. Wittbrodt, A. Wlotzka, Strong first order electroweak phase transition in the CP-conserving 2HDM revisited. JHEP **02**, 121 (2017). arXiv:1612.04086 [hep-ph]

45. B. Coleppa, F. Kling, S. Su, Exotic decays of a heavy neutral Higgs through HZ/AZ channel. JHEP **09**, 161 (2014). arXiv:1404.1922 [hep-ph]

46. ATLAS Collaboration, The ATLAS Experiment at the CERN Large Hadron Collider. JINST **3**, S08003 (2008)

47. ATLAS Collaboration, ATLAS insertable B-Layer Technical Design Report. CERN-LHCC-2010-013. ATLAS-TDR-19 (2010). https://cds.cern.ch/record/1291633. ATLAS Insertable B-Layer Technical Design Report Addendum. ATLAS-TDR-19-ADD-1 (2012) https://cds.cern.ch/record/1451888

48. B. Abbott et al., Production and integration of the ATLAS insertable B-layer. JINST **13**, T05008 (2018). arXiv:1803.00844 [physics.ins-det]

49. ATLAS Collaboration, Performance of the ATLAS trigger system in 2015. Eur. Phys. J. C **77**, 317 (2017). arXiv:1611.09661 [hep-ex]

50. ATLAS Collaboration, Luminosity determination in pp collisions at $\sqrt{s} = 7\,TeV$ using the ATLAS detector at the LHC. Eur. Phys. J. C **71**, 1630 (2011). arXiv:1101.2185 [hep-ex]

51. ATLAS Collaboration, Improved luminosity determination in pp collisions at $\sqrt{s} = 7\,TeV$ using the ATLAS detector at the LHC. Eur. Phys. J. C **73**, 2518 (2013). arXiv:1302.4393 [hep-ex]

52. ATLAS Collaboration, Luminosity determination in pp collisions at $\sqrt{s} = 8\,TeV$ using the ATLAS detector at the LHC. Eur. Phys. J. C **76**, 653 (2016). arXiv:1608.03953 [hep-ex]

53. G. Avoni et al., The new LUCID-2 detector for luminosity measurement and monitoring in ATLAS. JINST **13**, P07017 (2018)

54. ATLAS Collaboration, ATLAS data quality operations and performance for 2015–2018 data-taking. JINST **15**, P04003 (2020). arXiv:1911.04632 [physics.ins-det]

55. ATLAS Collaboration, Performance of the ATLAS muon triggers in Run 2. JINST **15**, P09015 (2020). arXiv:2004.13447 [hep-ex]

56. ATLAS Collaboration, Performance of electron and photon triggers in ATLAS during LHC Run 2. Eur. Phys. J. C **80**, 47 (2020). arXiv:1909.00761 [hep-ex]

57. J. Alwall, M. Herquet, F. Maltoni, O. Mattelaer, T. Stelzer, MadGraph 5: going beyond. JHEP **06**, 128 (2011). arXiv:1106.0522 [hep-ph]

58. J. Alwall et al., The automated computation of tree-level and next-to-leading order differential cross sections, and their

matching to parton shower simulations. JHEP **07**, 079 (2014). arXiv:1405.0301 [hep-ph]

59. T. Sjöstrand et al., An introduction to PYTHIA 8.2. Comput. Phys. Commun. **191**, 159 (2015). arXiv:1410.3012 [hep-ph]

60. ATLAS Collaboration, ATLAS Pythia 8 tunes to 7 TeV data. ATL-PHYS-PUB-2014-021 (2014). https://cds.cern.ch/record/1966419

61. S. Frixione, B.R. Webber, Matching NLO QCD computations with parton shower simulations: the POWHEG method. JHEP **06**, 029 (2002). arXiv:hep-ph/0204244

62. M. Wiesemann et al., Higgs production in association with bottom quarks. JHEP **02**, 132 (2015). arXiv:1409.5301 [hep-ph]

63. D. de Florian et al., Handbook of LHC Higgs cross sections: 4. Deciphering the nature of the Higgs Sector (2016). arXiv:1610.07922 [hep-ph]

64. R.D. Ball et al., Parton distributions with LHC data. Nucl. Phys. B **867**, 244 (2013). arXiv:1207.1303 [hep-ph]

65. H.-L. Lai et al., New parton distributions for collider physics. Phys. Rev. D **82**, 074024 (2010). arXiv:1007.2241 [hep-ph]

66. E. Bothmann et al., Event generation with Sherpa 2.2. SciPost Phys. **7**, 034 (2019). arXiv:1905.09127 [hep-ph]

67. T. Gleisberg, S. Höche, Comix, a new matrix element generator. JHEP **12**, 039 (2008). arXiv:0808.3674 [hep-ph]

68. F. Cascioli, P. Maierhöfer, S. Pozzorini, Scattering amplitudes with open loops. Phys. Rev. Lett. **108**, 111601 (2012). arXiv:1111.5206 [hep-ph]

69. A. Denner, S. Dittmaier, L. Hofer, Collier: a fortran-based complex one-loop library in extended regularizations. Comput. Phys. Commun. **212**, 220 (2017). arXiv:1604.06792 [hep-ph]

70. S. Schumann, F. Krauss, A parton shower algorithm based on Catani–eymour dipole factorisation. JHEP **03**, 038 (2008). arXiv:0709.1027 [hep-ph]

71. S. Höche, F. Krauss, M. Schönherr, F. Siegert, A critical appraisal of NLO+PS matching methods. JHEP **09**, 049 (2012). arXiv:1111.1220 [hep-ph]

72. S. Höche, F. Krauss, M. Schönherr, F. Siegert, QCD matrix elements + parton showers. The NLO case, JHEP **04**, 027 (2013). arXiv:1207.5030 [hep-ph]

73. S. Catani, F. Krauss, R. Kuhn, B.R. Webber, QCD matrix elements + parton showers. JHEP **11**, 063 (2001). arXiv:hep-ph/0109231

74. S. Höche, F. Krauss, S. Schumann, F. Siegert, QCD matrix elements and truncated showers. JHEP **05**, 053 (2009). arXiv:0903.1219 [hep-ph]

75. R.D. Ball et al., Parton distributions for the LHC Run II. JHEP **04**, 040 (2015). arXiv:1410.8849 [hep-ph]

76. C. Anastasiou, L.J. Dixon, K. Melnikov, F. Petriello, High-precision QCD at hadron colliders: electroweak gauge boson rapidity distributions at next-to-next-to leading order. Phys. Rev. D **69**, 094008 (2004). arXiv:hep-ph/0312266

77. S. Frixione, P. Nason, G. Ridolfi, A positive-weight next-to-leading-order Monte Carlo for heavy flavour hadroproduction. JHEP **09**, 126 (2007). arXiv:0707.3088 [hep-ph]

78. P. Nason, A new method for combining NLO QCD with shower Monte Carlo algorithms. JHEP **11**, 040 (2004). arXiv:hep-ph/0409146

79. S. Frixione, P. Nason, C. Oleari, Matching NLO QCD computations with Parton Shower simulations: the POWHEG method. JHEP **11**, 070 (2007). arXiv:0709.2092 [hep-ph]

80. S. Alioli, P. Nason, C. Oleari, E. Re, A general framework for implementing NLO calculations in shower Monte Carlo programs: the POWHEG BOX. JHEP **06**, 043 (2010). arXiv:1002.2581 [hep-ph]

81. ATLAS Collaboration, Studies on top-quark Monte Carlo modelling for Top2016. ATL-PHYS-PUB-2016-020 (2016). https://cds.cern.ch/record/2216168

82. D.J. Lange, The EvtGen particle decay simulation package. Nucl. Instrum. Methods A **462**, 152 (2001)

83. E. Re, Single-top Wt-channel production matched with parton showers using the POWHEG method. Eur. Phys. J. C **71**, 1547 (2011). arXiv:1009.2450 [hep-ph]

84. S. Alioli, P. Nason, C. Oleari, E. Re, NLO single-top production matched with shower in POWHEG: s- and t-channel contributions. JHEP **09**, 111 (2009). arXiv:0907.4076 [hep-ph] [Erratum: JHEP **02**, 011 (2010)]

85. S. Frixione, E. Laenen, P. Motylinski, B.R. Webber, C.D. White, Single-top hadroproduction in association with a W boson. JHEP **07**, 029 (2008). arXiv:0805.3067 [hep-ph]

86. P. Nason, C. Oleari, NLO Higgs boson production via vector-boson fusion matched with shower in POWHEG. JHEP **02**, 037 (2010). arXiv:0911.5299 [hep-ph]

87. T. Sjöstrand, S. Mrenna, P.Z. Skands, A brief introduction to PYTHIA 8.1. Comput. Phys. Commun. **178**, 852 (2008). arXiv:0710.3820 [hep-ph]

88. J. Butterworth et al., PDF4LHC recommendations for LHC Run II. J. Phys. G **43**, 023001 (2016). arXiv:1510.03865 [hep-ph]

89. ATLAS Collaboration, Measurement of the Z/γ^* boson transverse momentum distribution in pp collisions at $\sqrt{s} = 7\,TeV$ with the ATLAS detector. JHEP **09**, 145 (2014). arXiv:1406.3660 [hep-ex]

90. M.L. Ciccolini, S. Dittmaier, M. Krämer, Electroweak radiative corrections to associated WH and ZH production at hadron colliders. Phys. Rev. D **68**, 073003 (2003). arXiv:hep-ph/0306234

91. O. Brein, A. Djouadi, R. Harlander, NNLO QCD corrections to the Higgs-strahlung processes at hadron colliders. Phys. Lett. B **579**, 149 (2004). arXiv:hep-ph/0307206

92. O. Brein, R. Harlander, M. Wiesemann, T. Zirke, Top-quark mediated effects in hadronic Higgs-Strahlung. Eur. Phys. J. C **72**, 1868 (2012). arXiv:1111.0761 [hep-ph]

93. L. Altenkamp, S. Dittmaier, R.V. Harlander, H. Rzehak, T.J.E. Zirke, Gluon-induced Higgs-strahlung at next-to-leading order QCD. JHEP **02**, 078 (2013). arXiv:1211.5015 [hep-ph]

94. A. Denner, S. Dittmaier, S. Kallweit, A. Mück, HAWK 2.0: a Monte Carlo program for Higgs production in vector-boson fusion and Higgs strahlung at hadron colliders. Comput. Phys. Commun. **195** 161 (2015). arXiv:1412.5390 [hep-ph]

95. O. Brein, R.V. Harlander, T.J.E. Zirke, vh@nnlo—Higgs Strahlung at hadron colliders. Comput. Phys. Commun. **184**, 998 (2013). arXiv:1210.5347 [hep-ph]

96. R.V. Harlander, A. Kulesza, V. Theeuwes, T. Zirke, Soft gluon resummation for gluon-induced Higgs Strahlung. JHEP **11**, 082 (2014). arXiv:1410.0217 [hep-ph]

97. ATLAS Collaboration, The Pythia 8 A3 tune description of ATLAS minimum bias and inelastic measurements incorporating the Donnachie-Landshoff diffractive model. ATL-PHYS-PUB-2016-017 (2016). https://cds.cern.ch/record/2206965

98. ATLAS Collaboration, Measurement of the inelastic proton-proton cross section at $\sqrt{s} = 13\,TeV$ with the ATLAS detector at the LHC. Phys. Rev. Lett. **117**, 182002 (2016). arXiv:1606.02625 [hep-ex]

99. S. Agostinelli et al., GEANT4: a simulation toolkit. Nucl. Instrum. Methods A **506**, 250 (2003)

100. ATLAS Collaboration, The ATLAS simulation infrastructure. Eur. Phys. J. C **70**, 823 (2010). arXiv:1005.4568 [hep-ex]

101. ATLAS Collaboration, Electron and photon performance measurements with the ATLAS detector using the 2015-2017 LHC proton-proton collision data. JINST **14**, P12006 (2019). arXiv:1908.00005 [hep-ex]

102. ATLAS Collaboration, Muon reconstruction performance of the ATLAS detector in proton-proton collision data at $\sqrt{s} = 13\,TeV$. Eur. Phys. J. C **76**, 292 (2016). arXiv:1603.05598 [hep-ex]

103. ATLAS Collaboration, Muon reconstruction and identification efficiency in ATLAS using the full Run 2 pp collision data set at $\sqrt{s} = 13\,TeV$. ATLAS-CONF-2020-030 (2020). https://cds.cern.ch/record/2725736

104. ATLAS Collaboration, Topological cell clustering in the ATLAS calorimeters and its performance in LHC Run 1. Eur. Phys. J. C **77**, 490 (2017). arXiv:1603.02934 [hep-ex]

105. M. Cacciari, G.P. Salam, G. Soyez, The anti-k_t jet clustering algorithm. JHEP **04**, 063 (2008). arXiv:0802.1189 [hep-ph]

106. M. Cacciari, G.P. Salam, G. Soyez, FastJet user manual. Eur. Phys. J. C **72**, 1896 (2012). arXiv:1111.6097 [hep-ph]

107. ATLAS Collaboration, Jet energy scale and resolution measured in proton-proton collisions at $\sqrt{s} = 13\,TeV$ with the ATLAS detector (2020). arXiv:2007.02645 [hep-ex]

108. ATLAS Collaboration, Performance of pile-up mitigation techniques for jets in pp collisions at $\sqrt{s} = 8\,TeV$ using the ATLAS detector. Eur. Phys. J. C **76**, 581 (2016). arXiv:1510.03823 [hep-ex]

109. ATLAS Collaboration, Optimisation and performance studies of the ATLAS b-tagging algorithms for the 2017-18 LHC run. ATL-PHYS-PUB-2017-013 (2017). https://cds.cern.ch/record/2273281

110. ATLAS Collaboration, ATLAS b-jet identification performance and efficiency measurement with $t\bar{t}$ events in pp collisions at $\sqrt{s} = 13\,TeV$. Eur. Phys. J. C **79**, 970 (2019). arXiv:1907.05120 [hep-ex]

111. ATLAS Collaboration, Evidence for the $H \rightarrow b\bar{b}$ decay with the ATLAS detector. JHEP **12**, 024 (2017). arXiv:1708.03299 [hep-ex]

112. ATLAS Collaboration, Performance of missing transverse momentum reconstruction with the ATLAS detector using proton-proton collisions at $\sqrt{s} = 13\,TeV$. Eur. Phys. J. C **78**, 903 (2018). arXiv:1802.08168 [hep-ex]

113. ATLAS Collaboration, E_T^{miss} performance in the ATLAS detector using 2015-2016 LHC pp collisions. ATLAS-CONF-2018-023 (2018). https://cds.cern.ch/record/2625233

114. T. Gehrmann et al., W^+W^- production at hadron colliders in next to next to leading order QCD. Phys. Rev. Lett. **113**, 212001 (2014). arXiv:1408.5243 [hep-ph]

115. M. Grazzini, S. Kallweit, D. Rathlev, M. Wiesemann, $W^{\pm}Z$ production at hadron colliders in NNLO QCD. Phys. Lett. B **761**, 179 (2016). arXiv:1604.08576 [hep-ph]

116. M. Grazzini, S. Kallweit, D. Rathlev, ZZ production at the LHC: Fiducial cross sections and distributions in NNLO QCD. Phys. Lett. B **750**, 407 (2015). arXiv:1507.06257 [hep-ph]

117. F. Cascioli et al., ZZ production at hadron colliders in NNLO QCD. Phys. Lett. B **735**, 311 (2014). arXiv:1405.2219 [hep-ph]

118. N. Kidonakis, Next-to-next-to-leading logarithm resummation for s-channel single top quark production. Phys. Rev. D **81**, 054028 (2010). arXiv:1001.5034 [hep-ph]

119. N. Kidonakis, Next-to-next-to-leading-order collinear and soft gluon corrections for t-channel single top quark production. Phys. Rev. D **83**, 091503 (2011). arXiv:1103.2792 [hep-ph]

120. N. Kidonakis, Two-loop soft anomalous dimensions for single top quark associated production with a W- or H-. Phys. Rev. D **82**, 054018 (2010). arXiv:1005.4451 [hep-ph]

121. S. Das, A simple alternative to the Crystal Ball function (2016). arXiv:1603.08591 [hep-ex]

122. M. Oreglia, A study of the reactions $\psi' \rightarrow \gamma\gamma\psi$. SLAC-R-023 (1980). http://www.slac.stanford.edu/cgi-wrap/getdoc/slac-r-236.pdf

123. J. Duchon, Interpolation des fonctions de deux variables suivant le principe de la flexion des plaques minces. ESAIM: Mathematical Modelling and Numerical Analysis - Modélisation Mathématique et Analyse Numérique **10** , 5 (1976). https://eudml.org/doc/193284

124. ATLAS Collaboration, Luminosity determination in pp collisions a $\sqrt{s} = 13\,TeV$ using the ATLAS detector at the LHC. ATLAS-CONF-2019-021 (2019). https://cds.cern.ch/record/2677054

125. G. Cowan, K. Cranmer, E. Gross, O. Vitells, Asymptotic formulae for likelihood-based tests of new physics. Eur. Phys. J. C **71**, 1554 (2011). arXiv:1007.1727 [physics.data-an]. [Erratum: Eur. Phys. J. C **73**, 2501 (2013)]

126. L. Moneta et al., The RooStats Project. PoS ACAT **2010**, 057 (2010). arXiv:1009.1003 [physics.data-an]

127. W. Verkerke, D. Kirkby, The RooFit toolkit for data modeling (2003). arXiv:physics/0306116 [physics.data-an]

128. O. Vitells, E. Gross, Estimating the significance of a signal in a multi-dimensional search. Astropart. Phys. **35**, 230 (2011). arXiv:1105.4355 [astro-ph.IM]

129. A.L. Read, Presentation of search results: the CLs technique. J. Phys. G **28**, 2693 (2002)

130. R.V. Harlander, S. Liebler, H. Mantler, SusHi: a program for the calculation of Higgs production in gluon fusion and bottom-quark annihilation in the Standard Model and the MSSM. Comput. Phys. Commun. **184**, 1605 (2013). arXiv:1212.3249 [hep-ph]

131. R. Harlander, P. Kant, Higgs production and decay: analytic results at next-to-leading order QCD. JHEP **12**, 015 (2005). arXiv:hep-ph/0509189

132. R.V. Harlander, W.B. Kilgore, Higgs boson production in bottom quark fusion at next-to-next-to-leading order. Phys. Rev. D **68**, 013001 (2003). arXiv:hep-ph/0304035

133. R.V. Harlander, W.B. Kilgore, Next-to-next-to-leading order Higgs production at hadron colliders. Phys. Rev. Lett. **88**, 201801 (2002). arXiv:hep-ph/0201206

134. S. Dawson, C.B. Jackson, L. Reina, D. Wackeroth, Exclusive Higgs boson production with bottom quarks at hadron colliders. Phys. Rev. D **69**, 074027 (2004). arXiv:hep-ph/0311067

135. S. Dittmaier, M. Krämer, M. Spira, Higgs radiation off bottom quarks at the Fermilab Tevatron and the CERN LHC. Phys. Rev. D **70**, 074010 (2004). arXiv:hep-ph/0309204

136. R. Harlander, M. Krämer, M. Schumacher, Bottom-quark associated Higgs-boson production: reconciling the four- and five-flavour scheme approach (2011). arXiv:1112.3478 [hep-ph]

137. D. Eriksson, J. Rathsman, O. Stål, 2HDMC—two-Higgs-doublet model calculator physics and manual. Comput. Phys. Commun. **181**, 189 (2010). arXiv:0902.0851 [hep-ph]

138. ATLAS Collaboration, ATLAS Computing Acknowledgements. ATL-SOFT-PUB-2020-001. https://cds.cern.ch/record/2717821

ATLAS Collaboration

G. Aad[102], B. Abbott[128], D. C. Abbott[103], A. Abed Abud[36], K. Abeling[53], D. K. Abhayasinghe[94], S. H. Abidi[29], O. S. AbouZeid[40], N. L. Abraham[156], H. Abramowicz[161], H. Abreu[160], Y. Abulaiti[6], B. S. Acharya[67a,67b,o], B. Achkar[53], L. Adam[100], C. Adam Bourdarios[5], L. Adamczyk[84a], L. Adamek[167], J. Adelman[121], A. Adiguzel[12c,ad], S. Adorni[54], T. Adye[143], A. A. Affolder[145], Y. Afik[160], C. Agapopoulou[65], M. N. Agaras[38], A. Aggarwal[119], C. Agheorghiesei[27c], J. A. Aguilar-Saavedra[139f,139a,ac], A. Ahmad[36], F. Ahmadov[80], W. S. Ahmed[104], X. Ai[18], G. Aielli[74a,74b], S. Akatsuka[86], M. Akbiyik[100], T. P. A. Åkesson[97], E. Akilli[54], A. V. Akimov[111], K. Al Khoury[65], G. L. Alberghi[23a,23b], J. Albert[176], M. J. Alconada Verzini[161], S. Alderweireldt[36], M. Aleksa[36], I. N. Aleksandrov[80], C. Alexa[27b], T. Alexopoulos[10], A. Alfonsi[120], F. Alfonsi[23a,23b], M. Alhroob[128], B. Ali[141], S. Ali[158], M. Aliev[166], G. Alimonti[69a], C. Allaire[36], B. M. M. Allbrooke[156], B. W. Allen[131], P. P. Allport[21], A. Aloisio[70a,70b], F. Alonso[89], C. Alpigiani[148], E. Alunno Camelia[74a,74b], M. Alvarez Estevez[99], M. G. Alviggi[70a,70b], Y. Amaral Coutinho[81b], A. Ambler[104], L. Ambroz[134], C. Amelung[36], D. Amidei[106], S. P. Amor Dos Santos[139a], S. Amoroso[46], C. S. Amrouche[54], F. An[79], C. Anastopoulos[149], N. Andari[144], T. Andeen[11], J. K. Anders[20], S. Y. Andrean[45a,45b], A. Andreazza[69a,69b], V. Andrei[61a], C. R. Anelli[176], S. Angelidakis[9], A. Angerami[39], A. V. Anisenkov[122a,122b], A. Annovi[72a], C. Antel[54], M. T. Anthony[149], E. Antipov[129], M. Antonelli[51], D. J. A. Antrim[18], F. Anulli[73a], M. Aoki[82], J. A. Aparisi Pozo[174], M. A. Aparo[156], L. Aperio Bella[46], N. Aranzabal[36], V. Araujo Ferraz[81a], R. Araujo Pereira[81b], C. Arcangeletti[51], A. T. H. Arce[49], J-F. Arguin[110], S. Argyropoulos[52], J.-H. Arling[46], A. J. Armbruster[36], A. Armstrong[171], O. Arnaez[167], H. Arnold[120], Z. P. Arrubarrena Tame[114], G. Artoni[134], H. Asada[117], K. Asai[126], S. Asai[163], T. Asawatavonvanich[165], N. Asbah[59], E. M. Asimakopoulou[172], L. Asquith[156], J. Assahsah[35e], K. Assamagan[29], R. Astalos[28a], R. J. Atkin[33a], M. Atkinson[173], N. B. Atlay[19], H. Atmani[65], P. A. Atmasiddha[106], K. Augsten[141], V. A. Austrup[182], G. Avolio[36], M. K. Ayoub[15c], G. Azuelos[110,ak], D. Babal[28a], H. Bachacou[144], K. Bachas[162], F. Backman[45a,45b], P. Bagnaia[73a,73b], M. Bahmani[85], H. Bahrasemani[152], A. J. Bailey[174], V. R. Bailey[173], J. T. Baines[143], C. Bakalis[10], O. K. Baker[183], P. J. Bakker[120], E. Bakos[16], D. Bakshi Gupta[8], S. Balaji[157], R. Balasubramanian[120], E. M. Baldin[122a,122b], P. Balek[180], F. Balli[144], W. K. Balunas[134], J. Balz[100], E. Banas[85], M. Bandieramonte[138], A. Bandyopadhyay[19], Sw. Banerjee[181,j], L. Barak[161], W. M. Barbe[38], E. L. Barberio[105], D. Barberis[55a,55b], M. Barbero[102], G. Barbour[95], T. Barillari[115], M-S. Barisits[36], J. Barkeloo[131], T. Barklow[153], R. Barnea[160], B. M. Barnett[143], R. M. Barnett[18], Z. Barnovska-Blenessy[60a], A. Baroncelli[60a], G. Barone[29], A. J. Barr[134], L. Barranco Navarro[45a,45b], F. Barreiro[99], J. Barreiro Guimarães da Costa[15a], U. Barron[161], S. Barsov[137], F. Bartels[61a], R. Bartoldus[153], G. Bartolini[102], A. E. Barton[90], P. Bartos[28a], A. Basalaev[46], A. Basan[100], A. Bassalat[65,ah], M. J. Basso[167], C. R. Basson[101], R. L. Bates[57], S. Batlamous[35f], J. R. Batley[32], B. Batool[151], M. Battaglia[145], M. Bauce[73a,73b], F. Bauer[144,*], P. Bauer[24], H. S. Bawa[31], A. Bayirli[12c], J. B. Beacham[49], T. Beau[135], P. H. Beauchemin[170], F. Becherer[52], P. Bechtle[24], H. C. Beck[53], H. P. Beck[20,q], K. Becker[178], C. Becot[46], A. Beddall[12d], A. J. Beddall[12a], V. A. Bednyakov[80], M. Bedognetti[120], C. P. Bee[155], T. A. Beermann[182], M. Begalli[81b], M. Begel[29], A. Behera[155], J. K. Behr[46], F. Beisiegel[24], M. Belfkir[5], A. S. Bell[95], G. Bella[161], L. Bellagamba[23b], A. Bellerive[34], P. Bellos[9], K. Beloborodov[122a,122b], K. Belotskiy[112], N. L. Belyaev[112], D. Benchekroun[35a], N. Benekos[10], Y. Benhammou[161], D. P. Benjamin[6], M. Benoit[29], J. R. Bensinger[26], S. Bentvelsen[120], L. Beresford[134], M. Beretta[51], D. Berge[19], E. Bergeaas Kuutmann[172], N. Berger[5], B. Bergmann[141], L. J. Bergsten[26], J. Beringer[18], S. Berlendis[7], G. Bernardi[135], C. Bernius[153], F. U. Bernlochner[24], T. Berry[94], P. Berta[100], A. Berthold[48], I. A. Bertram[90], O. Bessidskaia Bylund[182], N. Besson[144], S. Bethke[115], A. Betti[42], A. J. Bevan[93], S. Bhatta[155], D. S. Bhattacharya[177], P. Bhattarai[26], V. S. Bhopatkar[6], R. Bi[138], R. M. Bianchi[138], O. Biebel[114], D. Biedermann[19], R. Bielski[36], K. Bierwagen[100], N. V. Biesuz[72a,72b], M. Biglietti[75a], T. R. V. Billoud[141], M. Bindi[53], A. Bingul[12d], C. Bini[73a,73b], S. Biondi[23a,23b], C. J. Birch-sykes[101], M. Birman[180], T. Bisanz[36], J. P. Biswal[3], D. Biswas[181,j], A. Bitadze[101], C. Bittrich[48], K. Bjørke[133], T. Blazek[28a], I. Bloch[46], C. Blocker[26], A. Blue[57], U. Blumenschein[93], G. J. Bobbink[120], V. S. Bobrovnikov[122a,122b], S. S. Bocchetta[97], D. Bogavac[14], A. G. Bogdanchikov[122a,122b], C. Bohm[45a], V. Boisvert[94], P. Bokan[172,53], T. Bold[84a], A. E. Bolz[61b], M. Bomben[135], M. Bona[93], J. S. Bonilla[131], M. Boonekamp[144], C. D. Booth[94], A. G. Borbély[57], H. M. Borecka-Bielska[91], L. S. Borgna[95], A. Borisov[123], G. Borissov[90], D. Bortoletto[134], D. Boscherini[23b], M. Bosman[14], J. D. Bossio Sola[104], K. Bouaouda[35a], J. Boudreau[138], E. V. Bouhova-Thacker[90], D. Boumediene[38], R. Bouquet[135], A. Boveia[127],

J. Boyd[36], D. Boye[33c], I. R. Boyko[80], A. J. Bozson[94], J. Bracinik[21], N. Brahimi[60c,60d], G. Brandt[182], O. Brandt[32], F. Braren[46], B. Brau[103], J. E. Brau[131], W. D. Breaden Madden[57], K. Brendlinger[46], R. Brener[160], L. Brenner[36], R. Brenner[172], S. Bressler[180], B. Brickwedde[100], D. L. Briglin[21], D. Britton[57], D. Britzger[115], I. Brock[24], R. Brock[107], G. Brooijmans[39], W. K. Brooks[146d], E. Brost[29], P. A. Bruckman de Renstrom[85], B. Brüers[46], D. Bruncko[28b], A. Bruni[23b], G. Bruni[23b], M. Bruschi[23b], N. Bruscino[73a,73b], L. Bryngemark[153], T. Buanes[17], Q. Buat[155], P. Buchholz[151], A. G. Buckley[57], I. A. Budagov[80], M. K. Bugge[133], O. Bulekov[112], B. A. Bullard[59], T. J. Burch[121], S. Burdin[91], C. D. Burgard[120], A. M. Burger[129], B. Burghgrave[8], J. T. P. Burr[46], C. D. Burton[11], J. C. Burzynski[103], V. Büscher[100], E. Buschmann[53], P. J. Bussey[57], J. M. Butler[25], C. M. Buttar[57], J. M. Butterworth[95], W. Buttinger[143], C. J. Buxo Vazquez[107], A. R. Buzykaev[122a,122b], G. Cabras[23a,23b], S. Cabrera Urbán[174], D. Caforio[56], H. Cai[138], V. M. M. Cairo[153], O. Cakir[4a], N. Calace[36], P. Calafiura[18], G. Calderini[135], P. Calfayan[66], G. Callea[57], L. P. Caloba[81b], A. Caltabiano[74a,74b], S. Calvente Lopez[99], D. Calvet[38], S. Calvet[38], T. P. Calvet[102], M. Calvetti[72a,72b], R. Camacho Toro[135], S. Camarda[36], D. Camarero Munoz[99], P. Camarri[74a,74b], M. T. Camerlingo[75a,75b], D. Cameron[133], C. Camincher[36], S. Campana[36], M. Campanelli[95], A. Camplani[40], V. Canale[70a,70b], A. Canesse[104], M. Cano Bret[78], J. Cantero[129], T. Cao[161], Y. Cao[173], M. Capua[41a,41b], R. Cardarelli[74a], F. Cardillo[174], G. Carducci[41a,41b], T. Carli[36], G. Carlino[70a], B. T. Carlson[138], E. M. Carlson[176,168a], L. Carminati[69a,69b], R. M. D. Carney[153], S. Caron[119], E. Carquin[146d], S. Carrá[46], G. Carratta[23a,23b], J. W. S. Carter[167], T. M. Carter[50], M. P. Casado[14,g], A. F. Casha[167], E. G. Castiglia[183], F. L. Castillo[174], L. Castillo Garcia[14], V. Castillo Gimenez[174], N. F. Castro[139a,139e], A. Catinaccio[36], J. R. Catmore[133], A. Cattai[36], V. Cavaliere[29], V. Cavasinni[72a,72b], E. Celebi[12b], F. Celli[134], K. Cerny[130], A. S. Cerqueira[81a], A. Cerri[156], L. Cerrito[74a,74b], F. Cerutti[18], A. Cervelli[23a,23b], S. A. Cetin[12b], Z. Chadi[35a], D. Chakraborty[121], J. Chan[181], W. S. Chan[120], W. Y. Chan[91], J. D. Chapman[32], B. Chargeishvili[159b], D. G. Charlton[21], T. P. Charman[93], M. Chatterjee[20], C. C. Chau[34], S. Che[127], S. Chekanov[6], S. V. Chekulaev[168a], G. A. Chelkov[80,af], B. Chen[79], C. Chen[60a], C. H. Chen[79], H. Chen[15c], H. Chen[29], J. Chen[60a], J. Chen[39], J. Chen[26], S. Chen[136], S. J. Chen[15c], X. Chen[15b], Y. Chen[60a], Y-H. Chen[46], H. C. Cheng[63a], H. J. Cheng[15a], A. Cheplakov[80], E. Cheremushkina[123], R. Cherkaoui El Moursli[35f], E. Cheu[7], K. Cheung[64], T. J. A. Chevalérias[144], L. Chevalier[144], V. Chiarella[51], G. Chiarelli[72a], G. Chiodini[68a], A. S. Chisholm[21], A. Chitan[27b], I. Chiu[163], Y. H. Chiu[176], M. V. Chizhov[80], K. Choi[11], A. R. Chomont[73a,73b], Y. Chou[103], Y. S. Chow[120], L. D. Christopher[33e], M. C. Chu[63a], X. Chu[15a,15d], J. Chudoba[140], J. J. Chwastowski[85], L. Chytka[130], D. Cieri[115], K. M. Ciesla[85], V. Cindro[92], I. A. Cioară[27b], A. Ciocio[18], F. Cirotto[70a,70b], Z. H. Citron[180,k], M. Citterio[69a], D. A. Ciubotaru[27b], B. M. Ciungu[167], A. Clark[54], P. J. Clark[50], S. E. Clawson[101], C. Clement[45a,45b], L. Clissa[23a,23b], Y. Coadou[102], M. Cobal[67a,67c], A. Coccaro[55b], J. Cochran[79], R. Coelho Lopes De Sa[103], H. Cohen[161], A. E. C. Coimbra[36], B. Cole[39], A. P. Colijn[120], J. Collot[58], P. Conde Muiño[139a,139h], S. H. Connell[33c], I. A. Connelly[57], S. Constantinescu[27b], F. Conventi[70a,al], A. M. Cooper-Sarkar[134], F. Cormier[175], K. J. R. Cormier[167], L. D. Corpe[95], M. Corradi[73a,73b], E. E. Corrigan[97], F. Corriveau[104,aa], M. J. Costa[174], F. Costanza[5], D. Costanzo[149], G. Cowan[94], J. W. Cowley[32], J. Crane[101], K. Cranmer[125], R. A. Creager[136], S. Crépé-Renaudin[58], F. Crescioli[135], M. Cristinziani[24], M. Cristoforetti[76a,76b], V. Croft[170], G. Crosetti[41a,41b], A. Cueto[5], T. Cuhadar Donszelmann[171], H. Cui[15a,15d], A. R. Cukierman[153], W. R. Cunningham[57], S. Czekierda[85], P. Czodrowski[36], M. M. Czurylo[61b], M. J. Da Cunha Sargedas De Sousa[60b], J. V. Da Fonseca Pinto[81b], C. Da Via[101], W. Dabrowski[84a], F. Dachs[36], T. Dado[47], S. Dahbi[33e], T. Dai[106], C. Dallapiccola[103], M. Dam[40], G. D'amen[29], V. D'Amico[75a,75b], J. Damp[100], J. R. Dandoy[136], M. F. Daneri[30], M. Danninger[152], V. Dao[36], G. Darbo[55b], O. Dartsi[5], A. Dattagupta[131], S. D'Auria[69a,69b], C. David[168b], T. Davidek[142], D. R. Davis[49], I. Dawson[149], K. De[8], R. De Asmundis[70a], M. De Beurs[120], S. De Castro[23a,23b], N. De Groot[119], P. de Jong[120], H. De la Torre[107], A. De Maria[15c], D. De Pedis[73a], A. De Salvo[73a], U. De Sanctis[74a,74b], M. De Santis[74a,74b], A. De Santo[156], J. B. De Vivie De Regie[65], D. V. Dedovich[80], A. M. Deiana[42], J. Del Peso[99], Y. Delabat Diaz[46], D. Delgove[65], F. Deliot[144], C. M. Delitzsch[7], M. Della Pietra[70a,70b], D. Della Volpe[54], A. Dell'Acqua[36], L. Dell'Asta[74a,74b], M. Delmastro[5], C. Delporte[65], P. A. Delsart[58], S. Demers[183], M. Demichev[80], G. Demontigny[110], S. P. Denisov[123], L. D'Eramo[121], D. Derendarz[85], J. E. Derkaoui[35e], F. Derue[135], P. Dervan[91], K. Desch[24], K. Dette[167], C. Deutsch[24], M. R. Devesa[30], P. O. Deviveiros[36], F. A. Di Bello[73a,73b], A. Di Ciaccio[74a,74b], L. Di Ciaccio[5], C. Di Donato[70a,70b], A. Di Girolamo[36], G. Di Gregorio[72a,72b], A. Di Luca[76a,76b], B. Di Micco[75a,75b], R. Di Nardo[75a,75b], R. Di Sipio[167], C. Diaconu[102], F. A. Dias[120], T. Dias Do Vale[139a], M. A. Diaz[146a], F. G. Diaz Capriles[24], J. Dickinson[18], M. Didenko[166], E. B. Diehl[106], J. Dietrich[19],

S. Díez Cornell[46], C. Diez Pardos[151], A. Dimitrievska[18], W. Ding[15b], J. Dingfelder[24], S. J. Dittmeier[61b],
F. Dittus[36], F. Djama[102], T. Djobava[159b], J. I. Djuvsland[17], M. A. B. Do Vale[147], M. Dobre[27b],
D. Dodsworth[26], C. Doglioni[97], J. Dolejsi[142], Z. Dolezal[142], M. Donadelli[81c], B. Dong[60c], J. Donini[38],
A. D'onofrio[15c], M. D'Onofrio[91], J. Dopke[143], A. Doria[70a], M. T. Dova[89], A. T. Doyle[57], E. Drechsler[152],
E. Dreyer[152], T. Dreyer[53], A. S. Drobac[170], D. Du[60b], T. A. du Pree[120], Y. Duan[60d], F. Dubinin[111],
M. Dubovsky[28a], A. Dubreuil[54], E. Duchovni[180], G. Duckeck[114], O. A. Ducu[36,27b], D. Duda[115],
A. Dudarev[36], A. C. Dudder[100], E. M. Duffield[18], M. D'uffizi[101], L. Duflot[65], M. Dührssen[36], C. Dülsen[182],
M. Dumancic[180], A. E. Dumitriu[27b], M. Dunford[61a], S. Dungs[47], A. Duperrin[102], H. Duran Yildiz[4a],
M. Düren[56], A. Durglishvili[159b], B. Dutta[46], D. Duvnjak[1], G. I. Dyckes[136], M. Dyndal[36], S. Dysch[101],
B. S. Dziedzic[85], M. G. Eggleston[49], T. Eifert[8], G. Eigen[17], K. Einsweiler[18], T. Ekelof[172], H. El Jarrari[35f],
V. Ellajosyula[172], M. Ellert[172], F. Ellinghaus[182], A. A. Elliot[93], N. Ellis[36], J. Elmsheuser[29], M. Elsing[36],
D. Emeliyanov[143], A. Emerman[39], Y. Enari[163], J. Erdmann[47], A. Ereditato[20], P. A. Erland[85], M. Errenst[182],
M. Escalier[65], C. Escobar[174], O. Estrada Pastor[174], E. Etzion[161], G. Evans[139a], H. Evans[66], M. O. Evans[156],
A. Ezhilov[137], F. Fabbri[57], L. Fabbri[23a,23b], V. Fabiani[119], G. Facini[178], R. M. Fakhrutdinov[123], S. Falciano[73a],
P. J. Falke[24], S. Falke[36], J. Faltova[142], Y. Fang[15a], Y. Fang[15a], G. Fanourakis[44], M. Fanti[69a,69b],
M. Faraj[67a,67c], A. Farbin[8], A. Farilla[75a], E. M. Farina[71a,71b], T. Farooque[107], S. M. Farrington[50],
P. Farthouat[36], F. Fassi[35f], P. Fassnacht[36], D. Fassouliotis[9], M. Faucci Giannelli[50], W. J. Fawcett[32],
L. Fayard[65], O. L. Fedin[137,p], W. Fedorko[175], A. Fehr[20], M. Feickert[173], L. Feligioni[102], A. Fell[149],
C. Feng[60b], M. Feng[49], M. J. Fenton[171], A. B. Fenyuk[123], S. W. Ferguson[43], J. Ferrando[46], A. Ferrari[172],
P. Ferrari[120], R. Ferrari[71a], A. Ferrer[174], D. Ferrere[54], C. Ferretti[106], F. Fiedler[100], A. Filipčič[92],
F. Filthaut[119], K. D. Finelli[25], M. C. N. Fiolhais[139a,139c,a], L. Fiorini[174], F. Fischer[114], J. Fischer[100],
W. C. Fisher[107], T. Fitschen[21], I. Fleck[151], P. Fleischmann[106], T. Flick[182], B. M. Flierl[114], L. Flores[136],
L. R. Flores Castillo[63a], F. M. Follega[76a,76b], N. Fomin[17], J. H. Foo[167], G. T. Forcolin[76a,76b], B. C. Forland[66],
A. Formica[144], F. A. Förster[14], A. C. Forti[101], E. Fortin[102], M. G. Foti[134], D. Fournier[65], H. Fox[90],
P. Francavilla[72a,72b], S. Francescato[73a,73b], M. Franchini[23a,23b], S. Franchino[61a], D. Francis[36], L. Franco[5],
L. Franconi[20], M. Franklin[59], G. Frattari[73a,73b], A. N. Fray[93], P. M. Freeman[21], B. Freund[110], W. S. Freund[81b],
E. M. Freundlich[47], D. C. Frizzell[128], D. Froidevaux[36], J. A. Frost[134], M. Fujimoto[126], C. Fukunaga[164],
E. Fullana Torregrosa[174], T. Fusayasu[116], J. Fuster[174], A. Gabrielli[23a,23b], A. Gabrielli[36], S. Gadatsch[54],
P. Gadow[115], G. Gagliardi[55a,55b], L. G. Gagnon[110], G. E. Gallardo[134], E. J. Gallas[134], B. J. Gallop[143],
R. Gamboa Goni[93], K. K. Gan[127], S. Ganguly[180], J. Gao[60a], Y. Gao[50], Y. S. Gao[31,m], F. M. Garay Walls[146a],
C. García[174], J. E. García Navarro[174], J. A. García Pascual[15a], C. Garcia-Argos[52], M. Garcia-Sciveres[18],
R. W. Gardner[37], N. Garelli[153], S. Gargiulo[52], C. A. Garner[167], V. Garonne[133], S. J. Gasiorowski[148],
P. Gaspar[81b], G. Gaudio[71a], P. Gauzzi[73a,73b], I. L. Gavrilenko[111], A. Gavrilyuk[124], C. Gay[175],
G. Gaycken[46], E. N. Gazis[10], A. A. Geanta[27b], C. M. Gee[145], C. N. P. Gee[143], J. Geisen[97], M. Geisen[100],
C. Gemme[55b], M. H. Genest[58], C. Geng[106], S. Gentile[73a,73b], S. George[94], T. Geralis[44], L. O. Gerlach[53],
P. Gessinger-Befurt[100], G. Gessner[47], M. Ghasemi Bostanabad[176], M. Ghneimat[151], A. Ghosh[65], A. Ghosh[78],
B. Giacobbe[23b], S. Giagu[73a,73b], N. Giangiacomi[167], P. Giannetti[72a], A. Giannini[70a,70b], G. Giannini[14],
S. M. Gibson[94], M. Gignac[145], D. T. Gil[84b], B. J. Gilbert[39], D. Gillberg[34], G. Gilles[182], N. E. K. Gillwald[46],
D. M. Gingrich[3,ak], M. P. Giordani[67a,67c], P. F. Giraud[144], G. Giugliarelli[67a,67c], D. Giugni[69a],
F. Giuli[74a,74b], S. Gkaitatzis[162], I. Gkialas[9,h], E. L. Gkougkousis[14], P. Gkountoumis[10], L. K. Gladilin[113],
C. Glasman[99], P. C. F. Glaysher[46], A. Glazov[46], G. R. Gledhill[131], I. Gnesi[41b,c], M. Goblirsch-Kolb[26],
D. Godin[110], S. Goldfarb[105], T. Golling[54], D. Golubkov[123], A. Gomes[139a,139b], R. Goncalves Gama[53],
R. Gonçalo[139a,139c], G. Gonella[131], L. Gonella[21], A. Gongadze[80], F. Gonnella[21], J. L. Gonski[39],
S. González de la Hoz[174], S. Gonzalez Fernandez[14], R. Gonzalez Lopez[91], C. Gonzalez Renteria[18],
R. Gonzalez Suarez[172], S. Gonzalez-Sevilla[54], G. R. Gonzalvo Rodriguez[174], L. Goossens[36], N. A. Gorasia[21],
P. A. Gorbounov[124], H. A. Gordon[29], B. Gorini[36], E. Gorini[68a,68b], A. Gorišek[92], A. T. Goshaw[49],
M. I. Gostkin[80], C. A. Gottardo[119], M. Gouighri[35b], A. G. Goussiou[148], N. Govender[33c], C. Goy[5],
I. Grabowska-Bold[84a], E. C. Graham[91], J. Gramling[171], E. Gramstad[133], S. Grancagnolo[19], M. Grandi[156],
V. Gratchev[137], P. M. Gravila[27f], F. G. Gravili[68a,68b], C. Gray[57], H. M. Gray[18], C. Grefe[24], K. Gregersen[97],
I. M. Gregor[46], P. Grenier[153], K. Grevtsov[46], C. Grieco[14], N. A. Grieser[128], A. A. Grillo[145], K. Grimm[31,l],
S. Grinstein[14,w], J.-F. Grivaz[65], S. Groh[100], E. Gross[180], J. Grosse-Knetter[53], Z. J. Grout[95],
C. Grud[106], A. Grummer[118], J. C. Grundy[134], L. Guan[106], W. Guan[181], C. Gubbels[175], J. Guenther[36],
A. Guerguichon[65], J. G. R. Guerrero Rojas[174], F. Guescini[115], D. Guest[77], R. Gugel[100], A. Guida[46],

T. Guillemin[5], S. Guindon[36], J. Guo[60c], W. Guo[106], Y. Guo[60a], Z. Guo[102], R. Gupta[46], S. Gurbuz[12c], G. Gustavino[128], M. Guth[52], P. Gutierrez[128], L. F. Gutierrez Zagazeta[136], C. Gutschow[95], C. Guyot[144], C. Gwenlan[134], C. B. Gwilliam[91], E. S. Haaland[133], A. Haas[125], C. Haber[18], H. K. Hadavand[8], A. Hadef[100], M. Haleem[177], J. Haley[129], J. J. Hall[149], G. Halladjian[107], G. D. Hallewell[102], K. Hamano[176], H. Hamdaoui[35f], M. Hamer[24], G. N. Hamity[50], K. Han[60a], L. Han[15c], L. Han[60a], S. Han[18], Y. F. Han[167], K. Hanagaki[82,u], M. Hance[145], D. M. Handl[114], M. D. Hank[37], R. Hankache[135], E. Hansen[97], J. B. Hansen[40], J. D. Hansen[40], M. C. Hansen[24], P. H. Hansen[40], E. C. Hanson[101], K. Hara[169], T. Harenberg[182], S. Harkusha[108], P. F. Harrison[178], N. M. Hartman[153], N. M. Hartmann[114], Y. Hasegawa[150], A. Hasib[50], S. Hassani[144], S. Haug[20], R. Hauser[107], M. Havranek[141], C. M. Hawkes[21], R. J. Hawkings[36], S. Hayashida[117], D. Hayden[107], C. Hayes[106], R. L. Hayes[175], C. P. Hays[134], J. M. Hays[93], H. S. Hayward[91], S. J. Haywood[143], F. He[60a], Y. He[165], M. P. Heath[50], V. Hedberg[97], A. L. Heggelund[133], N. D. Hehir[93], C. Heidegger[52], K. K. Heidegger[52], W. D. Heidorn[79], J. Heilman[34], S. Heim[46], T. Heim[18], B. Heinemann[46,ai], J. G. Heinlein[136], J. J. Heinrich[131], L. Heinrich[36], J. Hejbal[140], L. Helary[46], A. Held[125], S. Hellesund[133], C. M. Helling[145], S. Hellman[45a,45b], C. Helsens[36], R. C. W. Henderson[90], L. Henkelmann[32], A. M. Henriques Correia[36], H. Herde[26], Y. Hernández Jiménez[33e], H. Herr[100], M. G. Herrmann[114], T. Herrmann[48], G. Herten[52], R. Hertenberger[114], L. Hervas[36], G. G. Hesketh[95], N. P. Hessey[168a], H. Hibi[83], S. Higashino[82], E. Higón-Rodriguez[174], K. Hildebrand[37], J. C. Hill[32], K. K. Hill[29], K. H. Hiller[46], S. J. Hillier[21], M. Hils[48], I. Hinchliffe[18], F. Hinterkeuser[24], M. Hirose[132], S. Hirose[169], D. Hirschbuehl[182], B. Hiti[92], O. Hladik[140], J. Hobbs[155], R. Hobincu[27e], N. Hod[180], M. C. Hodgkinson[149], A. Hoecker[36], D. Hohn[52], D. Hohov[65], T. Holm[24], T. R. Holmes[37], M. Holzbock[115], L. B. A. H. Hommels[32], T. M. Hong[138], J. C. Honig[52], A. Hönle[115], B. H. Hooberman[173], W. H. Hopkins[6], Y. Horii[117], P. Horn[48], L. A. Horyn[37], S. Hou[158], A. Hoummada[35a], J. Howarth[57], J. Hoya[89], M. Hrabovsky[130], J. Hrivnac[65], A. Hrynevich[109], T. Hryn'ova[5], P. J. Hsu[64], S.-C. Hsu[148], Q. Hu[39], S. Hu[60c], Y. F. Hu[15a,15d,am], D. P. Huang[95], X. Huang[15c], Y. Huang[60a], Y. Huang[15a], Z. Hubacek[141], F. Hubaut[102], M. Huebner[24], F. Huegging[24], T. B. Huffman[134], M. Huhtinen[36], R. Hulsken[58], R. F. H. Hunter[34], N. Huseynov[80,ab], J. Huston[107], J. Huth[59], R. Hyneman[153], S. Hyrych[28a], G. Iacobucci[54], G. Iakovidis[29], I. Ibragimov[151], L. Iconomidou-Fayard[65], P. Iengo[36], R. Ignazzi[40], R. Iguchi[163], T. Iizawa[54], Y. Ikegami[82], M. Ikeno[82], N. Ilic[119,167,aa], F. Iltzsche[48], H. Imam[35a], G. Introzzi[71a,71b], M. Iodice[75a], K. Iordanidou[168a], V. Ippolito[73a,73b], M. F. Isacson[172], M. Ishino[163], W. Islam[129], C. Issever[19,46], S. Istin[12c], J. M. Iturbe Ponce[63a], R. Iuppa[76a,76b], A. Ivina[180], J. M. Izen[43], V. Izzo[70a], P. Jacka[140], P. Jackson[1], R. M. Jacobs[46], B. P. Jaeger[152], V. Jain[2], G. Jäkel[182], K. B. Jakobi[100], K. Jakobs[52], T. Jakoubek[180], J. Jamieson[57], K. W. Janas[84a], R. Jansky[54], M. Janus[53], P. A. Janus[84a], G. Jarlskog[97], A. E. Jaspan[91], N. Javadov[80,ab], T. Javůrek[36], M. Javurkova[103], F. Jeanneau[144], L. Jeanty[131], J. Jejelava[159a], P. Jenni[52,d], N. Jeong[46], S. Jézéquel[5], J. Jia[155], Z. Jia[15c], Y. Jiang[60a], S. Jiggins[52], F. A. Jimenez Morales[38], J. Jimenez Pena[115], S. Jin[15c], A. Jinaru[27b], O. Jinnouchi[165], H. Jivan[33e], P. Johansson[149], K. A. Johns[7], C. A. Johnson[66], E. Jones[178], R. W. L. Jones[90], S. D. Jones[156], T. J. Jones[91], J. Jovicevic[36], X. Ju[18], J. J. Junggeburth[115], A. Juste Rozas[14,w], A. Kaczmarska[85], M. Kado[73a,73b], H. Kagan[127], M. Kagan[153], A. Kahn[39], C. Kahra[100], T. Kaji[179], E. Kajomovitz[160], C. W. Kalderon[29], A. Kaluza[100], A. Kamenshchikov[123], M. Kaneda[163], N. J. Kang[145], S. Kang[79], Y. Kano[117], J. Kanzaki[82], L. S. Kaplan[181], D. Kar[33e], K. Karava[134], M. J. Kareem[168b], I. Karkanias[162], S. N. Karpov[80], Z. M. Karpova[80], V. Kartvelishvili[90], A. N. Karyukhin[123], E. Kasimi[162], A. Kastanas[45a,45b], C. Kato[60d], J. Katzy[46], K. Kawade[150], K. Kawagoe[88], T. Kawaguchi[117], T. Kawamoto[144], G. Kawamura[53], E. F. Kay[176], F. I. Kaya[170], S. Kazakos[14], V. F. Kazanin[122a,122b], J. M. Keaveney[33a], R. Keeler[176], J. S. Keller[34], E. Kellermann[97], D. Kelsey[156], J. J. Kempster[21], J. Kendrick[21], K. E. Kennedy[39], O. Kepka[140], S. Kersten[182], B. P. Kerševan[92], S. Ketabchi Haghighat[167], F. Khalil-Zada[13], M. Khandoga[144], A. Khanov[129], A. G. Kharlamov[122a,122b], T. Kharlamova[122a,122b], E. E. Khoda[175], T. J. Khoo[77], G. Khoriauli[177], E. Khramov[80], J. Khubua[159b], S. Kido[83], M. Kiehn[36], E. Kim[165], Y. K. Kim[37], N. Kimura[95], A. Kirchhoff[53], D. Kirchmeier[48], J. Kirk[143], A. E. Kiryunin[115], T. Kishimoto[163], D. P. Kisliuk[167], V. Kitali[46], C. Kitsaki[10], O. Kivernyk[24], T. Klapdor-Kleingrothaus[52], M. Klassen[61a], C. Klein[34], M. H. Klein[106], M. Klein[91], U. Klein[91], K. Kleinknecht[100], P. Klimek[36], A. Klimentov[29], F. Klimpel[36], T. Klingl[24], T. Klioutchnikova[36], F. F. Klitzner[114], P. Kluit[120], S. Kluth[115], E. Kneringer[77], E. B. F. G. Knoops[102], A. Knue[52], D. Kobayashi[88], M. Kobel[48], M. Kocian[153], T. Kodama[163], P. Kodys[142], D. M. Koeck[156], P. T. Koenig[24], T. Koffas[34], N. M. Köhler[36], M. Kolb[144], I. Koletsou[5], T. Komarek[130], T. Kondo[82], K. Köneke[52], A. X. Y. Kong[1], A. C. König[119], T. Kono[126], V. Konstantinides[95],

N. Konstantinidis[95], B. Konya[97], R. Kopeliansky[66], S. Koperny[84a], K. Korcyl[85], K. Kordas[162], G. Koren[161], A. Korn[95], I. Korolkov[14], E. V. Korolkova[149], N. Korotkova[113], O. Kortner[115], S. Kortner[115], V. V. Kostyukhin[149,166], A. Kotsokechagia[65], A. Kotwal[49], A. Koulouris[10], A. Kourkoumeli-Charalampidi[71a,71b], C. Kourkoumelis[9], E. Kourlitis[6], V. Kouskoura[29], R. Kowalewski[176], W. Kozanecki[101], A. S. Kozhin[123], V. A. Kramarenko[113], G. Kramberger[92], D. Krasnopevtsev[60a], M. W. Krasny[135], A. Krasznahorkay[36], J. A. Kremer[100], J. Kretzschmar[91], K. Kreul[19], P. Krieger[167], F. Krieter[114], S. Krishnamurthy[103], A. Krishnan[61b], M. Krivos[142], K. Krizka[18], K. Kroeninger[47], H. Kroha[115], J. Kroll[140], J. Kroll[136], K. S. Krowpman[107], U. Kruchonak[80], H. Krüger[24], N. Krumnack[79], M. C. Kruse[49], J. A. Krzysiak[85], A. Kubota[165], O. Kuchinskaia[166], S. Kuday[4b], D. Kuechler[46], J. T. Kuechler[46], S. Kuehn[36], T. Kuhl[46], V. Kukhtin[80], Y. Kulchitsky[108,ae], S. Kuleshov[146b], Y. P. Kulinich[173], M. Kumar[33e], M. Kuna[58], A. Kupco[140], T. Kupfer[47], O. Kuprash[52], H. Kurashige[83], L. L. Kurchaninov[168a], Y. A. Kurochkin[108], A. Kurova[112], M. G. Kurth[15a,15d], E. S. Kuwertz[36], M. Kuze[165], A. K. Kvam[148], J. Kvita[130], T. Kwan[104], C. Lacasta[174], F. Lacava[73a,73b], D. P. J. Lack[101], H. Lacker[19], D. Lacour[135], E. Ladygin[80], R. Lafaye[5], B. Laforge[135], T. Lagouri[146c], S. Lai[53], I. K. Lakomiec[84a], J. E. Lambert[128], S. Lammers[66], W. Lampl[7], C. Lampoudis[162], E. Lançon[29], U. Landgraf[52], M. P. J. Landon[93], V. S. Lang[52], J. C. Lange[53], R. J. Langenberg[103], A. J. Lankford[171], F. Lanni[29], K. Lantzsch[24], A. Lanza[71a], A. Lapertosa[55a,55b], J. F. Laporte[144], T. Lari[69a], F. Lasagni Manghi[23a,23b], M. Lassnig[36], V. Latonova[140], T. S. Lau[63a], A. Laudrain[100], A. Laurier[34], M. Lavorgna[70a,70b], S. D. Lawlor[94], M. Lazzaroni[69a,69b], B. Le[101], E. Le Guirriec[102], A. Lebedev[79], M. LeBlanc[7], T. LeCompte[6], F. Ledroit-Guillon[58], A. C. A. Lee[95], C. A. Lee[29], G. R. Lee[17], L. Lee[59], S. C. Lee[158], S. Lee[79], B. Lefebvre[168a], H. P. Lefebvre[94], M. Lefebvre[176], C. Leggett[18], K. Lehmann[152], N. Lehmann[20], G. Lehmann Miotto[36], W. A. Leight[46], A. Leisos[162,v], M. A. L. Leite[81c], C. E. Leitgeb[114], R. Leitner[142], K. J. C. Leney[42], T. Lenz[24], S. Leone[72a], C. Leonidopoulos[50], A. Leopold[135], C. Leroy[110], R. Les[107], C. G. Lester[32], M. Levchenko[137], J. Levêque[5], D. Levin[106], L. J. Levinson[180], D. J. Lewis[21], B. Li[15b], B. Li[106], C-Q. Li[60c,60d], F. Li[60c], H. Li[60a], H. Li[60b], J. Li[60c], K. Li[148], L. Li[60c], M. Li[15a,15d], Q. Y. Li[60a], S. Li[60c,60d,b], X. Li[46], Y. Li[46], Z. Li[60b], Z. Li[134], Z. Li[104], Z. Li[91], Z. Liang[15a], M. Liberatore[46], B. Liberti[74a], K. Lie[63c], S. Lim[29], C. Y. Lin[32], K. Lin[107], R. A. Linck[66], R. E. Lindley[7], J. H. Lindon[21], A. Linss[46], A. L. Lionti[54], E. Lipeles[136], A. Lipniacka[17], T. M. Liss[173,aj], A. Lister[175], J. D. Little[8], B. Liu[79], B. X. Liu[152], H. B. Liu[29], J. B. Liu[60a], J. K. K. Liu[37], K. Liu[60c,60d], M. Liu[60a], M. Y. Liu[60a], P. Liu[15a], X. Liu[60a], Y. Liu[46], Y. Liu[15a,15d], Y. L. Liu[106], Y. W. Liu[60a], M. Livan[71a,71b], A. Lleres[58], J. Llorente Merino[152], S. L. Lloyd[93], C. Y. Lo[63b], E. M. Lobodzinska[46], P. Loch[7], S. Loffredo[74a,74b], T. Lohse[19], K. Lohwasser[149], M. Lokajicek[140], J. D. Long[173], R. E. Long[90], I. Longarini[73a,73b], L. Longo[36], R. Longo[173], I. Lopez Paz[101], A. Lopez Solis[149], J. Lorenz[114], N. Lorenzo Martinez[5], A. M. Lory[114], A. Lösle[52], X. Lou[45a,45b], X. Lou[15a], A. Lounis[65], J. Love[6], P. A. Love[90], J. J. Lozano Bahilo[174], M. Lu[60a], Y. J. Lu[64], H. J. Lubatti[148], C. Luci[73a,73b], F. L. Lucio Alves[15c], A. Lucotte[58], F. Luehring[66], I. Luise[155], L. Luminari[73a], B. Lund-Jensen[154], N. A. Luongo[131], M. S. Lutz[161], D. Lynn[29], H. Lyons[91], R. Lysak[140], E. Lytken[97], F. Lyu[15a], V. Lyubushkin[80], T. Lyubushkina[80], H. Ma[29], L. L. Ma[60b], Y. Ma[95], D. M. Mac Donell[176], G. Maccarrone[51], C. M. Macdonald[149], J. C. MacDonald[149], J. Machado Miguens[136], R. Madar[38], W. F. Mader[48], M. Madugoda Ralalage Don[129], N. Madysa[48], J. Maeda[83], T. Maeno[29], M. Maerker[48], V. Magerl[52], N. Magini[79], J. Magro[67a,67c,r], D. J. Mahon[39], C. Maidantchik[81b], A. Maio[139a,139b,139d], K. Maj[84a], O. Majersky[28a], S. Majewski[131], Y. Makida[82], N. Makovec[65], B. Malaescu[135], Pa. Malecki[85], V. P. Maleev[137], F. Malek[58], D. Malito[41a,41b], U. Mallik[78], C. Malone[32], S. Maltezos[10], S. Malyukov[80], J. Mamuzic[174], G. Mancini[51], J. P. Mandalia[93], I. Mandić[92], L. Manhaes de Andrade Filho[81a], I. M. Maniatis[162], J. Manjarres Ramos[48], K. H. Mankinen[97], A. Mann[114], A. Manousos[77], B. Mansoulie[144], I. Manthos[162], S. Manzoni[120], A. Marantis[162], L. Marchese[134], G. Marchiori[135], M. Marcisovsky[140], L. Marcoccia[74a,74b], C. Marcon[97], M. Marjanovic[128], Z. Marshall[18], M. U. F. Martensson[172], S. Marti-Garcia[174], C. B. Martin[127], T. A. Martin[178], V. J. Martin[50], B. Martin dit Latour[17], L. Martinelli[75a,75b], M. Martinez[14,w], P. Martinez Agullo[174], V. I. Martinez Outschoorn[103], S. Martin-Haugh[143], V. S. Martoiu[27b], A. C. Martyniuk[95], A. Marzin[36], S. R. Maschek[115], L. Masetti[100], T. Mashimo[163], R. Mashinistov[111], J. Masik[101], A. L. Maslennikov[122a,122b], L. Massa[23a,23b], P. Massarotti[70a,70b], P. Mastrandrea[72a,72b], A. Mastroberardino[41a,41b], T. Masubuchi[163], D. Matakias[29], A. Matic[114], N. Matsuzawa[163], P. Mättig[24], J. Maurer[27b], B. Maček[92], D. A. Maximov[122a,122b], R. Mazini[158], I. Maznas[162], S. M. Mazza[145], C. Mc Ginn[29], J. P. Mc Gowan[104], S. P. Mc Kee[106],

T. G. McCarthy[115], W. P. McCormack[18], E. F. McDonald[105], A. E. McDougall[120], J. A. Mcfayden[18], G. Mchedlidze[159b], M. A. McKay[42], K. D. McLean[176], S. J. McMahon[143], P. C. McNamara[105], C. J. McNicol[178], R. A. McPherson[176,aa], J. E. Mdhluli[33e], Z. A. Meadows[103], S. Meehan[36], T. Megy[38], S. Mehlhase[114], A. Mehta[91], B. Meirose[43], D. Melini[160], B. R. Mellado Garcia[33e], J. D. Mellenthin[53], M. Melo[28a], F. Meloni[46], A. Melzer[24], E. D. Mendes Gouveia[139a,139e], A. M. Mendes Jacques Da Costa[21], H. Y. Meng[167], L. Meng[36], X. T. Meng[106], S. Menke[115], E. Meoni[41a,41b], S. Mergelmeyer[19], S. A. M. Merkt[138], C. Merlassino[134], P. Mermod[54], L. Merola[70a,70b], C. Meroni[69a], G. Merz[106], O. Meshkov[111,113], J. K. R. Meshreki[151], J. Metcalfe[6], A. S. Mete[6], C. Meyer[66], J-P. Meyer[144], M. Michetti[19], R. P. Middleton[143], L. Mijović[50], G. Mikenberg[180], M. Mikestikova[140], M. Mikuž[92], H. Mildner[149], A. Milic[167], C. D. Milke[42], D. W. Miller[37], L. S. Miller[34], A. Milov[180], D. A. Milstead[45a,45b], A. A. Minaenko[123], I. A. Minashvili[159b], L. Mince[57], A. I. Mincer[125], B. Mindur[84a], M. Mineev[80], Y. Minegishi[163], Y. Mino[86], L. M. Mir[14], M. Mironova[134], T. Mitani[179], J. Mitrevski[114], V. A. Mitsou[174], M. Mittal[60c], O. Miu[167], A. Miucci[20], P. S. Miyagawa[93], A. Mizukami[82], J. U. Mjörnmark[97], T. Mkrtchyan[61a], M. Mlynarikova[121], T. Moa[45a,45b], S. Mobius[53], K. Mochizuki[110], P. Moder[46], P. Mogg[114], S. Mohapatra[39], G. Mokgatitswane[33e], R. Moles-Valls[24], B. Mondal[151], S. Mondal[141], K. Mönig[46], E. Monnier[102], A. Montalbano[152], J. Montejo Berlingen[36], M. Montella[95], F. Monticelli[89], S. Monzani[69a], N. Morange[65], A. L. Moreira De Carvalho[139a], D. Moreno[22a], M. Moreno Llácer[174], C. Moreno Martinez[14], P. Morettini[55b], M. Morgenstern[160], S. Morgenstern[48], D. Mori[152], M. Morii[59], M. Morinaga[179], V. Morisbak[133], A. K. Morley[36], G. Mornacchi[36], A. P. Morris[95], L. Morvaj[36], P. Moschovakos[36], B. Moser[120], M. Mosidze[159b], T. Moskalets[144], P. Moskvitina[119], J. Moss[31,n], E. J. W. Moyse[103], S. Muanza[102], J. Mueller[138], R. S. P. Mueller[114], D. Muenstermann[90], G. A. Mullier[97], J. J. Mullin[136], D. P. Mungo[69a,69b], J. L. Munoz Martinez[14], F. J. Munoz Sanchez[101], P. Murin[28b], W. J. Murray[178,143], A. Murrone[69a,69b], J. M. Muse[128], M. Muškinja[18], C. Mwewa[33a], A. G. Myagkov[123,af], A. A. Myers[138], G. Myers[66], J. Myers[131], M. Myska[141], B. P. Nachman[18], O. Nackenhorst[47], A.Nag Nag[48], K. Nagai[134], K. Nagano[82], Y. Nagasaka[62], J. L. Nagle[29], E. Nagy[102], A. M. Nairz[36], Y. Nakahama[117], K. Nakamura[82], T. Nakamura[163], H. Nanjo[132], F. Napolitano[61a], R. F. Naranjo Garcia[46], R. Narayan[42], I. Naryshkin[137], M. Naseri[34], T. Naumann[46], G. Navarro[22a], J. Navarro-Gonzalez[174], P. Y. Nechaeva[111], F. Nechansky[46], T. J. Neep[21], A. Negri[71a,71b], M. Negrini[23b], C. Nellist[119], C. Nelson[104], M. E. Nelson[45a,45b], S. Nemecek[140], M. Nessi[36,f], M. S. Neubauer[173], F. Neuhaus[100], M. Neumann[182], R. Newhouse[175], P. R. Newman[21], C. W. Ng[138], Y. S. Ng[19], Y. W. Y. Ng[171], B. Ngair[35f], H. D. N. Nguyen[102], T. Nguyen Manh[110], E. Nibigira[38], R. B. Nickerson[134], R. Nicolaidou[144], D. S. Nielsen[40], J. Nielsen[145], M. Niemeyer[53], N. Nikiforou[11], V. Nikolaenko[123,af], I. Nikolic-Audit[135], K. Nikolopoulos[21], P. Nilsson[29], H. R. Nindhito[54], A. Nisati[73a], N. Nishu[60c], R. Nisius[115], I. Nitsche[47], T. Nitta[179], T. Nobe[163], D. L. Noel[32], Y. Noguchi[86], I. Nomidis[135], M. A. Nomura[29], M. Nordberg[36], J. Novak[92], T. Novak[92], O. Novgorodova[48], R. Novotny[118], L. Nozka[130], K. Ntekas[171], E. Nurse[95], F. G. Oakham[34,ak], J. Ocariz[135], A. Ochi[83], I. Ochoa[139a], J. P. Ochoa-Ricoux[146a], K. O'Connor[26], S. Oda[88], S. Odaka[82], S. Oerdek[53], A. Ogrodnik[84a], A. Oh[101], C. C. Ohm[154], H. Oide[165], R. Oishi[163], M. L. Ojeda[167], H. Okawa[169], Y. Okazaki[86], M. W. O'Keefe[91], Y. Okumura[163], A. Olariu[27b], L. F. Oleiro Seabra[139a], S. A. Olivares Pino[146a], D. Oliveira Damazio[29], J. L. Oliver[1], M. J. R. Olsson[171], A. Olszewski[85], J. Olszowska[85], Ö. O. Öncel[24], D. C. O'Neil[152], A. P. O'neill[134], A. Onofre[139a,139e], P. U. E. Onyisi[11], H. Oppen[133], R. G. Oreamuno Madriz[121], M. J. Oreglia[37], G. E. Orellana[89], D. Orestano[75a,75b], N. Orlando[14], R. S. Orr[167], V. O'Shea[57], R. Ospanov[60a], G. Otero y Garzon[30], H. Otono[88], P. S. Ott[61a], G. J. Ottino[18], M. Ouchrif[35e], J. Ouellette[29], F. Ould-Saada[133], A. Ouraou[144,*], Q. Ouyang[15a], M. Owen[57], R. E. Owen[143], V. E. Ozcan[12c], N. Ozturk[8], J. Pacalt[130], H. A. Pacey[32], K. Pachal[49], A. Pacheco Pages[14], C. Padilla Aranda[14], S. Pagan Griso[18], G. Palacino[66], S. Palazzo[50], S. Palestini[36], M. Palka[84b], P. Palni[84a], C. E. Pandini[54], J. G. Panduro Vazquez[94], P. Pani[46], G. Panizzo[67a,67c], L. Paolozzi[54], C. Papadatos[110], K. Papageorgiou[9,h], S. Parajuli[42], A. Paramonov[6], C. Paraskevopoulos[10], D. Paredes Hernandez[63b], S. R. Paredes Saenz[134], B. Parida[180], T. H. Park[167], A. J. Parker[31], M. A. Parker[32], F. Parodi[55a,55b], E. W. Parrish[121], J. A. Parsons[39], U. Parzefall[52], L. Pascual Dominguez[135], V. R. Pascuzzi[18], J. M. P. Pasner[145], F. Pasquali[120], E. Pasqualucci[73a], S. Passaggio[55b], F. Pastore[94], P. Pasuwan[45a,45b], S. Pataraia[100], J. R. Pater[101], A. Pathak[181,j], J. Patton[91], T. Pauly[36], J. Pearkes[153], M. Pedersen[133], L. Pedraza Diaz[119], R. Pedro[139a], T. Peiffer[53], S. V. Peleganchuk[122a,122b], O. Penc[140], C. Peng[63b], H. Peng[60a], B. S. Peralva[81a], M. M. Perego[65], A. P. Pereira Peixoto[139a], L. Pereira Sanchez[45a,45b], D. V. Perepelitsa[29], E. Perez Codina[168a], L. Perini[69a,69b], H. Pernegger[36], S. Perrella[36], A. Perrevoort[120],

K. Peters[46], R. F. Y. Peters[101], B. A. Petersen[36], T. C. Petersen[40], E. Petit[102], V. Petousis[141], C. Petridou[162], F. Petrucci[75a,75b], M. Pettee[183], N. E. Pettersson[103], K. Petukhova[142], A. Peyaud[144], R. Pezoa[146d], L. Pezzotti[71a,71b], T. Pham[105], P. W. Phillips[143], M. W. Phipps[173], G. Piacquadio[155], E. Pianori[18], A. Picazio[103], R. H. Pickles[101], R. Piegaia[30], D. Pietreanu[27b], J. E. Pilcher[37], A. D. Pilkington[101], M. Pinamonti[67a,67c], J. L. Pinfold[3], C. Pitman Donaldson[95], M. Pitt[161], L. Pizzimento[74a,74b], A. Pizzini[120], M.-A. Pleier[29], V. Plesanovs[52], V. Pleskot[142], E. Plotnikova[80], P. Podberezko[122a,122b], R. Poettgen[97], R. Poggi[54], L. Poggioli[135], I. Pogrebnyak[107], D. Pohl[24], I. Pokharel[53], G. Polesello[71a], A. Poley[152,168a], A. Policicchio[73a,73b], R. Polifka[142], A. Polini[23b], C. S. Pollard[46], V. Polychronakos[29], D. Ponomarenko[112], L. Pontecorvo[36], S. Popa[27a], G. A. Popeneciu[27d], L. Portales[5], D. M. Portillo Quintero[58], S. Pospisil[141], P. Postolache[27c], K. Potamianos[134], I. N. Potrap[80], C. J. Potter[32], H. Potti[11], T. Poulsen[97], J. Poveda[174], T. D. Powell[149], G. Pownall[46], M. E. Pozo Astigarraga[36], A. Prades Ibanez[174], P. Pralavorio[102], M. M. Prapa[44], S. Prell[79], D. Price[101], M. Primavera[68a], M. L. Proffitt[148], N. Proklova[112], K. Prokofiev[63c], F. Prokoshin[80], S. Protopopescu[29], J. Proudfoot[6], M. Przybycien[84a], D. Pudzha[137], A. Puri[173], P. Puzo[65], D. Pyatiizbyantseva[112], J. Qian[106], Y. Qin[101], A. Quadt[53], M. Queitsch-Maitland[36], G. Rabanal Bolanos[59], M. Racko[28a], F. Ragusa[69a,69b], G. Rahal[98], J. A. Raine[54], S. Rajagopalan[29], A. Ramirez Morales[93], K. Ran[15a,15d], D. F. Rassloff[61a], D. M. Rauch[46], F. Rauscher[114], S. Rave[100], B. Ravina[57], I. Ravinovich[180], M. Raymond[36], A. L. Read[133], N. P. Readioff[149], M. Reale[68a,68b], D. M. Rebuzzi[71a,71b], G. Redlinger[29], K. Reeves[43], D. Reikher[161], A. Reiss[100], A. Rej[151], C. Rembser[36], A. Renardi[46], M. Renda[27b], M. B. Rendel[115], A. G. Rennie[57], S. Resconi[69a], E. D. Resseguie[18], S. Rettie[95], B. Reynolds[127], E. Reynolds[21], O. L. Rezanova[122a,122b], P. Reznicek[142], E. Ricci[76a,76b], R. Richter[115], S. Richter[46], E. Richter-Was[84b], M. Ridel[135], P. Rieck[115], O. Rifki[46], M. Rijssenbeek[155], A. Rimoldi[71a,71b], M. Rimoldi[46], L. Rinaldi[23b], T. T. Rinn[173], G. Ripellino[154], I. Riu[14], P. Rivadeneira[46], J. C. Rivera Vergara[176], F. Rizatdinova[129], E. Rizvi[93], C. Rizzi[36], S. H. Robertson[104,aa], M. Robin[46], D. Robinson[32], C. M. Robles Gajardo[146d], M. Robles Manzano[100], A. Robson[57], A. Rocchi[74a,74b], C. Roda[72a,72b], S. Rodriguez Bosca[174], A. Rodriguez Rodriguez[52], A. M. Rodríguez Vera[168b], S. Roe[36], J. Roggel[182], O. Røhne[133], R. A. Rojas[146d], B. Roland[52], C. P. A. Roland[66], J. Roloff[29], A. Romaniouk[112], M. Romano[23a,23b], N. Rompotis[91], M. Ronzani[125], L. Roos[135], S. Rosati[73a], G. Rosin[103], B. J. Rosser[136], E. Rossi[46], E. Rossi[75a,75b], E. Rossi[70a,70b], L. P. Rossi[55b], L. Rossini[46], R. Rosten[14], M. Rotaru[27b], B. Rottler[52], D. Rousseau[65], G. Rovelli[71a,71b], A. Roy[11], D. Roy[33e], A. Rozanov[102], Y. Rozen[160], X. Ruan[33e], T. A. Ruggeri[1], F. Rühr[52], A. Ruiz-Martinez[174], A. Rummler[36], Z. Rurikova[52], N. A. Rusakovich[80], H. L. Russell[104], L. Rustige[38,47], J. P. Rutherfoord[7], E. M. Rüttinger[149], M. Rybar[142], G. Rybkin[65], E. B. Rye[133], A. Ryzhov[123], J. A. Sabater Iglesias[46], P. Sabatini[174], L. Sabetta[73a,73b], S. Sacerdoti[65], H.F-W. Sadrozinski[145], R. Sadykov[80], F. Safai Tehrani[73a], B. Safarzadeh Samani[156], M. Safdari[153], P. Saha[121], S. Saha[104], M. Sahinsoy[115], A. Sahu[182], M. Saimpert[36], M. Saito[163], T. Saito[163], H. Sakamoto[163], D. Salamani[54], G. Salamanna[75a,75b], A. Salnikov[153], J. Salt[174], A. Salvador Salas[14], D. Salvatore[41a,41b], F. Salvatore[156], A. Salvucci[63a], A. Salzburger[36], D. Sammel[52], D. Sampsonidis[162], D. Sampsonidou[60c,60d], J. Sánchez[174], A. Sanchez Pineda[67a,36,67c], H. Sandaker[133], C. O. Sander[46], I. G. Sanderswood[90], M. Sandhoff[182], C. Sandoval[22b], D. P. C. Sankey[143], M. Sannino[55a,55b], Y. Sano[117], A. Sansoni[51], C. Santoni[38], H. Santos[139a,139b], S. N. Santpur[18], A. Santra[180], K. A. Saoucha[149], A. Sapronov[80], J. G. Saraiva[139a,139d], O. Sasaki[82], K. Sato[169], F. Sauerburger[52], E. Sauvan[5], P. Savard[167,ak], R. Sawada[163], C. Sawyer[143], L. Sawyer[96], I. Sayago Galvan[174], C. Sbarra[23b], A. Sbrizzi[67a,67c], T. Scanlon[95], J. Schaarschmidt[148], P. Schacht[115], D. Schaefer[37], L. Schaefer[136], U. Schäfer[100], A. C. Schaffer[65], D. Schaile[114], R. D. Schamberger[155], E. Schanet[114], C. Scharf[19], N. Scharmberg[101], V. A. Schegelsky[137], D. Scheirich[142], F. Schenck[19], M. Schernau[171], C. Schiavi[55a,55b], L. K. Schildgen[24], Z. M. Schillaci[26], E. J. Schioppa[68a,68b], M. Schioppa[41a,41b], K. E. Schleicher[52], S. Schlenker[36], K. R. Schmidt-Sommerfeld[115], K. Schmieden[100], C. Schmitt[100], S. Schmitt[46], L. Schoeffel[144], A. Schoening[61b], P. G. Scholer[52], E. Schopf[134], M. Schott[100], J. F. P. Schouwenberg[119], J. Schovancova[36], S. Schramm[54], F. Schroeder[182], A. Schulte[100], H-C. Schultz-Coulon[61a], M. Schumacher[52], B. A. Schumm[145], Ph. Schune[144], A. Schwartzman[153], T. A. Schwarz[106], Ph. Schwemling[144], R. Schwienhorst[107], A. Sciandra[145], G. Sciolla[26], F. Scuri[72a], F. Scutti[105], L. M. Scyboz[115], C. D. Sebastiani[91], K. Sedlaczek[47], P. Seema[19], S. C. Seidel[118], A. Seiden[145], B. D. Seidlitz[29], T. Seiss[37], C. Seitz[46], J. M. Seixas[81b], G. Sekhniaidze[70a], S. J. Sekula[42], N. Semprini-Cesari[23a,23b], S. Sen[49], C. Serfon[29], L. Serin[65], L. Serkin[67a,67b], M. Sessa[60a], H. Severini[128], S. Sevova[153], F. Sforza[55a,55b], A. Sfyrla[54], E. Shabalina[53], J. D. Shahinian[136], N. W. Shaikh[45a,45b],

D. Shaked Renous[180], L. Y. Shan[15a], M. Shapiro[18], A. Sharma[36], A. S. Sharma[1], P. B. Shatalov[124], K. Shaw[156], S. M. Shaw[101], M. Shehade[180], Y. Shen[128], A. D. Sherman[25], P. Sherwood[95], L. Shi[95], C. O. Shimmin[183], Y. Shimogama[179], M. Shimojima[116], J. D. Shinner[94], I. P. J. Shipsey[134], S. Shirabe[165], M. Shiyakova[80,y], J. Shlomi[180], A. Shmeleva[111], M. J. Shochet[37], J. Shojaii[105], D. R. Shope[154], S. Shrestha[127], E. M. Shrif[33e], M. J. Shroff[176], E. Shulga[180], P. Sicho[140], A. M. Sickles[173], E. Sideras Haddad[33e], O. Sidiropoulou[36], A. Sidoti[23a,23b], F. Siegert[48], Dj. Sijacki[16], M.Jr. Silva[181], M. V. Silva Oliveira[36], S. B. Silverstein[45a], S. Simion[65], R. Simoniello[100], C. J. Simpson-allsop[21], S. Simsek[12b], P. Sinervo[167], V. Sinetckii[113], S. Singh[152], S. Sinha[33e], M. Sioli[23a,23b], I. Siral[131], S.Yu. Sivoklokov[113], J. Sjölin[45a,45b], A. Skaf[53], E. Skorda[97], P. Skubic[128], M. Slawinska[85], K. Sliwa[170], V. Smakhtin[180], B. H. Smart[143], J. Smiesko[28b], N. Smirnov[112], S.Yu. Smirnov[112], Y. Smirnov[112], L. N. Smirnova[113,s], O. Smirnova[97], E. A. Smith[37], H. A. Smith[134], M. Smizanska[90], K. Smolek[141], A. Smykiewicz[85], A. A. Snesarev[111], H. L. Snoek[120], I. M. Snyder[131], S. Snyder[29], R. Sobie[176,aa], A. Soffer[161], A. Søgaard[50], F. Sohns[53], C. A. Solans Sanchez[36], E.Yu. Soldatov[112], U. Soldevila[174], A. A. Solodkov[123], A. Soloshenko[80], O. V. Solovyanov[123], V. Solovyev[137], P. Sommer[149], H. Son[170], A. Sonay[14], W. Y. Song[168b], A. Sopczak[141], A. L. Sopio[95], F. Sopkova[28b], S. Sottocornola[71a,71b], R. Soualah[67a,67c], A. M. Soukharev[122a,122b], D. South[46], S. Spagnolo[68a,68b], M. Spalla[115], M. Spangenberg[178], F. Spanò[94], D. Sperlich[52], T. M. Spieker[61a], G. Spigo[36], M. Spina[156], D. P. Spiteri[57], M. Spousta[142], A. Stabile[69a,69b], B. L. Stamas[121], R. Stamen[61a], M. Stamenkovic[120], A. Stampekis[21], E. Stanecka[85], B. Stanislaus[134], M. M. Stanitzki[46], M. Stankaityte[134], B. Stapf[120], E. A. Starchenko[123], G. H. Stark[145], J. Stark[58], P. Staroba[140], P. Starovoitov[61a], S. Stärz[104], R. Staszewski[85], G. Stavropoulos[44], M. Stegler[46], P. Steinberg[29], A. L. Steinhebel[131], B. Stelzer[152,168a], H. J. Stelzer[138], O. Stelzer-Chilton[168a], H. Stenzel[56], T. J. Stevenson[156], G. A. Stewart[36], M. C. Stockton[36], G. Stoicea[27b], M. Stolarski[139a], S. Stonjek[115], A. Straessner[48], J. Strandberg[154], S. Strandberg[45a,45b], M. Strauss[128], T. Strebler[102], P. Strizenec[28b], R. Ströhmer[177], D. M. Strom[131], R. Stroynowski[42], A. Strubig[45a,45b], S. A. Stucci[29], B. Stugu[17], J. Stupak[128], N. A. Styles[46], D. Su[153], W. Su[60d,148,60c], X. Su[60a], N. B. Suarez[138], V. V. Sulin[111], M. J. Sullivan[91], D. M. S. Sultan[54], S. Sultansoy[4c], T. Sumida[86], S. Sun[106], X. Sun[101], C. J. E. Suster[157], M. R. Sutton[156], S. Suzuki[82], M. Svatos[140], M. Swiatlowski[168a], S. P. Swift[2], T. Swirski[177], A. Sydorenko[100], I. Sykora[28a], M. Sykora[142], T. Sykora[142], D. Ta[100], K. Tackmann[46,x], J. Taenzer[161], A. Taffard[171], R. Tafirout[168a], E. Tagiev[123], R. H. M. Taibah[135], R. Takashima[87], K. Takeda[83], T. Takeshita[150], E. P. Takeva[50], Y. Takubo[82], M. Talby[102], A. A. Talyshev[122a,122b], K. C. Tam[63b], N. M. Tamir[161], J. Tanaka[163], R. Tanaka[65], S. Tapia Araya[173], S. Tapprogge[100], A. Tarek Abouelfadl Mohamed[107], S. Tarem[160], K. Tariq[60b], G. Tarna[27b,e], G. F. Tartarelli[69a], P. Tas[142], M. Tasevsky[140], E. Tassi[41a,41b], G. Tateno[163], A. Tavares Delgado[139a], Y. Tayalati[35f], A. J. Taylor[50], G. N. Taylor[105], W. Taylor[168b], H. Teagle[91], A. S. Tee[90], R. Teixeira De Lima[153], P. Teixeira-Dias[94], H. Ten Kate[36], J. J. Teoh[120], K. Terashi[163], J. Terron[99], S. Terzo[14], M. Testa[51], R. J. Teuscher[167,aa], N. Themistokleous[50], T. Theveneaux-Pelzer[19], D. W. Thomas[94], J. P. Thomas[21], E. A. Thompson[46], P. D. Thompson[21], E. Thomson[136], E. J. Thorpe[93], V. O. Tikhomirov[111,ag], Yu.A. Tikhonov[122a,122b], S. Timoshenko[112], P. Tipton[183], S. Tisserant[102], K. Todome[23a,23b], S. Todorova-Nova[142], S. Todt[48], J. Tojo[88], S. Tokár[28a], K. Tokushuku[82], E. Tolley[127], R. Tombs[32], K. G. Tomiwa[33e], M. Tomoto[82,117], L. Tompkins[153], P. Tornambe[103], E. Torrence[131], H. Torres[48], E. Torró Pastor[174], M. Toscani[30], C. Tosciri[134], J. Toth[102,z], D. R. Tovey[149], A. Traeet[17], C. J. Treado[125], T. Trefzger[177], F. Tresoldi[156], A. Tricoli[29], I. M. Trigger[168a], S. Trincaz-Duvoid[135], D. A. Trischuk[175], W. Trischuk[167], B. Trocmé[58], A. Trofymov[65], C. Troncon[69a], F. Trovato[156], L. Truong[33c], M. Trzebinski[85], A. Trzupek[85], F. Tsai[46], P. V. Tsiareshka[108,ae], A. Tsirigotis[162,v], V. Tsiskaridze[155], E. G. Tskhadadze[159a], M. Tsopoulou[162], I. I. Tsukerman[124], V. Tsulaia[18], S. Tsuno[82], D. Tsybychev[155], Y. Tu[63b], A. Tudorache[27b], V. Tudorache[27b], A. N. Tuna[36], S. Turchikhin[80], D. Turgeman[180], I. Turk Cakir[4b,t], R. J. Turner[21], R. Turra[69a], P. M. Tuts[39], S. Tzamarias[162], E. Tzovara[100], K. Uchida[163], F. Ukegawa[169], G. Unal[36], M. Unal[11], A. Undrus[29], G. Unel[171], F. C. Ungaro[105], Y. Unno[82], K. Uno[163], J. Urban[28b], P. Urquijo[105], G. Usai[8], Z. Uysal[12d], V. Vacek[141], B. Vachon[104], K. O. H. Vadla[133], T. Vafeiadis[36], A. Vaidya[95], C. Valderanis[114], E. Valdes Santurio[45a,45b], M. Valente[168a], S. Valentinetti[23a,23b], A. Valero[174], L. Valéry[46], R. A. Vallance[21], A. Vallier[36], J. A. Valls Ferrer[174], T. R. Van Daalen[14], P. Van Gemmeren[6], S. Van Stroud[95], I. Van Vulpen[120], M. Vanadia[74a,74b], W. Vandelli[36], M. Vandenbroucke[144], E. R. Vandewall[129], D. Vannicola[73a,73b], R. Vari[73a], E. W. Varnes[7], C. Varni[55a,55b], T. Varol[158], D. Varouchas[65], K. E. Varvell[157], M. E. Vasile[27b], G. A. Vasquez[176], F. Vazeille[38], D. Vazquez Furelos[14], T. Vazquez Schroeder[36], J. Veatch[53], V. Vecchio[101], M. J. Veen[120], L. M. Veloce[167],

F. Veloso[139a,139c], S. Veneziano[73a], A. Ventura[68a,68b], A. Verbytskyi[115], V. Vercesi[71a], M. Verducci[72a,72b], C. M. Vergel Infante[79], C. Vergis[24], W. Verkerke[120], A. T. Vermeulen[120], J. C. Vermeulen[120], C. Vernieri[153], P. J. Verschuuren[94], M. C. Vetterli[152,ak], N. Viaux Maira[146d], T. Vickey[149], O. E. Vickey Boeriu[149], G. H. A. Viehhauser[134], L. Vigani[61b], M. Villa[23a,23b], M. Villaplana Perez[174], E. M. Villhauer[50], E. Vilucchi[51], M. G. Vincter[34], G. S. Virdee[21], A. Vishwakarma[50], C. Vittori[23a,23b], I. Vivarelli[156], M. Vogel[182], P. Vokac[141], J. Von Ahnen[46], S. E. von Buddenbrock[33e], E. Von Toerne[24], V. Vorobel[142], K. Vorobev[112], M. Vos[174], J. H. Vossebeld[91], M. Vozak[101], N. Vranjes[16], M. Vranjes Milosavljevic[16], V. Vrba[141,*], M. Vreeswijk[120], N. K. Vu[102], R. Vuillermet[36], I. Vukotic[37], S. Wada[169], P. Wagner[24], W. Wagner[182], J. Wagner-Kuhr[114], S. Wahdan[182], H. Wahlberg[89], R. Wakasa[169], V. M. Walbrecht[115], J. Walder[143], R. Walker[114], S. D. Walker[94], W. Walkowiak[151], V. Wallangen[45a,45b], A. M. Wang[59], A. Z. Wang[181], C. Wang[60a], C. Wang[60c], H. Wang[18], H. Wang[3], J. Wang[63a], P. Wang[42], Q. Wang[128], R.-J. Wang[100], R. Wang[60a], R. Wang[121], S. M. Wang[158], S. Wang[60b], T. Wang[60a], W. T. Wang[60a], W. Wang[15c], W. X. Wang[60a], Y. Wang[60a], Z. Wang[106], C. Wanotayaroj[46], A. Warburton[104], C. P. Ward[32], R. J. Ward[21], N. Warrack[57], A. T. Watson[21], M. F. Watson[21], G. Watts[148], B. M. Waugh[95], A. F. Webb[11], C. Weber[29], M. S. Weber[20], S. A. Weber[34], S. M. Weber[61a], Y. Wei[134], A. R. Weidberg[134], J. Weingarten[47], M. Weirich[100], C. Weiser[52], P. S. Wells[36], T. Wenaus[29], B. Wendland[47], T. Wengler[36], S. Wenig[36], N. Wermes[24], M. Wessels[61a], T. D. Weston[20], K. Whalen[131], A. M. Wharton[90], A. S. White[106], A. White[8], M. J. White[1], D. Whiteson[171], B. W. Whitmore[90], W. Wiedenmann[181], C. Wiel[48], M. Wielers[143], N. Wieseotte[100], C. Wiglesworth[40], L. A. M. Wiik-Fuchs[52], H. G. Wilkens[36], L. J. Wilkins[94], D. M. Williams[39], H. H. Williams[136], S. Williams[32], S. Willocq[103], P. J. Windischhofer[134], I. Wingerter-Seez[5], E. Winkels[156], F. Winklmeier[131], B. T. Winter[52], M. Wittgen[153], M. Wobisch[96], A. Wolf[100], R. Wölker[134], J. Wollrath[52], M. W. Wolter[85], H. Wolters[139a,139c], V. W. S. Wong[175], A. F. Wongel[46], N. L. Woods[145], S. D. Worm[46], B. K. Wosiek[85], K. W. Woźniak[85], K. Wraight[57], S. L. Wu[181], X. Wu[54], Y. Wu[60a], J. Wuerzinger[134], T. R. Wyatt[101], B. M. Wynne[50], S. Xella[40], J. Xiang[63c], X. Xiao[106], X. Xie[60a], I. Xiotidis[156], D. Xu[15a], H. Xu[60a], H. Xu[60a], L. Xu[29], R. Xu[136], T. Xu[144], W. Xu[106], Y. Xu[15b], Z. Xu[60b], Z. Xu[153], B. Yabsley[157], S. Yacoob[33a], D. P. Yallup[95], N. Yamaguchi[88], Y. Yamaguchi[165], A. Yamamoto[82], M. Yamatani[163], H. Yamauchi[169], T. Yamazaki[163], Y. Yamazaki[83], J. Yan[60c], Z. Yan[25], H. J. Yang[60c,60d], H. T. Yang[18], S. Yang[60a], T. Yang[63c], X. Yang[60a], X. Yang[15a,58], Y. Yang[163], Z. Yang[106,60a], W-M. Yao[18], Y. C. Yap[46], H. Ye[15c], J. Ye[42], S. Ye[29], I. Yeletskikh[80], M. R. Yexley[90], P. Yin[39], K. Yorita[179], K. Yoshihara[79], C. J. S. Young[36], C. Young[153], R. Yuan[60b,i], X. Yue[61a], M. Zaazoua[35f], B. Zabinski[85], G. Zacharis[10], E. Zaffaroni[54], J. Zahreddine[135], A. M. Zaitsev[123,af], T. Zakareishvili[159b], N. Zakharchuk[34], S. Zambito[36], D. Zanzi[52], S. V. Zeißner[47], C. Zeitnitz[182], G. Zemaityte[134], J. C. Zeng[173], O. Zenin[123], T. Ženiš[28a], S. Zenz[93], S. Zerradi[35a], D. Zerwas[65], M. Zgubič[134], B. Zhang[15c], D. F. Zhang[15b], G. Zhang[15b], J. Zhang[6], K. Zhang[15a], L. Zhang[15c], L. Zhang[60a], M. Zhang[173], R. Zhang[181], S. Zhang[106], X. Zhang[60c], X. Zhang[60b], Y. Zhang[15a,15d], Z. Zhang[63a], Z. Zhang[65], P. Zhao[49], Y. Zhao[145], Z. Zhao[60a], A. Zhemchugov[80], Z. Zheng[106], D. Zhong[173], B. Zhou[106], C. Zhou[181], H. Zhou[7], M. Zhou[155], N. Zhou[60c], Y. Zhou[7], C. G. Zhu[60b], C. Zhu[15a,15d], H. L. Zhu[60a], H. Zhu[15a], J. Zhu[106], Y. Zhu[60a], X. Zhuang[15a], K. Zhukov[111], V. Zhulanov[122a,122b], D. Zieminska[66], N. I. Zimine[80], S. Zimmermann[52,*], Z. Zinonos[115], M. Ziolkowski[151], L. Živković[16], G. Zobernig[181], A. Zoccoli[23a,23b], K. Zoch[53], T. G. Zorbas[149], R. Zou[37], L. Zwalinski[36]

[1] Department of Physics, University of Adelaide, Adelaide, Australia

[2] Physics Department, SUNY Albany, Albany, NY, USA

[3] Department of Physics, University of Alberta, Edmonton, AB, Canada

[4] (a)Department of Physics, Ankara University, Ankara, Turkey; (b)Application and Research Center for Advanced Studies, Istanbul Aydin University, Istanbul, Turkey; (c)Division of Physics, TOBB University of Economics and Technology, Ankara, Turkey

[5] LAPP, Université Grenoble Alpes, Université Savoie Mont Blanc, CNRS/IN2P3, Annecy, France

[6] High Energy Physics Division, Argonne National Laboratory, Argonne, IL, USA

[7] Department of Physics, University of Arizona, Tucson, AZ, USA

[8] Department of Physics, University of Texas at Arlington, Arlington, TX, USA

[9] Physics Department, National and Kapodistrian University of Athens, Athens, Greece

[10] Physics Department, National Technical University of Athens, Zografou, Greece

[11] Department of Physics, University of Texas at Austin, Austin, TX, USA

12 (a)Bahcesehir University, Faculty of Engineering and Natural Sciences, Istanbul, Turkey; (b)Istanbul Bilgi University, Faculty of Engineering and Natural Sciences, Istanbul, Turkey; (c)Department of Physics, Bogazici University, Istanbul, Turkey; (d)Department of Physics Engineering, Gaziantep University, Gaziantep, Turkey

13 Institute of Physics, Azerbaijan Academy of Sciences, Baku, Azerbaijan

14 Institut de Física d'Altes Energies (IFAE), Barcelona Institute of Science and Technology, Barcelona, Spain

15 (a)Institute of High Energy Physics, Chinese Academy of Sciences, Beijing, China; (b)Physics Department, Tsinghua University, Beijing, China; (c)Department of Physics, Nanjing University, Nanjing, China; (d)University of Chinese Academy of Science (UCAS), Beijing, China

16 Institute of Physics, University of Belgrade, Belgrade, Serbia

17 Department for Physics and Technology, University of Bergen, Bergen, Norway

18 Physics Division, Lawrence Berkeley National Laboratory and University of California, Berkeley, CA, USA

19 Institut für Physik, Humboldt Universität zu Berlin, Berlin, Germany

20 Albert Einstein Center for Fundamental Physics and Laboratory for High Energy Physics, University of Bern, Bern, Switzerland

21 School of Physics and Astronomy, University of Birmingham, Birmingham, UK

22 (a)Facultad de Ciencias y Centro de Investigaciónes, Universidad Antonio Nariño, Bogotá, Colombia; (b)Departamento de Física, Universidad Nacional de Colombia, Bogotá, Colombia

23 (a)Dipartimento di Fisica, INFN Bologna, Universita' di Bologna, Bologna, Italy; (b)INFN Sezione di Bologna, Bologna, Italy

24 Physikalisches Institut, Universität Bonn, Bonn, Germany

25 Department of Physics, Boston University, Boston, MA, USA

26 Department of Physics, Brandeis University, Waltham, MA, USA

27 (a)Transilvania University of Brasov, Brasov, Romania; (b)Horia Hulubei National Institute of Physics and Nuclear Engineering, Bucharest, Romania; (c)Department of Physics, Alexandru Ioan Cuza University of Iasi, Iasi, Romania; (d)Physics Department, National Institute for Research and Development of Isotopic and Molecular Technologies, Cluj-Napoca, Romania; (e)University Politehnica Bucharest, Bucharest, Romania; (f)West University in Timisoara, Timisoara, Romania

28 (a)Faculty of Mathematics, Physics and Informatics, Comenius University, Bratislava, Slovak Republic; (b)Department of Subnuclear Physics, Institute of Experimental Physics of the Slovak Academy of Sciences, Kosice, Slovak Republic

29 Physics Department, Brookhaven National Laboratory, Upton, NY, USA

30 Departamento de Física, Universidad de Buenos Aires, Buenos Aires, Argentina

31 California State University, Long Beach, CA, USA

32 Cavendish Laboratory, University of Cambridge, Cambridge, UK

33 (a)Department of Physics, University of Cape Town, Cape Town, South Africa; (b)iThemba Labs, Western Cape, South Africa; (c)Department of Mechanical Engineering Science, University of Johannesburg, Johannesburg, South Africa; (d)University of South Africa, Department of Physics, Pretoria, South Africa; (e)School of Physics, University of the Witwatersrand, Johannesburg, South Africa

34 Department of Physics, Carleton University, Ottawa, ON, Canada

35 (a)Faculté des Sciences Ain Chock, Réseau Universitaire de Physique des Hautes Energies-Université Hassan II, Casablanca, Morocco; (b)Faculté des Sciences, Université Ibn-Tofail, Kénitra, Morocco; (c)Faculté des Sciences Semlalia, Université Cadi Ayyad, LPHEA, Marrakech, Morocco; (d)Moroccan Foundation for Advanced Science Innovation and Research (MAScIR), Rabat, Morocco; (e)LPMR, Faculté des Sciences, Université Mohamed Premier, Oujda, Morocco; (f)Faculté des sciences, Université Mohammed V, Rabat, Morocco

36 CERN, Geneva, Switzerland

37 Enrico Fermi Institute, University of Chicago, Chicago, IL, USA

38 LPC, Université Clermont Auvergne, CNRS/IN2P3, Clermont-Ferrand, France

39 Nevis Laboratory, Columbia University, Irvington, NY, USA

40 Niels Bohr Institute, University of Copenhagen, Copenhagen, Denmark

41 (a)Dipartimento di Fisica, Università della Calabria, Rende, Italy; (b)Laboratori Nazionali di Frascati, INFN Gruppo Collegato di Cosenza, Rende, Italy

42 Physics Department, Southern Methodist University, Dallas, TX, USA

43 Physics Department, University of Texas at Dallas, Richardson, TX, USA

44 National Centre for Scientific Research "Demokritos", Agia Paraskevi, Greece

45 [(a)]Department of Physics, Stockholm University, Stockholm, Sweden; [(b)]Oskar Klein Centre, Stockholm, Sweden

46 Deutsches Elektronen-Synchrotron DESY, Hamburg and Zeuthen, Germany

47 Lehrstuhl für Experimentelle Physik IV, Technische Universität Dortmund, Dortmund, Germany

48 Institut für Kern- und Teilchenphysik, Technische Universität Dresden, Dresden, Germany

49 Department of Physics, Duke University, Durham, NC, USA

50 SUPA-School of Physics and Astronomy, University of Edinburgh, Edinburgh, UK

51 INFN e Laboratori Nazionali di Frascati, Frascati, Italy

52 Physikalisches Institut, Albert-Ludwigs-Universität Freiburg, Freiburg, Germany

53 II. Physikalisches Institut, Georg-August-Universität Göttingen, Göttingen, Germany

54 Département de Physique Nucléaire et Corpusculaire, Université de Genève, Geneva, Switzerland

55 [(a)]Dipartimento di Fisica, Università di Genova, Genoa, Italy; [(b)]INFN Sezione di Genova, Genoa, Italy

56 II. Physikalisches Institut, Justus-Liebig-Universität Giessen, Giessen, Germany

57 SUPA-School of Physics and Astronomy, University of Glasgow, Glasgow, UK

58 LPSC, Université Grenoble Alpes, CNRS/IN2P3, Grenoble INP, Grenoble, France

59 Laboratory for Particle Physics and Cosmology, Harvard University, Cambridge, MA, USA

60 [(a)]Department of Modern Physics and State Key Laboratory of Particle Detection and Electronics, University of Science and Technology of China, Hefei, China; [(b)]Institute of Frontier and Interdisciplinary Science and Key Laboratory of Particle Physics and Particle Irradiation (MOE), Shandong University, Qingdao, China; [(c)]School of Physics and Astronomy, Key Laboratory for Particle Astrophysics and Cosmology (MOE), SKLPPC, Shanghai Jiao Tong University, Shanghai, China; [(d)]Tsung-Dao Lee Institute, Shanghai, China

61 [(a)]Kirchhoff-Institut für Physik, Ruprecht-Karls-Universität Heidelberg, Heidelberg, Germany; [(b)]Physikalisches Institut, Ruprecht-Karls-Universität Heidelberg, Heidelberg, Germany

62 Faculty of Applied Information Science, Hiroshima Institute of Technology, Hiroshima, Japan

63 [(a)]Department of Physics, Chinese University of Hong Kong, Shatin, N.T., Hong Kong; [(b)]Department of Physics, University of Hong Kong, Pok Fu Lam, Hong Kong; [(c)]Department of Physics and Institute for Advanced Study, Hong Kong University of Science and Technology, Clear Water Bay, Kowloon, Hong Kong, China

64 Department of Physics, National Tsing Hua University, Hsinchu, Taiwan

65 IJCLab, Université Paris-Saclay, CNRS/IN2P3, 91405, Orsay, France

66 Department of Physics, Indiana University, Bloomington, IN, USA

67 [(a)]INFN Gruppo Collegato di Udine, Sezione di Trieste, Udine, Italy; [(b)]ICTP, Trieste, Italy; [(c)]Dipartimento Politecnico di Ingegneria e Architettura, Università di Udine, Udine, Italy

68 [(a)]INFN Sezione di Lecce, Lecce, Italy; [(b)]Dipartimento di Matematica e Fisica, Università del Salento, Lecce, Italy

69 [(a)]INFN Sezione di Milano, Milan, Italy; [(b)]Dipartimento di Fisica, Università di Milano, Milan, Italy

70 [(a)]INFN Sezione di Napoli, Naples, Italy; [(b)]Dipartimento di Fisica, Università di Napoli, Naples, Italy

71 [(a)]INFN Sezione di Pavia, Pavia, Italy; [(b)]Dipartimento di Fisica, Università di Pavia, Pavia, Italy

72 [(a)]INFN Sezione di Pisa, Pisa, Italy; [(b)]Dipartimento di Fisica E. Fermi, Università di Pisa, Pisa, Italy

73 [(a)]INFN Sezione di Roma, Rome, Italy; [(b)]Dipartimento di Fisica, Sapienza Università di Roma, Rome, Italy

74 [(a)]INFN Sezione di Roma Tor Vergata, Rome, Italy; [(b)]Dipartimento di Fisica, Università di Roma Tor Vergata, Rome, Italy

75 [(a)]INFN Sezione di Roma Tre, Rome, Italy; [(b)]Dipartimento di Matematica e Fisica, Università Roma Tre, Rome, Italy

76 [(a)]INFN-TIFPA, Trento, Italy; [(b)]Università degli Studi di Trento, Trento, Italy

77 Institut für Astro- und Teilchenphysik, Leopold-Franzens-Universität, Innsbruck, Austria

78 University of Iowa, Iowa City, IA, USA

79 Department of Physics and Astronomy, Iowa State University, Ames, IA, USA

80 Joint Institute for Nuclear Research, Dubna, Russia

81 [(a)]Departamento de Engenharia Elétrica, Universidade Federal de Juiz de Fora (UFJF), Juiz de Fora, Brazil; [(b)]Universidade Federal do Rio De Janeiro COPPE/EE/IF, Rio de Janeiro, Brazil; [(c)]Instituto de Física, Universidade de São Paulo, São Paulo, Brazil

82 KEK, High Energy Accelerator Research Organization, Tsukuba, Japan

83 Graduate School of Science, Kobe University, Kobe, Japan

84 [(a)]AGH University of Science and Technology, Faculty of Physics and Applied Computer Science, Kraków, Poland ; [(b)]Marian Smoluchowski Institute of Physics, Jagiellonian University, Kraków, Poland

85 Institute of Nuclear Physics Polish Academy of Sciences, Kraków, Poland

[86] Faculty of Science, Kyoto University, Kyoto, Japan

[87] Kyoto University of Education, Kyoto, Japan

[88] Research Center for Advanced Particle Physics and Department of Physics, Kyushu University, Fukuoka , Japan

[89] Instituto de Física La Plata, Universidad Nacional de La Plata and CONICET, La Plata, Argentina

[90] Physics Department, Lancaster University, Lancaster, UK

[91] Oliver Lodge Laboratory, University of Liverpool, Liverpool, UK

[92] Department of Experimental Particle Physics, Jožef Stefan Institute and Department of Physics, University of Ljubljana, Ljubljana, Slovenia

[93] School of Physics and Astronomy, Queen Mary University of London, London, UK

[94] Department of Physics, Royal Holloway University of London, Egham, UK

[95] Department of Physics and Astronomy, University College London, London, UK

[96] Louisiana Tech University, Ruston, LA, USA

[97] Fysiska institutionen, Lunds universitet, Lund, Sweden

[98] Centre de Calcul de l'Institut National de Physique Nucléaire et de Physique des Particules (IN2P3), Villeurbanne, France

[99] Departamento de Física Teorica C-15 and CIAFF, Universidad Autónoma de Madrid, Madrid, Spain

[100] Institut für Physik, Universität Mainz, Mainz, Germany

[101] School of Physics and Astronomy, University of Manchester, Manchester, UK

[102] CPPM, Aix-Marseille Université, CNRS/IN2P3, Marseille, France

[103] Department of Physics, University of Massachusetts, Amherst, MA, USA

[104] Department of Physics, McGill University, Montreal, QC, Canada

[105] School of Physics, University of Melbourne, Victoria, Australia

[106] Department of Physics, University of Michigan, Ann Arbor, MI, USA

[107] Department of Physics and Astronomy, Michigan State University, East Lansing, MI, USA

[108] B.I. Stepanov Institute of Physics, National Academy of Sciences of Belarus, Minsk, Belarus

[109] Research Institute for Nuclear Problems of Byelorussian State University, Minsk, Belarus

[110] Group of Particle Physics, University of Montreal, Montreal, QC, Canada

[111] P.N. Lebedev Physical Institute of the Russian Academy of Sciences, Moscow, Russia

[112] National Research Nuclear University MEPhI, Moscow, Russia

[113] D.V. Skobeltsyn Institute of Nuclear Physics, M.V. Lomonosov Moscow State University, Moscow, Russia

[114] Fakultät für Physik, Ludwig-Maximilians-Universität München, Munich, Germany

[115] Max-Planck-Institut für Physik (Werner-Heisenberg-Institut), Munich, Germany

[116] Nagasaki Institute of Applied Science, Nagasaki, Japan

[117] Graduate School of Science and Kobayashi-Maskawa Institute, Nagoya University, Nagoya, Japan

[118] Department of Physics and Astronomy, University of New Mexico, Albuquerque, NM, USA

[119] Institute for Mathematics, Astrophysics and Particle Physics, Radboud University/Nikhef, Nijmegen, The Netherlands

[120] Nikhef National Institute for Subatomic Physics and University of Amsterdam, Amsterdam, The Netherlands

[121] Department of Physics, Northern Illinois University, DeKalb, IL, USA

[122] (a)Budker Institute of Nuclear Physics and NSU, SB RAS, Novosibirsk, Russia; (b)Novosibirsk State University Novosibirsk, Novosibirsk, Russia

[123] Institute for High Energy Physics of the National Research Centre Kurchatov Institute, Protvino, Russia

[124] Institute for Theoretical and Experimental Physics named by A.I. Alikhanov of National Research Centre "Kurchatov Institute", Moscow, Russia

[125] Department of Physics, New York University, New York, NY, USA

[126] Ochanomizu University, Otsuka, Bunkyo-ku, Tokyo, Japan

[127] Ohio State University, Columbus, OH, USA

[128] Homer L. Dodge Department of Physics and Astronomy, University of Oklahoma, Norman, OK, USA

[129] Department of Physics, Oklahoma State University, Stillwater, OK, USA

[130] Palacký University, RCPTM, Joint Laboratory of Optics, Olomouc, Czech Republic

[131] Institute for Fundamental Science, University of Oregon, Eugene, OR, USA

[132] Graduate School of Science, Osaka University, Osaka, Japan

[133] Department of Physics, University of Oslo, Oslo, Norway

[134] Department of Physics, Oxford University, Oxford, UK

[135] LPNHE, Sorbonne Université, Université de Paris, CNRS/IN2P3, Paris, France

[136] Department of Physics, University of Pennsylvania, Philadelphia, PA, USA

[137] Konstantinov Nuclear Physics Institute of National Research Centre "Kurchatov Institute", PNPI, St. Petersburg, Russia

[138] Department of Physics and Astronomy, University of Pittsburgh, Pittsburgh, PA, USA

[139] [a]Laboratório de Instrumentação e Física Experimental de Partículas-LIP, Lisbon, Portugal; [b]Departamento de Física, Faculdade de Ciências, Universidade de Lisboa, Lisbon, Portugal; [c]Departamento de Física, Universidade de Coimbra, Coimbra, Portugal; [d]Centro de Física Nuclear da Universidade de Lisboa, Lisbon, Portugal; [e]Departamento de Física, Universidade do Minho, Braga, Portugal; [f]Departamento de Física Teórica y del Cosmos, Universidad de Granada, Granada, Spain; [g]Dep Física and CEFITEC of Faculdade de Ciências e Tecnologia, Universidade Nova de Lisboa, Caparica, Portugal; [h]Instituto Superior Técnico, Universidade de Lisboa, Lisbon, Portugal

[140] Institute of Physics of the Czech Academy of Sciences, Prague, Czech Republic

[141] Czech Technical University in Prague, Prague, Czech Republic

[142] Charles University, Faculty of Mathematics and Physics, Prague, Czech Republic

[143] Particle Physics Department, Rutherford Appleton Laboratory, Didcot, UK

[144] IRFU, CEA, Université Paris-Saclay, Gif-sur-Yvette, France

[145] Santa Cruz Institute for Particle Physics, University of California Santa Cruz, Santa Cruz, CA, USA

[146] [a]Departamento de Física, Pontificia Universidad Católica de Chile, Santiago, Chile; [b]Universidad Andres Bello, Department of Physics, Santiago, Chile; [c]Instituto de Alta Investigación, Universidad de Tarapacá, Santiago, Chile; [d]Departamento de Física, Universidad Técnica Federico Santa María, Valparaíso, Chile

[147] Universidade Federal de São João del Rei (UFSJ), São João del Rei, Brazil

[148] Department of Physics, University of Washington, Seattle, WA, USA

[149] Department of Physics and Astronomy, University of Sheffield, Sheffield, UK

[150] Department of Physics, Shinshu University, Nagano, Japan

[151] Department Physik, Universität Siegen, Siegen, Germany

[152] Department of Physics, Simon Fraser University, Burnaby, BC, Canada

[153] SLAC National Accelerator Laboratory, Stanford, CA, USA

[154] Physics Department, Royal Institute of Technology, Stockholm, Sweden

[155] Departments of Physics and Astronomy, Stony Brook University, Stony Brook, NY, USA

[156] Department of Physics and Astronomy, University of Sussex, Brighton, UK

[157] School of Physics, University of Sydney, Sydney, Australia

[158] Institute of Physics, Academia Sinica, Taipei, Taiwan

[159] [a]E. Andronikashvili Institute of Physics, Iv. Javakhishvili Tbilisi State University, Tbilisi, Georgia; [b]High Energy Physics Institute, Tbilisi State University, Tbilisi, Georgia

[160] Department of Physics, Technion, Israel Institute of Technology, Haifa, Israel

[161] Raymond and Beverly Sackler School of Physics and Astronomy, Tel Aviv University, Tel Aviv, Israel

[162] Department of Physics, Aristotle University of Thessaloniki, Thessaloniki, Greece

[163] International Center for Elementary Particle Physics and Department of Physics, University of Tokyo, Tokyo, Japan

[164] Graduate School of Science and Technology, Tokyo Metropolitan University, Tokyo, Japan

[165] Department of Physics, Tokyo Institute of Technology, Tokyo, Japan

[166] Tomsk State University, Tomsk, Russia

[167] Department of Physics, University of Toronto, Toronto, ON, Canada

[168] [a]TRIUMF, Vancouver, BC, Canada; [b]Department of Physics and Astronomy, York University, Toronto, ON, Canada

[169] Division of Physics and Tomonaga Center for the History of the Universe, Faculty of Pure and Applied Sciences, University of Tsukuba, Tsukuba, Japan

[170] Department of Physics and Astronomy, Tufts University, Medford, MA, USA

[171] Department of Physics and Astronomy, University of California Irvine, Irvine, CA, USA

[172] Department of Physics and Astronomy, University of Uppsala, Uppsala, Sweden

[173] Department of Physics, University of Illinois, Urbana, IL, USA

[174] Instituto de Física Corpuscular (IFIC), Centro Mixto Universidad de Valencia - CSIC, Valencia, Spain

[175] Department of Physics, University of British Columbia, Vancouver, BC, Canada

[176] Department of Physics and Astronomy, University of Victoria, Victoria, BC, Canada

[177] Fakultät für Physik und Astronomie, Julius-Maximilians-Universität Würzburg, Würzburg, Germany

[178] Department of Physics, University of Warwick, Coventry, UK

[179] Waseda University, Tokyo, Japan
[180] Department of Particle Physics and Astrophysics, Weizmann Institute of Science, Rehovot, Israel
[181] Department of Physics, University of Wisconsin, Madison, WI, USA
[182] Fakultät für Mathematik und Naturwissenschaften, Fachgruppe Physik, Bergische Universität Wuppertal, Wuppertal, Germany
[183] Department of Physics, Yale University, New Haven, CT, USA

[a] Also at Borough of Manhattan Community College, City University of New York, New York, NY, USA
[b] Also at Center for High Energy Physics, Peking University, China
[c] Also at Centro Studi e Ricerche Enrico Fermi, Rome, Italy
[d] Also at CERN, Geneva, Switzerland
[e] Also at CPPM, Aix-Marseille Université, CNRS/IN2P3, Marseille, France
[f] Also at Département de Physique Nucléaire et Corpusculaire, Université de Genève, Geneva, Switzerland
[g] Also at Departament de Fisica de la Universitat Autonoma de Barcelona, Barcelona, Spain
[h] Also at Department of Financial and Management Engineering, University of the Aegean, Chios, Greece
[i] Also at Department of Physics and Astronomy, Michigan State University, East Lansing, MI, USA
[j] Also at Department of Physics and Astronomy, University of Louisville, Louisville, KY, USA
[k] Also at Department of Physics, Ben Gurion University of the Negev, Beer Sheva, Israel
[l] Also at Department of Physics, California State University, East Bay, USA
[m] Also at Department of Physics, California State University, Fresno, USA
[n] Also at Department of Physics, California State University, Sacramento, USA
[o] Also at Department of Physics, King's College London, London, UK
[p] Also at Department of Physics, St. Petersburg State Polytechnical University, St. Petersburg, Russia
[q] Also at Department of Physics, University of Fribourg, Fribourg, Switzerland
[r] Also at Dipartimento di Matematica, Informatica e Fisica, Università di Udine, Udine, Italy
[s] Also at Faculty of Physics, M.V. Lomonosov Moscow State University, Moscow, Russia
[t] Also at Giresun University, Faculty of Engineering, Giresun, Turkey
[u] Also at Graduate School of Science, Osaka University, Osaka, Japan
[v] Also at Hellenic Open University, Patras, Greece
[w] Also at Institucio Catalana de Recerca i Estudis Avancats, ICREA, Barcelona, Spain
[x] Also at Institut für Experimentalphysik, Universität Hamburg, Hamburg, Germany
[y] Also at Institute for Nuclear Research and Nuclear Energy (INRNE) of the Bulgarian Academy of Sciences, Sofia, Bulgaria
[z] Also at Institute for Particle and Nuclear Physics, Wigner Research Centre for Physics, Budapest, Hungary
[aa] Also at Institute of Particle Physics (IPP), Montreal, Canada
[ab] Also at Institute of Physics, Azerbaijan Academy of Sciences, Baku, Azerbaijan
[ac] Also at Instituto de Fisica Teorica, IFT-UAM/CSIC, Madrid, Spain
[ad] Also at Istanbul University, Dept. of Physics, Istanbul, Turkey
[ae] Also at Joint Institute for Nuclear Research, Dubna, Russia
[af] Also at Moscow Institute of Physics and Technology State University, Dolgoprudny, Russia
[ag] Also at National Research Nuclear University MEPhI, Moscow, Russia
[ah] Also at Physics Department, An-Najah National University, Nablus, Palestine
[ai] Also at Physikalisches Institut, Albert-Ludwigs-Universität Freiburg, Freiburg, Germany
[aj] Also at The City College of New York, New York, NY, USA
[ak] Also at TRIUMF, Vancouver, BC, Canada
[al] Also at Universita di Napoli Parthenope, Napoli, Italy
[am] Also at University of Chinese Academy of Sciences (UCAS), Beijing, China
*Deceased